TRANSPORT OF SURFACE-MODIFIED IRON NANOPARTICLES THROUGH MODEL SUBSURFACE POROUS MEDIA

by

Trishikhi Raychoudhury

Department of Civil Engineering and Applied Mechanics
McGill University, Montreal

A THESIS SUBMITTED TO McGILL UNIVERSITY
IN PARTIAL FULFILLMENT OF THE REQUIREMENTS FOR THE DEGREE
OF DOCTOR OF PHILOSOPHY

May 2011

Abstract

A rapidly emerging remediation technique for source zone remediation of chlorinated solvent- or heavy metal contaminated aquifers is the application of nano-sized zero valent iron (NZVI) particles. However, the efficient remediation of aquifers will depend on the feasibility of transport of NZVI from injection wells to the zones of elevated contamination. Bare NZVI has limited potential for transport in subsurface porous media due to its tendency to aggregate into larger particles and to deposit on granular subsurface media. Polymer-coatings on NZVI however reduce aggregation and improve its transport in porous media and thus may facilitate NZVI-based *in situ* remediation of contaminated aquifers.

The overall objective of this research is to evaluate significant mechanisms for deposition of surface-modified NZVI in granular subsurface media during transport. Although surface-modified NZVI have been shown to transport more easily than bare NZVI, there is a lack of knowledge of how different parameters such NZVI particle concentration, NZVI size, aqueous-phase flow velocity, and sand particle size influence nanoparticle transport. To investigate the effects of these parameters on transport, a number of laboratory experiments were conducted with NZVI synthesized from ferrous sulfate in the presence of polymers that were effective in colloidal stabilization of the particles. The bare and surface modified-NZVI was characterized for size and surface chemistry by a wide array of analytical instruments. The polymer-stabilized NZVI were employed in three different studies to identify parameters that influence deposition of NZVI in model, granular, subsurface media.

In the first study, the breakthrough patterns of carboxymethyl cellulose (CMC)- and polyacrylic acid (PAA)- stabilized NZVI eluted from packed sand columns under a range of pore water velocities and NZVI influent concentrations were investigated. The NZVI effluent relative concentrations of both types of particles decreased with decreasing flow velocities and increasing particle concentrations. PAA-NZVI exhibited slower elution from the columns than CMC-NZVI under identical experimental conditions, and this is attributed to more rapid aggregation kinetics of PAA-NZVI. The second study focused on the quantitative evaluation of aggregation kinetics and the possible effects of aggregation on NZVI deposition. Aggregation of CMC-NZVI particles resulted in a change in particle size distribution (PSD) with time, and the changes in particle size were evaluated by nanoparticle tracking analyzer (NTA). The effects of particle concentrations on the transport in porous media were evaluated by comparing the time profiles of elution of CMC-NZVI from packed sand columns. Changes in PSD over time were responsible for a gradual increase in effluent concentration between 1 and 4 pore volumes, and beyond 4 pore volumes particle detachment contributed to non-steady state effluent concentrations. The NZVI elution profiles had a good fit with aggregation kinetics equations coupled to colloid transport equations that account for particle deposition and detachment.

The third study focused on assessing the significance of straining of CMC-NZVI particles during transport in model subsurface porous media. Laboratory experiment were conducted to assess the transport of CMC-NZVI in columns packed with four different sized sands and with three different concentrations .

Breakthrough curves (BTC) and retention profiles of CMC-NZVI along the column length were analyzed to characterize CMC-NZVI transport. The breakthrough curves suggest that with decrease in mean sand diameter, the effluent concentrations decrease. Very high CMC-NZVI particle retention towards the inlet, particularly for the finer sands was observed. These observations are consistent with particle retention in porous media due to straining and/or wedging. Two colloid transport models considering 1) particle deposition by attachment only, and 2) particle retention by straining along with particle deposition by attachment were fitted to the experimental data. Comparison of experimental data and the model calculations suggest that in addition to deposition on collector surface, CMC-NZVI particles are removed from the solution by straining in packed sand beds, with straining rate coefficients that decrease with increase in sand diameter. This study adds to the very recent reports that nanoparticles of different materials, despite their small size, may be removed by straining during transport through granular subsurface media.

Résumé

Une technique d’assainissement en plein essor pour l’assainissement de la zone source des aquifères contaminés aux solvants chlorés ou métaux lourds est l’application des particules nano-métriques de fer zéro-valent (NZVI). Cependant, l’assainissement efficace des aquifères dépendra de la faisabilité du transport des particules NZVI à partir des puits d’injection jusqu’aux zones de contamination élevée.Les particules NZVI nues ont un potentiel limité de transport dans le milieu poreux subsurfacique en raison de leur tendance à s’agréger en particules plus grandes et à se déposer sur les milieux granuleux subsurfaciques. Toutefois, les revêtements polymériques des particules NZVI réduisent l’agrégation et améliorent leur transport dans les milieux poreux, facilitant ainsi l’assainissement in situ basé sur les particules NZVI, des aquifères contaminés.

L’objectif global de cette recherche est d’évaluer les mécanismes importants de déposition des particules NZVI modifiées en surface dans les milieux granulaires subsurfaciques pendant le transport.

Bien que les particules NZVI modifiées en surface aient montré un transport plus facile que les particules NZVI nues, il y a un manque de connaissance sur la façon dont des simples paramètres, tel que la concentration des particules NZVI, leur taille, la vitesse d’écoulement de la phase aqueuse et la taille des particules de sable, influencent le transport des nanoparticules.

Pour étudier les effets de ces paramètres sur le transport, un certain nombre d’expériences de laboratoire ont été menées avec des particules NZVI synthétisées à partir du sulfate ferreux en présence de polymères qui seraient efficaces dans la stabilisation colloïdale des particules. Les particules NZVI nues et modifiées en surface ont été caractérisées pour leur taille et leur chimie de surface par un large éventail d’instruments analytiques. Les particules NZVI stabilisées par des polymères (polymère-NZVI) ont été employées dans trois études différentes afin d’identifier les paramètres qui influencent leur déposition dans les milieux modèle, granulaire et subsurfacique.

Dans la première étude, on a étudié les modèles des particules CMC- et PAA-ZVI élues des colonnes remplies de sable dans une gamme de vitesses de l’eau des pores, et des concentrations influentes de particules NZVI. . Les concentrations effluentes relatives des deux types de particules NZVI ont diminué avec la diminution des vitesses d’écoulement et avec l’augmentation des concentrations des particules. Les particules PAA-NZVI présentaient une élution plus lente que les particules CMC-NZVI dans des conditions expérimentales identiques, ceci étant attribué à une cinétique d’agrégation plus rapide pour les particules PAA-NZVI. La réduction de la stabilité colloïdale due à l’agrégation des particules CMC- et PAA-NZVI a été vérifiée en utilisant les tests de sédimentation et on a trouvé que les particules PAA-NZVI ont été moins stables que les particules CMC-NZVI.

La deuxième étude portait sur l’évaluation quantitative de la cinétique d’agrégation et les effets d’agrégation possibles sur la déposition des particules NZVI. L’agrégation des particules CMC-NZVI a entraîné un changement dans la distribution de la taille des particules (PSD) avec le temps, et les changements dans la taille des particules étaient évalués par l’analyse de suivi des

nanoparticules (NTA). Les effets de la concentration des particules dans la gamme sur le transport dans les milieux poreux ont été évalués en comparant les profils de temps d’élution des particules CMC-NZVI dans les colonnes remplies de sable. Les profils d’élution des particules NZVI ont eu un bon ajustement avec les équations cinétiques d’agrégation couplées aux équations de transport colloïdal, qui tiennent compte de la déposition des particules et de détachement.

La troisième étude portait sur l’évaluation de l’importance de la filtration des particules CMC-NZVI pendant le transport dans les milieux poreux subsurfaciques modèles. Des expériences de laboratoire ont été effectuées pour évaluer le transport des particules CMC-NZVI dans les colonnes et trois concentrations différentes. Les courbes percées (BTC) et les profils de rétention des particules CMC-NZVI le long de la colonne ont été analysés afin de caractériser le transport. Les courbes BTC suggèrent que les concentrations effluentes diminuent avec la diminution du diamètre moyen du sable. Une très élevée rétention des particules CMC-NZVI a été observée, particulièrement pour les sables plus fins. Ces observations sont en accord avec la rétention des particules dans les milieux poreux due à la filtration et au calage. Deux modèles de transport colloïdal qui considèrent 1) la déposition des particules uniquement par attachement, et 2) la rétention des particules par filtration et déposition par attachement, ont été ajustés aux données expérimentales. La comparaison des données expérimentales avec les calculs du modèle suggèrent qu’en plus de la déposition sur la surface du collecteur, les particules CMC-NZVI sont retirées de la solution par filtration dans les lits remplis de sable, avec des coefficients de filtration qui diminuent avec le diamètre du sable. Cette étude s'ajoute à des très récents rapports qui démontrent que les nanoparticules de matériaux différents, malgré leur petite taille, peuvent être retirées par filtration pendant le transport à travers les milieux granulaires subsurfaciques.

Dedication

I would like to dedicate my thesis to

My Parents

&
My Sister: Prishati

Acknowledgments

I express my deepest gratitude to my supervisor Prof. Subhasis Ghoshal. It was a great experience to work under his guidance. I really appreciate his support throughout the course of my PhD and I enjoyed all discussion with him which was encouraging and helped me to gain more insight on my research problem. I would like to thank my co-supervisor Prof. Nathalie Tufenkji for her valuable comment and feedback at each stages of my work starting from research protocol to manuscript writing.

I would like to thank Dr. Ghinwa Naja from whom I have learnt not only to synthesis iron nanoparticles but also how to behave in the Lab as I didn’t have any experimental background. I would like to thank our whole NZVI research group starting from Prof. Audrey Moores and Dr. Mihai Ciprian Cirtiu for all the interesting discussion and guidance on particle characterization. It was my pleasure to work with Ciprian on particle characterization and I am really thankful to him for his contribution by translating the abstract in French. I would like to acknowledge that the characterization results for different polymers included in appendix have an equal contribution from Dr. Cirtiu. I would like to thanks Prof. Kevin Wilkinson for letting me use NTA in the University de Montreal and for his valuable comment related to aggregation studies. I am really enjoyed sharing my views with Mohan, Sai, Jing and Julien. I would like to thank Carolyn and Catharine for your contribution and help during your summer project.

Within environmental research group I would like to thank Prof. Frigon and Prof Gehr for participation in Water Resources and Environmental Engineering seminar series from which we all get good feedback on our research at different stages. Without Sai’s infinite enthusiasm and his ‘it’s okay” attitude towards everything we could not able to make such an enjoyable working environment. I ‘really appreciate’ Ali’s help regarding GC analysis. and Arti for spending her time on reading few of my thesis chapters   How can I forget to thank Jing, Sharmin, Bing, Siavash, Stoyan and Usman for your help and interesting conversation on various topics? Mohammad’s ‘how is it going’ concern really helped and kept me very alert on my day-to-day research progress.

I think all of us have learnt to be cool in hard time from Stoyan. Thanks to Sormeh, Basant, Wonjae and Diana and John for all of your support and help. I would like to thank all of you, and life without these would be pretty dull in the Lab.

I would like to acknowledge McGill Engineering Doctoral Award (MEDA) and the Natural Sciences and Engineering Research Council of Canada (NSERC) for their financial support.

My parents deserve more thanks than I could ever give for their unfailing support and generosity throughout my graduate career. I can't even imagine beginning such a huge commitment like PhD without my sister's support. I can count her always at my side that raised my level of confidence. I would like to thank Samit for encouraging and inspiring whenever I need. Finally, how can I even begin to thank my husband Dipanjan, for his support and love during this time in doctoral school? He gave more than I deserve and it's really hard to imagine completing my PhD without his support.

Table of Contents

ABSTRACT……………………………………………………….i
DEDICATION……………………..………………………...v
ACKNOWLEDGMENTS……………………………….…….vi
TABLE OF CONTENTS……………………………………..viii
LIST OF TABLE ……………………………………….…...xi
LIST OF FIGURES ………………………………..............xii
LIST OF ABREVIATION………………………………..xv
LIST OF SYMBOL………………………………..…....xvi

CHAPTER 1…………………………………………..……..1
INTRODUCTION ……………………………………..……1
1.1 Introduction…………………………………………..…...1
   1.1.1 Source of contamination……………………...........1
   1.1.2 Comparisons of different remediation techniques and advantage of NZVI………..……………………….…….1
   1.1.3 Motivation for research……..……………….………..3
1.2 Objectives……………………………………………..……..4
1.3 Scope and structure of thesis…………………….………..5
   1.3.1Organization of thesis………………………...……6
   1.3.2 Contributions of authors….………………..……………6
Literature cited………………………………………..………8

CHAPTER 2……………………………………………..…12
LITERATURE REVIEW……………………………......…12
2.1 Transport of colloid particles in porous media…..…………....12
   2.1.1 Attachment of colloid on collector surfaces..…………..12
   2.1.2 Colloid retention by other physical mechanisms……….14
   2.1.2.1 Wedging and straining….……………………..…....14
   2.1.2.2 Detachment……………………...…………..15
   2.1.2.3 Ripening……………………………………………..16
   2.1.2.4 Blocking…………………………………..……...16
   2.1.3 Transport of surface modified –NZVI in porous media...17
2.2 Aggregation of NZVI in aqueous solutions……………………19
   2.2.1 Inter-particle forces controlling aggregation……………19
   2.2.2 Aggregation kinetics…………………………….....20
   2.2.3 Colloid transport with aggregation…………………...22
Literature cited………………………………………….……...23

CHAPTER 3……………………………………………………......28
ASSESSMENT OF TRANSPORT OF TWO POLYELECTROLYTE-STABILIZED ZERO-VALENT IRON NANOPARTICLES IN POROUS MEDIA…………..................28
3.1 Introduction……………………………………………………29
3.2 Materials and Methods………………………………….......30
    3.2.1 Chemicals…………………………………….........30
    3.2.2 Zerovalent iron nano-particles synthesis and characterization……………………………………..…..31
    3.2.3 Sedimentation tests………………………….……33
    3.2.4 Column experiments……………………….........33
3.3 Result and discussion……………………………..………34
    3.3.1 Nano-particle characterization…………………………..34
    3.3.2 Assesesment of NZVI aggregation and colloidial stability…..36
    3.3.3Column transport of CMC- and PAA-NZVI.....................40
        3.3.3.1 Effect of flow velocity of NZVI transport ……..40
        3.3.3.2 Effect of concentration on transport…………....46
3.4 Conclusion…………………………………………………49
    Acknowledgement ………………………………………50
    Supplementary data………………………………………51
    References…………………………………………...52

CONNECTING TEXT: CHAPTER 3 AND 4…………………....55

CHAPTER 4…………………………………………………..…56
AGGREGATION AND DEPOSITION KINETICS OF CARBOXYMETHYL CELLULOSE-MODIFIED ZERO-VALENT IRON NANOPARTICLES IN POROUS MEDIA …..56
4.1 Introduction…………………………………………...57
4.2 Materials and Methods…………………………….......60
    4.2.1 Synthesis of CMC-NZVI……………………………...60
    4.2.2 Particle size analysis of CMC-NZVI for assessment of aggregation kinetics……………………………………61
    4.2.3 Packed column experiments…………………….…..62
4.3 Result and discussion……………………………………63
    4.3.1 Aggregation Kinetics of CMC-NZVI……..…………....63

4.3.2 Framework for Assessing the Effect of Aggregation Kinetics on transport of CMC-NZVI……..……………..67
4.3.3 Break Through Curves of CMC-NZVI from Column Transport Experiments……………… …………………..70
4.4 Conclusion…………………………………………….………....75
Acknowledgement………………………………...…………76
Supplementary Information…………………….….……….76
References………………………..…………………….……81

CONNECTING TEXT: CHAPTER 4 AND 5…………………..85

CHAPTER 5……………………………………………….…86
STRAINING OF CMC-NZVI DURING TRANSPORT THROUGH POROUS MEDIA……………………………..….86
5.1 Introduction…………………………………………….…...87
5.2 Theoretical Background……………………………….....89
5.3 Materials and Methods………………………………..…...91
5.3.1 Synthesis and characterization of CMC-NZVI…...……91
5.3.2 Packed column experiments…………………….…92
5.4 Result and discussion……………………………………....94
5.4.1 Transport of CMC-NZVI at different concentrations through coarse and fine sands…..…………………………....94
5.4.2 Model 1: Particle attachment to sand surface….………99
5.4.3 Model 2: Particle attachment and straining……...…..100
Supplementary data……………………………………..….106
References…………………………………………………....108

CHAPTER 6…………………………………………………112
INTELLECTUAL CONTRIBUTION…...……………….……..112

APPENDIX…………………………………….………….117

LIST OF TABLES

TBALE 3.1. Experimental conditions and different parameters for column experiments……………………………..…………………………….…..34

TABLE 3.2. Characteristic of different types of NZVI……………..…………..…..36

NOMENCLATURE…………………………………………………………59

TABLE 4.1: Specifications of experimental conditions …...………...…..…......63

TABLE 4.2. Fitted values of particle-particle attachment efficiency (α_{pp}), particle-collector attachment efficiency (α_{pc}) and detachment rate constant (k_{det}) for different experimental conditions. ……………………….……….....………..72

TABLE 5.1: Experimental conditions and different parameters for column experiments…………………………………………………..…………..…99

TABLE 5.2: Transport results and strained mass at different experimental conditions ………………………………………………..………………99

TABLE A.1: Characteristics of bare and different polymer-NZVI ……………………………………………..………………………….....118

TABLE A.2: DLVO interaction energies between particle-particle and particle-collector ...…………………………………………………………….…...119

TABLE A.3: Parameter values used for DLVO calculation …….……...……..121

LIST OF FIGURE

FIGURE 2.1. Schematic of colloid straining and wedging in the porous medium ……………………………………..……………………………………….....14

FIGURE 2.2. Schematic of colloid detachment from collector surface ……………………………………………….………………..…………15

FIGURE 2.3. Schematic representations of colloid ripening and blocking ……17

FIGURE 3.1. TEM images of PAA-NZVI: (a) smaller (3-15 nm) particle sub-population (typical particles indicated by circles). (b) larger (25-100 nm) particle sub-population……………………………………………………………....35

FIGURE 3.2. Changes in relative absorbance over time in sedimentation tests with different NZVI at a suspension concentration of 0.2 g L^{-1}…………………37

FIGURE 3.3. Particle-particle DLVO interaction with steric effect for (a) CMC-NZVI and PAA-NZVI of 5nm size and (b) for different size of PAA-NZV...38-39

FIGURE 3.4: Changes in average particle diameter with time as determined by NTA of CMC-NZVI of particle suspension concentration of 0.2gL^{-1}……….......40

FIGURE 3.5. Experimental breakthrough curves for varying pore water velocities in packed sand columns of L =4.5 cm, C_0 = 0.5 g L^{-1}. **(a)** CMC-NZVI (**b)** PAA-NZVI……………………………...……………………………………...41

FIGURE 3.6. (a) XDLVO total interaction energies between sand collector surface and PAA-NZVI (4.6 nm, 25 nm and 50 nm diameter) and CMC-NZVI (5.7 nm diameter). The plots for PAA-NZVI (4.6 nm) and CMC-NZVI (5.7 nm) overlap (b) Change in single collector efficiency (η_0) with particle size...………43

FIGURE 3.7. Effect of particle size on BTC of particles with diameter ranging between (a) 2.5-10nm and (b) 25-100nm. Each BTC corresponds to a fixed particle size, except in (b) the line connecting the circles has been drawn to illustrate the approximate BTC for particles that aggregate from 25 nm at 1 PV to 100 nm at 4 PV…......................................……………………………….……45

FIGURE 3.8. Experimental breakthrough curves with varying particle concentrations in packed sand columns of L =4.5 cm, v = 0.2 cm min^{-1} **(a)** CMC-NZVI (**b)** PAA-NZVI..……………………………………………….…………48

FIGURE 3.S1. Variation in influent concentration of iron nanoparticles at the inlet with time…………………………………………………………………51

FIGURE 3.S2. Experimental breakthrough curves of CMC-NZVI with varying column lengths in packed sand columns where, v = 0.2 cm min^{-1} , C_0 = 0.1 g L^{-1} ………………………………………………………………..………………51

FIGURE 4.1. Schematic of concurrent aggregation and particle deposition processes in porous medium.……………………………………………………60

FIGURE 4.2. (A) Changes in mean particle size over time for suspensions of CMC-NZVI obtained by nanoparticle tracking analysis (NTA). The lines show the best fit of the aggregation kinetics model to the 0.2 gL^{-1} and 0.725 gL^{-1} CMC-NZVI. (B) Change in Na^{+} concentration with increase in CMC-NZVI concentration in suspensions prepared in 0.1 mM NaHCO$_3$..…………………..……..64

FIGURE 4.3. (A) Change in single-collector contact efficiency with particle size in the range 40-400 nm, and (B) change in CMC-NZVI breakthrough curves computed for different particle sizes with a α_{pp}= 2.5×10^4 and α_{pc}=0.34 with an assumed total particle number concentration of 5×10^{17} (number/mL). The values of α_{pp} , α_{pc} and number concentration were the average values for different experimental conditions in this study……………………………………………69

FIGURE 4.4. Experimental breakthrough curves of CMC-NZVI with model fit considering (A) particle aggregation and transport but no detachment, and (B) particle aggregation, transport and detachment. The BTCs were obtained using particle suspensions of concentrations of 0.07 gL^{-1}, 0.2 gL^{-1} and 0.725 gL^{-1}. The column bed depth was 9 cm and flow velocity 0.445 cm.min^{-1}. ………………...71

FIGURE 4.5. Breakthrough curves of CMC-NZVI for column experiments with 0.2 gL^{-1} particle suspensions prepared in 0.1 mM and 10 mM IS. The column bed depth was 9 cm and flow velocity 0.445 cm.min^{-1}……………………………75

FIGURE 4.S1. CMC-NZVI concentration at inlet over time………..………77

FIGURE 4.S2. Extended DLVO interaction energy calculations for CMC-NZVI (A) particle-particle and (B) sand-particle (70 nm diameter) interactions. ……………………………………………………………….……………………78

Figure 4.S3. Calculated particle size distributions at various times for a particle size range of 45-220 nm in particle suspensions with concentrations of (A) 0.20 gL^{-1} and (B) 0.725 gL^{-1} CMC-NZVI particles. The maximum aggregate size was set at 220 nm, as discrete aggregate sizes larger than 220 nm were not observed by TEM in particle suspensions maintained up to 65 min………………………79

Figure 4.S4. (A) Ratio of torque due to drag (T_{applied}) and DLVO interaction energy (T_{adhesive})………………………….........……………………………80

Figure 4.S5. Breakthrough curves of CMC-NZVI with electrolyte flushing indicate tailing effect. The column bed depth was 9 cm, particle concentration of 0.2 gL^{-1}, flow velocity 0.445 cm.min^{-1} and IS was 0.1mM……………………80

FIGURE 5.1. : Experimental and simulated (a) breakthrough curves and (b) retention profiles along the column length of CMC-NZVI through different sized sands packed columns of *L* =9.0 cm, C_0 = 0.085 g•L^{-1}, considering Model 1….100

FIGURE 5.2. Experimental and simulated (a) breakthrough curves and (b) retention profiles along the column length of CMC-NZVI through different sized sands packed columns of *L* =9.0 cm, C_0 = 0.085 g•L^{-1},considering Model 2 ……………….……………………………………………………………….102

FIGURE 5.3. Experimental and simulated (a) breakthrough curves and (b) retention profiles along the column length of CMC-NZVI through different sized sands packed columns of *L* =9.0 cm, C_0 = 0.35 g•L^{-1},considering Model 2 ………………………………………………………………………………..103

FIGURE 5.4. Experimental and simulated (a) breakthrough curves and (b) retention profiles along the column length of CMC-NZVI through different sized sands packed columns of *L* =9.0 cm, C_0 = 1.70 g•L^{-1},considering Model 2 ………….……………………………………………..……………..104

FIGURE5. 5. Fitted straining rate coefficient, evaluated using Model 2, varies linearly with d_p/d_c ratio. Here, d_p is based on NTA image analysis…...……......105

FIGURE 5.S1. (a) Experimental and simulated (a) breakthrough curves and (b) retention profiles along the column length of CMC-NZVI through different sized sands packed columns of *L* =9.0 cm, C_0 = 0.35 g•L^{-1},considering Model……………………………………………………………………...108

FIGURE 5.S2. Experimental and simulated (a) breakthrough curves and (b) retention profiles along the column length of CMC-NZVI through different sized sands packed columns of *L* =9.0 cm, C_0 = 1.70 g•L^{-1},considering Model 1…………………………………..………………………………..109

FIGURE A.1. Sedimentation test results of bare and different surface modified NZVI…………..……………………………………………………………119

LIST OF ABBREVIATION

AAS: Atomic Absorption Spectroscopy
BTC: Break Through Curves
CCC: Critical Coagulation Concentration
CMC: Carboxymethyl Cellulose
CF: Coalesced Fractal
CFT: Colloid Filtration Theory
CS: Coalesced Sphere
DLA: Diffusion Limited Aggregation
DLS: Dynamic Light Scattering
DLVO: Darjaguin-Landue-Varwey-Overbeek
DNAPL: Dense Non-Aqueous Phase Liquids
FTIR: Fourier Transform Infrared Spectroscopy
IS: Ionic Strength
MW: Molecular Weight
NAPL: Non-Aqueous Phase Liquids
NTA: Nanoparticle Tracking Analyzer
NZVI: Nano-scale Zero-Valent Iron
PAA: Polyacrylic acid
PAM: Polyacrylamide
PSD: Particle Size Distribution
PSS : Polystyrenesulfonate
PV: Pore Volume
RLA: Reaction Limited Aggregation
TEM: Transmission Electron Microscopy
XPS: X-ray Photoelectron Spectroscopy
XRD: X-Ray Diffraction

LIST OF SYMBOLS

A: Hamaker constant

C: effluent particle mass concentration

C_0: influent particle mass concentration

C_i: Mass concentration of i^{th} size aggregate

D : hydrodynamic dispersion coefficient,

D_f: Fractal dimension of aggregates

Fe^0: Zero valent iron

Fe_0: Percentage of zero valent iron in nano particle

$F_{adhesive}$: Adhesive force

F_{drag}: Drag force

M_s : saturation magnetization

$N_{0:}$ primary particle number concentration

N_a: Avogadro's constant

N_i : number of single particles forming the aggregates

N_p: Number of segment of polyelectrolyte chain

T: Temperature

$T_{adhesive}$: Adhesive torque

$T_{applied}$: Torque applied

V_{es}: electrostatic interaction energy

V_m: magnetic interaction energy

V_{steric} : steric interaction energy

V_{tot}: total interaction energy

V_{vdw}: ven dar Waal interaction energy

$\frac{\partial V}{\partial r}$: velocity gradient within the pore space due to shear on the collector surface

W : stability ratio

Z: maximum number of size categories

a: radius of the colloid particles

c_i: ion concentration of i^{th} ion

d_{Navg} : Number-averaged mean diameter measured by NTA
d^{*}_{Navg} : Number-averaged mean diameter calculated from model
d_{c}: mean collector diameter
$d_{\mathrm{p(i)}}$: particle diameter of i^{th} aggregates
$d_{\mathrm{p(i=1)}}$: diameter of the smallest particle size
d_{p}: mean particle size
d_{p}^{*}: Measured particle size by NTA
e : elcron charge
$k_{11:}$ initial aggregation rate constant
k_{att} : particle attachment rate coefficient
k_{b}: Boltzmann constant
k_{deb} :Debye screening length
k_{dep} : particle deposition rate coefficient
$k_{\mathrm{dep,i}}$: deposition rate coefficient of the i^{th} sized particles
k_{det} : particle detachment rate coefficient
k_{str} : straining rate co-efficient
l : length of each segment of polyelectrolyte chain.
$mass_{i}$: Mass of i^{th} particles
n: particle number concentration
$n_{\mathrm{i,:}}$ particle number concentrations of ith aggregates
r_{h}: hydrodynamic radius
s : separation distance between surface of two particles
s_{att} : solid phase attached mass on collector
s_{dep} : solid phase deposited mass on collector
s_{str} : phase strained mass
s_{total}: Total solid phase mass retained
t: time
t_{p} : polyelectrlyte layer thickness
v : Darcy's velocity
v_{x} : pore water velocity
x : space or down gradient distance along porous media

z_i : valency of i^{th} ion

α_{pc}: particle-collector attachment efficiency

α_{pp}: particle-particle attachment efficiency

α_x: longitudinal dispersivity

β : particle-particle collision frequency

β': fitted parameter

δ: distance of the energy minima from particle surface

ε: porosity

ε_o : vacuum permeability

ε_r : relative permeability of water

φ_{min} : Energy at secondary minima

$\eta_{0:}$ single collector efficiency

$\eta_{0,i:}$ single collector efficiency of i^{th} sized aggregate

μ :dynamic viscosity

μ_0 : permeability of free space

ρ : bulk density of sand

σ_p : surface density of polymer layer segment

ψ : zeta potential

ψ_{str} : dimensionless colloid straining function

Chapter 1

Introduction

1.1 Introduction

1.1.1. Source of contamination

Chlorinated solvents are used in large volumes by various industries, especially as degreasers by metal parts manufacturing industry; organic solvent for dry cleaning industry. Uncontrolled or accidental discharges of chlorinated solvents into the subsurface of many industrial and military sites have led to extensive soil and groundwater contamination. Approximately 1.8 million pounds of chlorinated solvents have been improperly discharged in groundwater at different sites in the US which resulted in contamination of up to several thousand aquifers [1].

Chlorinated solvents which are denser than water are referred to as dense non-aqueous phase liquids or DNAPLs. As they migrate through the subsurface, significant volumes are trapped as immobile residual saturation blobs in permeable porous media or collected in pools on top of low permeability regions. The DNAPLs in residual saturation and in pools act as a source for groundwater contamination from which chlorinated organic compounds are slowly but continuously released [2, 3]. Therefore, effective technologies for remediation of chlorinated solvent source zones are needed.

1.1.2. Comparison of different remediation techniques and advantage of NZVI

Surfactant flushing, chemical oxidation, air-sparging, thermal treatment technologies such as hot water flushing, and bioremediation are the most well known source zone remediation techniques for chlorinated solvent-contaminated sites. However, there has been limited success with these remediation technologies and efforts to restore groundwater concentrations to meet drinking water standards have not yet been successful at any large DNAPL-contaminated site [1]. For example, Pennell et al [4] have suggested surfactant-enhanced remediation by mobilization of DNAPLs, however there are concerns with uncontrolled mobilization of DNAPLs. Schnarr et al [5] demonstrated that *in situ* oxidation can remove chlorinated solvent such as TCE and PCE efficiently from homogeneous porous media, but removal efficiency decreased in heterogeneous media. Rogers and Ong [6] demonstrated air-sparging also have limited efficiency for source zone remediation of DNAPL. A review by Soga et al [7], suggest effect of source zone remediation activities on mass flux depends on the complexity in heterogeneity of the media and re-distribution of NAPL morphology due NAPL mass removal.

Bioremediation when employed as a source zone remediation technique, may have limited efficiency because high concentrations of chlorinated organic compounds at DNAPL source zones are often toxic for microorganisms [8, 9]. In addition, *in situ* bioremediation rates are very slow and often result in the production of potentially toxic intermediates [10].

A rapidly emerging remediation technique that can be applied for source zone remediation of chlorinated solvent-contaminated sites is the application of nano-sized zero-valent iron (NZVI) particles. Zero-valent iron is a strong reducing agent that can spontaneously degrade and detoxify many chlorinated organic compounds [11] and is also effective in adsorbing and/or reducing heavy metals such as chromium and arsenic and degrading inorganic anions [12, 13]. Zero-valent iron in granular form was first used in permeable reactive barriers (PRB). PRBs are employed as a passive in-situ method to remediate contaminated groundwater containing chlorinated hydrocarbons [14, 15]. A major limitation of a permeable barrier is that it can only be applied for treatment of pollutants in shallow groundwater.

Injection of NZVI is an emerging technique for *in situ* groundwater remediation. The primary advantages of NZVI-based remediation are (i) very rapid rates of degradation of chlorinated solvents or heavy metals due to the large specific surface area of NZVI, and (ii) the potential for injection of the reactive

NZVI into deeper locations in the aquifers where chlorinated solvents or DNAPL pools are often found.

The use of NZVI for *in situ* groundwater remediation is limited by its rapid aggregation and deposition onto the mineral surface [16]. Several recent studies have focused on facilitating colloidal stabilization and transport by surface modification of NZVI particles with different polymer and polyelectrolyte. Water soluble starch, polyacrylic acid (PAA), sodium carboxymethyl cellulose (CMC) and several polymers are found to be very effective in colloidal stabilization of NZVI [12, 17-21].

There is, however, concern over the toxicity of nanoparticles in aquifers which may serve as drinking water sources, and the risks of the addition of iron nanoparticles need to be carefully evaluated. However, recent studies have suggested that the risk of adding NZVI to contaminated aquifers may not be high, especially for polymer-stabilized NZVI [22]. The polymer coating prevents direct contact of the metal nanoparticle surface with live cells. In addition, the toxicity of NZVI reduces with age as they are oxidized and dissolved over time.

1.1.3. Motivation for the research

The efficient remediation of DNAPL source zones in aquifers will depend on the feasibility of transport of NZVI from injection wells to the DNAPL pools and zones of residual saturation that act as source zones for groundwater contamination. Bare NZVI has been found to have limited potential for transport in subsurface porous media due to its tendency to aggregate into larger particles and to deposit on granular subsurface media [16]. Field application of NZVI suggests NZVI transport limited within few foot in the subsurface porous media [23, 24]

Different polymers and polyelectrolytes can achieve different levels of colloidal stability [25-27] and thus have variable impacts on transport and deposition of modified-NZVI particles in porous media. CMC-NZVI was found to be more colloidal stable [27] and and an *in situ* assessment for chlorinated solvent destruction was carried out by He et al [28].

Currently, there is limited information on the different parameters that influence transport and deposition of polymer-stabilized NZVI in granular subsurface media. A number of studies have investigated the transport of various nanoparticles in subsurface porous media [29]. However, there are some unique aspects of NZVI and its use for groundwater remediation, which require in-depth investigation. It is expected that for effective remediation, NZVI in g/L doses have to be delivered to contaminated zones. Most studies on nanoparticle transport have assessed transport behavior at much lower concentrations [29] . Furthermore, unlike most other nanomaterials of environmental significance, there is strong magnetic attraction between NZVI particles. Electrosteric stabilization of these nanoparticles by polyelectrolytes surface coating can limit aggregation of NZVI; however, in most cases it can not eliminate aggregation completely with the doses commonly reported in literature [25, 26, 30]. Therefore, it is important to understand the aggregation kinetics and the resulting effects of changes in particle size distribution on deposition during transport.

The deposition of surface modified-NZVI on sand grain surfaces have been shown to be influenced by van der Waals attraction, electrostatic repulsion, and steric hindrance due to polymer coatings [25, 31]. Often, polymer-stabilized NZVI are deposited on the sand collector surface at the secondary minimum. Thus, these particles are weekly associated on the collector surface and are easily detachable during groundwater flushing. Furthermore, in many cases colloids with high energy barriers to collector surfaces are retained in the porous media by wedging (particle retention at the grain-to-grain contact point) or straining (blocking of small pores near inlet) [32-34]. There are few studies reported in the literature which suggest that nanoparticles can be retained due to straining [35-37]. However these studies have not assessed straining systematically with respect to sand size, retention profile and with quantitative assessments of the straining rate coefficients.

1.2 Objectives

The overall objective of this research is to identify and evaluate several significant mechanisms that contribute to deposition of surface-modified NZVI in granular subsurface media during transport.

The specific objectives of this study are to:

Specific Objectives

- Evaluate the transport efficiency of NZVI stabilized with two polyelectrolytes, CMC and PAA, at different flow velocities and particle concentrations.
- Evaluate the effect of nanoparticle concentration on CMC-NZVI aggregation and transport.
- Develop a coupled aggregation-transport model, incorporating deposition and detachment and evaluate the fit of the model to the experimental data.
- Assess CMC-NZVI transport efficiency through beds of different sized sand grains, for a range of CMC-NZVI concentrations.
- Assess the significance of straining of CMC-NZI particles in porous media by evaluating the fit of a colloid transport model accounting for particle retention by straining to experimental data for column experiments.

1.3 Scope and structure of thesis

Different sizes of polymer-stabilized NZVI were used in the study. In all cases the NZVI were synthesized in the laboratory using well established procedures. Average particle diameters of polymer-modified NZVI were controlled by altering polymer/Fe^{2+} ratio and were characterized extensively for size and surface chemistry as described in Cirtiu et al. [27]. The first study discussed in Chapter 3 was carried out with a small particle size of 4-10 nm range for CMC-NZVI, whereas, in Chapter 4 and Chapter 5; all experiments were conducted with particles of bigger size in the range of 45-250 nm. Two NZVI transport experiments were conducted in laboratory columns packed with clean sand, and NZVI suspension were prepared with aqueous solutions of known chemistry. NZVI concentrations ranged from the mgL^{-1} to the gL^{-1} level in the different studies. Details of these procedures are presented in Chapter 3, 4 and 5.

1.3.1 Organization of thesis

The following remarks serve as a guide in reading this manuscript based thesis.

Chapter 1 provides the introduction, scope, motivation, objectives and structure of the thesis.

Chapter 2 provides a detailed literature review on colloid transport through subsurface porous media. Colloid transport with deposition and other physical mechanisms for colloid retention in porous media are discussed in detail. Literature on colloid aggregation kinetics and probable effect of aggregation on transport are discussed.

Chapters 3 to 5 are three journal manuscripts that address the specific objectives mentioned above. The manuscript in Chapter 3 has been published in the Journal of Contaminated Hydrology. The manuscript contained in Chapter 4 is submitted in Water Research and the manuscript in Chapter 5 will be submitted to Environmental Science and Technology.

Chapter 6 summarizes the conclusions and intellectual contributions of the research performed.

The Appendix provides information on surface-modified NZVI synthesis and characterizations. Equations and parameters used for particle-particle and particle-collector DLVO analysis are stated in appendix.

1.3.2 Contributions of Authors

The contribution of authors of the manuscripts contained in Chapters 3, 4 and 5 are stated below.

Chapter 3

Assessment of transport of two polyelectrolyte-stabilized zero-valent iron nanoparticles in porous media. **T. Raychoudhury , G. Naja, and S. Ghoshal**. Journal of Contaminant Hydrology, (2010).118, 143-151.

Dr. G. Naja, a Research Associate , worked with Prof. Ghoshal, synthesized the polyelectrolyte-stabilized NZVI particles and conducted transmission electron microscopy (TEM) of CMC-NZVI. Dr. Naja also provided guidance and assistance with the sedimentation experiments, column transport experiments. The nanoparticle tracking analysis experiments, TEM of PAA-NZVI, calculation of the extended DLVO interaction energies and single collector efficiencies, calculation of NZVI transport patterns and the discussion of the results were performed by me. Prof. S. Ghoshal supervised the research and edited the manuscript.

Chapter 4

Effects of particle concentration on aggregation and transport of carboxymethyl cellulose-modified zero-valent iron nanoparticles in porous media. **T. Raychoudhury , N. Tufenkji, and S. Ghoshal.** To be submitted to Water Research, May 2011.

Experimental design, execution, analysis of experimental data, aggregation and transport model development and solution were carried out by me. Prof. N. Tufenkji and Prof. S. Ghoshal supervised the research and experimental design, and edited the manuscript.

Chapter 5

Straining of CMC-NZVI during transport through porous media. To be submitted to Environmental Science and Technology, May 2011. **T. Raychoudhury , N. Tufenkji, and S. Ghoshal**

Experimental design, execution, analysis of experimental data, straining based transport model calculations were carried out by me. Prof. N. Tufenkji and Prof.

S. Ghoshal supervised the research and experimental design, and edited the manuscript.

Appendix

Synthesis and surface characterization of different surface-modified NZVI presented in appendix was carried out by me and Dr. Cirtiu, postodoctoral researcher in the Department of Chemistry, working under the supervision of Dr. Audrey Moores. Assessment of colloidal stability of different surface-modified NZVI by sedimentation test was performed by me.

Literature cited

[1] *Cleanup of the Nation's Waste Sites: Markets and Technology Trends. EPA 542-R-96-005;* ***1997*** *U.S. Environmental Protection Agency; U.S. Government Printing Office: Washington, DC.*

[2] Bradford, S.A., Rathfelder, Klaus M.,Lang, John,Abriola, Linda M., Brown Jr, George E., *Entrapment and dissolution of DNAPLs in heterogeneous porous media.* Journal of Contaminant Hydrology, 2003. **67**(Compendex): p. 133-157.

[3] Pantazidou, M. and K. Liu, *DNAPL distribution in the source zone: Effect of soil structure and uncertainty reduction with increased sampling density.* Journal of Contaminant Hydrology, 2008. **96**(Compendex): p. 169-186.

[4] Pennell, K.D., M. Jin, L.M. Abriola and G.A. Pope, *Surfactant enhanced remediation of soil columns contaminated by residual tetrachloroethylene.* Journal of Contaminant Hydrology, 1994. **16**(Compendex): p. 35-53.

[5] Schnarr, M., C. Truax, G. Farquhar, E. Hood, T. Gonulu and B. Stickney, *Laboratory and controlled field experiments using potassium permanganate to remediate trichloroethylene and perchloroethylene DNAPLs in porous media.* Journal of Contaminant Hydrology, 1998. **29**(Compendex): p. 205-224.

[6] Rogers, S.W. and S.K. Ong, *Influence of porous media, airflow rate, and air channel spacing on benzene NAPL removal during air sparging.* Environmental science and technology, 2000. **34**(Compendex): p. 764-770.

[7] Soga, K., J.W.E. Page and T.H. Illangasekare. *A review of NAPL source zone remediation efficiency and the mass flux approach*. 2004. Elsevier.

[8] Haest, P.J., D. Springael and E. Smolders, *Erratum to "Dechlorination kinetics of TCE at toxic TCE concentrations: Assessment of different models" [Water Research 44 (2010) 1] (DOI:10.1016/j.watres.2009.09.033).* Water Research, 2010. **44**(Compendex): p. 2995.

[9] Haest, P.J., D. Springael and E. Smolders, *Dechlorination kinetics of TCE at toxic TCE concentrations: Assessment of different models.* Water Research, 2010. **44**(Compendex): p. 331-339.

[10] Wako Takami, H.N., Hisakazu Yamane and Toshio Omori, *Degradation of trichloroethylene by recombinant E. coli in continuous culture.* Biotechnology Letters, 2000. **22**: p. 211-217.

[11] Liu, Y., T. Phenrat and G.V. Lowry, *Effect of TCE concentration and dissolved groundwater solutes on NZVI-promoted TCE dechlorination and H2 evolution.* Environmental science and technology, 2007. **41**(22): p. 7881-7887.

[12] Kanel, S., D. Nepal, B. Manning and H. Choi, *Transport of surface-modified iron nanoparticle in porous media and application to arsenic(III) remediation.* Journal of Nanoparticle Research, 2007. **9**(5): p. 725-735.

[13] Li, X.-Q., J. Cao and W.-X. Zhang, *Stoichiometry of Cr(VI) immobilization using nanoscale zero valent iron (nZVI): A study with high-resolution X-ray photoelectron spectroscopy (HR-XPS).* Industrial and Engineering Chemistry Research, 2008. **47**(Compendex): p. 2131-2139.

[14] VanStone, N., A. Przepiora, J. Vogan, G. Lacrampe-Couloume, B. Powers, E. Perez, S. Mabury and B. Sherwood Lollar, *Monitoring trichloroethene remediation at an iron permeable reactive barrier using stable carbon isotopic analysis.* Journal of Contaminant Hydrology, 2005. **78**(Compendex): p. 313-325.

[15] Ebert, M., R. Kober, A. Parbs, V. Plagentz, D. Schafer and A. Dahmke, *Assessing degradation rates of chlorinated ethylenes in column experiments with commercial iron materials used in permeable reactive barriers.* Environmental science and technology, 2006. **40**(Compendex): p. 2004-2010.

[16] Phenrat, T., N. Saleh, K. Sirk, R.D. Tilton and G.V. Lowry, *Aggregation and sedimentation of aqueous nanoscale zerovalent iron dispersions.* Environmental science and technology, 2007. **41**(1): p. 284-290.

[17] He, F., M. Zhang, T. Qian and D. Zhao, *Transport of carboxymethyl cellulose stabilized iron nanoparticles in porous media: Column experiments and modeling.* Journal of Colloid and Interface Science, 2009. **334**(1): p. 96-102.

[18] Phenrat, T., Y. Liu, R.D. Tilton and G.V. Lowry, *Adsorbed polyelectrolyte coatings decrease Feo nanoparticle reactivity with TCE in water: Conceptual model and mechanisms.* Environmental science and technology, 2009. **43**(5): p. 1507-1514.

[19] Raychoudhury, T., G. Naja and S. Ghoshal, *Assessment of transport of two polyelectrolyte-stabilized zero-valent iron nanoparticles in porous media.* Journal of Contaminant Hydrology, 2010. **118**(Compendex): p. 143-151.

[20] Schrick, B., B.W. Hydutsky, J.L. Blough and T.E. Mallouk, *Delivery vehicles for zerovalent metal nanoparticles in soil and groundwater.* Chemistry of Materials, 2004. **16**(11): p. 2187-2193.

[21] Yang, G.C.C., H.-C. Tu and C.-H. Hung, *Stability of nanoiron slurries and their transport in the subsurface environment.* Separation and Purification Technology, 2007. **58**(1): p. 166-172.

[22] Phenrat, T., T.C. Long, G.V. Lowry and B. Veronesi, *Partial oxidation ("Aging") and surface modification decrease the toxicity of nanosized zerovalent Iron.* Environmental science and technology, 2009. **43**(1): p. 195-200.

[23] Ahmadimoghaddam, M., F. Mashhoon, R. Kavch and F. Tarkian. *Nano iron particles application in ground water remediation*. 2008. Postfach 10 10 54, dusseldorf, 40001, Germany: VDI Verlag GMBH.

[24] Tratnyek, P.G. and R.L. Johnson, *Nanotechnologies for environmental cleanup.* Nano Today, 2006. **1**(Compendex): p. 44-48.

[25] Phenrat, T., N. Saleh, K. Sirk, H.-J. Kim, R.D. Tilton and G.V. Lowry, *Stabilization of aqueous nanoscale zerovalent iron dispersions by anionic polyelectrolytes: Adsorbed anionic polyelectrolyte layer properties and their effect on aggregation and sedimentation.* Journal of Nanoparticle Research, 2008. **10**(5): p. 795-814.

[26] Saleh, N., K. Sirk, Y. Liu, T. Phenrat, B. Dufour, K. Matyjaszewski, R.D. Tilton and G.V. Lowry, *Surface modifications enhance nanoiron transport and NAPL targeting in saturated porous media.* Environmental Engineering Science, 2007. **24**(1): p. 45-57.

[27] Cirtiu, M.C., T. Raychoudhury, S. Ghoshal and A. Moores, *Systematic Comparison of the Size, Surface Characteristics and Colloidal Stability of Zero Valent Iron Nanoparticles Preand Post-Grafted with Common Polymers.* Colloids and Surfaces A: Physicochem. Eng. Aspects, 2011. doi:10.1016/j.colsurfa.2011.09.011.

[28] He, F., D. Zhao and C. Paul, *Field assessment of carboxymethyl cellulose stabilized iron nanoparticles for in situ destruction of chlorinated solvents in source zones.* Water Research, 2010. **44**(Compendex): p. 2360-2370.

[29] Petosa, A.R., D.P. Jaisi, I.R. Quevedo, M. Elimelech and N. Tufenkji, *Aggregation and deposition of engineered nanomaterials in aquatic environments: Role of physicochemical interactions.* Environmental science and technology, 2010. **44**(17): p. 6532-6549.

[30] Phenrat, T., H.-J. Kim, F. Fagerlund, T. Illangasekare, R.D. Tilton and G.V. Lowry, *Particle size distribution, concentration, and magnetic attraction affect transport of polymer-modified Fe0 nanoparticles in sand columns.* Environmental science and technology, 2009. **43**(13): p. 5079-5085.

[31] Fatisson, J., S. Ghoshal and N. Tufenkji, *Deposition of carboxymethylcellulose-coated zero-valent iron nanoparticles onto silica: Roles of solution chemistry and organic molecules.* Langmuir, 2010. **26**(Compendex): p. 12832-12840.

[32] Bradford, S.A., H.N. Kim, B.Z. Haznedaroglu, S. Torkzaban and S.L. Walker, *Coupled factors influencing concentration-dependent colloid transport and retention in saturated porous media.* Environmental science and technology, 2009. **43**(Compendex): p. 6996-7002.

[33] Johnson, W.P., E. Pazmino and H. Ma, *Direct observations of colloid retention in granular media in the presence of energy barriers, and implications for inferred mechanisms from indirect observations.* Water Research, 2010. **44**(Compendex): p. 1158-1169.

[34] Li, X., C.-L. Lin, J.D. Miller and W.P. Johnson, *Role of grain-to-grain contacts on profiles of retained colloids in porous media in the presence of an energy barrier to deposition.* Environmental science and technology, 2006. **40**(Compendex): p. 3769-3774.

[35] Hong, Y., R.J. Honda, N.V. Myung and S.L. Walker, *Transport of iron-based nanoparticles: Role of magnetic properties.* Environmental science and technology, 2009. **43**(Compendex): p. 8834-8839.

[36] Jaisi, D.P., N.B. Saleh, R.E. Blake and M. Elimelech, *Transport of single-walled carbon nanotubes in porous media: Filtration mechanisms and reversibility.* Environmental science and technology, 2008. **42**(Compendex): p. 8317-8323.

[37] Tosco, T. and R. Sethi, *Transport of non-newtonian suspensions of highly concentrated micro- and nanoscale iron particles in porous media: A modeling approach.* Environmental science and technology, 2010. **44**(Compendex): p. 9062-9068.

Chapter 2

Literature Review

2.1 Transport of colloidal particles in porous media

2.1.1 Attachment of colloids on collector surfaces

Colloid particle transport in granular porous media is often described by the colloid transport equation [1-3] that include advection (velocity component), dispersion (hydrodynamic dispersivity), and deposition on collector surfaces as expressed in Equation 2.1.

$$\frac{\partial C}{\partial t} = D\frac{\partial^2 C}{\partial x^2} - v_x\frac{\partial C}{\partial x} - k_{att}C \tag{2.1}$$

where, C is the suspended particle mass concentration, D is the hydrodynamic dispersion coefficient, x is the space or down gradient distance along porous media, t is time, v_x is the pore water velocity and k_{att} is the particle deposition rate coefficient described as follows

$$k_{att} = \left[\frac{3(1-\varepsilon)v}{2d_c\varepsilon}\alpha_{pc}\right]\eta_0 \tag{2.2}$$

where, α_{pc}, is the particle-collector attachment efficiency, ε is porosity, v is the Darcy's velocity. d_c is the average grain size and η_0 is the single collector contact efficiency, that could be calculated using Tufenkji & Elimelech equation [4]. The solid phase deposition rate of colloid particles is described [2, 3] as follows,

$$\rho\frac{\delta S_{att}}{\delta t} = \varepsilon k_{att}C \tag{2.3}$$

where, ρ (ML^{-3}) is bulk density of sand and it is constant with time and S_{att} in solid phase deposited mass on collector. The overall particle deposition rate coefficient (k_{att}) is presented in Eq. 2.2.

The packed porous media bed through which transport occurs is idealized as composed of individual spherical particles, called collectors. Particle deposition is represented as a combined effect of α_{pc} and η_0. The collector contact efficiency is the probability of collision of a particle with the collector and the attachment efficiency is the probability of sticking of a particle on the collector after collision [3]. The collector efficiency is governed by three mechanisms; namely, sedimentation, interception and diffusion. Calculations of single-collector contact efficiency using T&E equation [4] indicate diffusion is considered to be the predominant deposition mechanism if the particles are small. Beyond a certain critical size, interception and gravity become the governing mechanisms for deposition. This critical size limit depends upon particle density and viscosity. Particle-collector attachment efficiency depends upon solution chemistry and surface properties, and thus on particle-collector interaction energy. Particle-collector interaction energy could be described by extended DLVO which considers flat plate-sphere van der Waals, electrostatic and steric interaction as described in several studies [5-8].

According to classical colloid filtration theory (CFT), which is the solution of Equation 2.1considering the steady state condition, the suspended and solid phase deposited particle concentrations vary exponentially along the column length. However, deviations from the CFT could be explained by several different mechanisms, such as pore blocking [1, 9], wedging and straining [10-12], ripening [13], aggregation and detachment of deposited particles. Tufenkji et al. [3] showed that deviations from clean-bed CFT due to those factors resulted in non-exponential patterns of particle deposition.

In the presence of an energy barrier, a particle can deposit at the secondary energy minima [8, 14]. However, these particles are weakly deposited and can be removed easily by hydrodynamic drag [15]. Many studies have suggested that particles with energy minima can be retained in the porous media by other mechanisms such as surface charge heterogeneity [16], straining or wedging at grain to grain contact [10, 12, 16], aggregation of particles during transport [7, 8, 17, 18], detachment of deposited or strained particles [19, 20] and by ripening [1].

2.1.2 Colloid retention by other physical mechanisms

2.1.2.1 Wedging and straining

Bradford et al. [15] suggested colloid particles with high energy barrier were retained in the porous media mainly by physical mechanisms such as straining. Straining is the clogging of small pores as presented in Figure 2.1. As a result some colloids are retained in those pores while other colloids are transported through a limited number of connected larger pores. Bradford et al. [11, 15] found particle straining resulted in a hyper-exponential particle retention profile along the column depth. They also demonstrated that the effluent concentration decreases with increase in particle (colloid) size and with decrease in sand size due to straining. Johnson et al. [21] proposed that more particles are retained in the flow stagnation zone at the bounding surfaces either by wedging (between two surfaces) and/or by straining (between three surface).

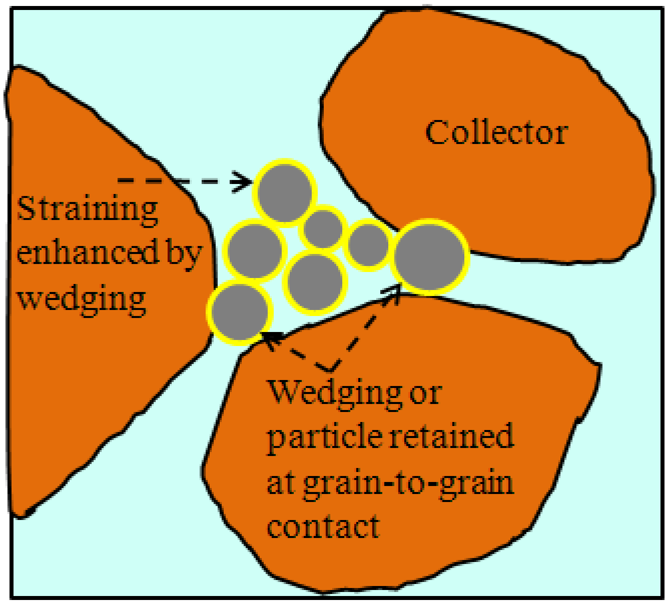

Figure 2.1 Schematic of colloid straining and wedging in the porous medium

Xu et al. [22] reported that straining decays exponentially with strained colloid mass. Bradford and Bettahar [19] addressed this phenomenon as blocking of straining sites. Those authors have explained that potential retention sites are filled up quickly at higher colloid concentrations and the solid phase mass transfer rate reduces with increase in solid phase particle deposition. This mechanism results in an unsteady break through curve (BTC).

2.1.2.2 Detachment

Many studies [10, 16, 21, 23-26] suggest that colloids deposited on secondary minimum of the collector surfaces are easily detachable by shear and drag. Bradford et al. [10] suggested that with increase in solid phase mass concentration more frequent particle-particle collisions at the retention sites results in sliding or rolling of weakly associated particles and eventually resulted in detachment. Recent studies [6, 26-28] have suggested that if the torque on a deposited colloidal particle due to shear force and hydrodynamic drag is greater than the adhesive torque on the particles created by particle-collector DLVO interaction energies, then the deposited particles on collector surface are easily detachable. The conceptual detachment phenomenon is presented in Figure 2.2.

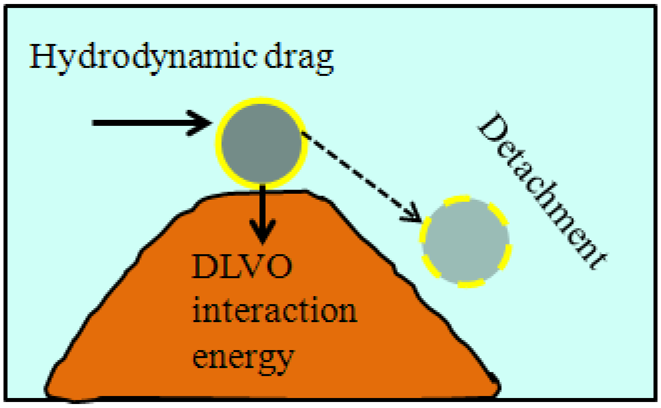

Figure 2.2 Schematic of colloid detachment from collector surface

Several studies have demonstrated detachment of colloids including nanoparticles [6, 20, 29, 30]. Bradford and Bettahar.[19] suggests detachment of strained particles (called liberation) is possible by hydrodynamic forces due to high flow velocity.

2.1.2.3 Ripening

In colloid transport equation the deposition rate coefficients are generally assumed to be constant. However depending upon the difference in the particle-particle interaction energies and particle-collector interaction energies, a time dependent deposition rate coefficient may be observed.

In the case of very high particle-particle attraction, if the particle-particle attachment efficiency becomes higher than the particle-collector attachment efficiency then multi-layer particle deposition can be observed. With time, total surface area of the deposited particle increases and thus more suspended particles tend to deposit on the surface of already deposited particles [13]. This results in an increasing trend in deposition rate with time and thus a decreasing trend in BTC with increasing pore volumes of colloid injection. Many studies demonstrated that with increase in ionic strength (IS) the ripening effect increases [13, 18] resulting in a decreasing trend in the BTC.

2.1.2.4 Blocking

Blocking could be considered as a reverse mechanism of ripening. The physical process of blocking and ripening are presented schematically in Figure 2.3. If the particle-collector attraction is significantly higher than the particle-particle interaction energy, then the suspended particles may be repelled from the already deposited particles. As a result, deposition rates reduce with time or with increases in the solid phase deposited mass [1, 9]. Typical trends for blocking are an increasing trend in the BTC with (i) more pore volumes of colloid injection, and (ii) higher influent concentrations. With increase in colloid concentrations, the available surface coverage for deposition of suspended particles becomes saturated faster and results in more particle elution. The particle deposition profile according to clean bed classical colloid filtration (CFT) theory is exponential along the column depth. However (iii) with blocking, deposition profiled deviate from the exponential pattern and more particles are observed to be deposited towards the outlet of the column [3].

Liu et al. [13] demonstrated that at very low IS, when the particle-particle interaction energy is very low, blocking of deposition sites control the transport mechanism. However with increase in IS, particle-particle attachment efficiency increases and ripening becomes predominant with a decreasing trend in BTC.

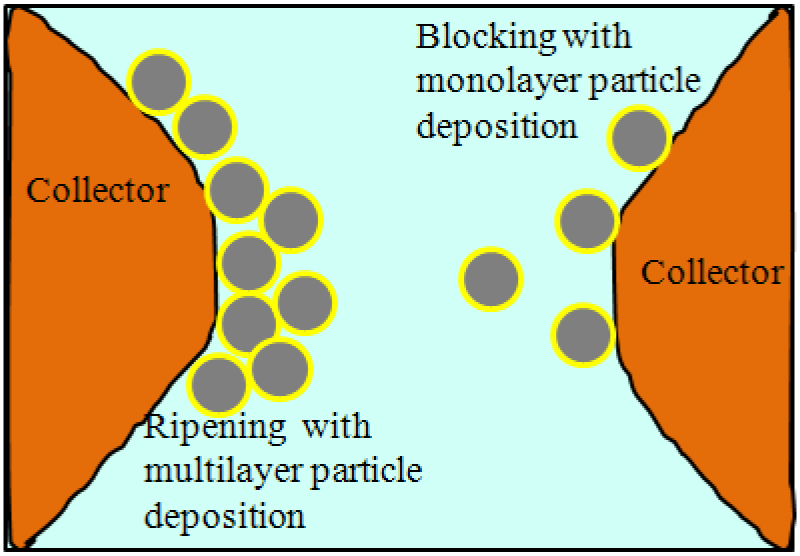

Figure 2.3 Schematic representations of colloid ripening and blocking

2.1.3 Transport of surface-modified NZVI in porous media

Field assessment of NZVI based *in situ* remediation suggests NZVI mobility is limited within few foot from the point of injection, in addition, formation of big aggregates reduce its reactivity and decreases overall performance of NZVI [31, 32]. Microscopic observations of NZVI transport through a sand bed in a microfluidic cell show that bare NZVI is deposited on sand grains during transport. After an initial particle-grain attachment, further NZVI-particles attached to the already deposited NZVI particles and lead to pore plugging. In contrast, surface-modified NZVI transported through the porous media without significant pore plugging [33].

Although surface-modified NZVI are transported more effectively than bare NZVI, their transport efficiency in subsurface porous media is still dependent on environmental factors such as the pH and ionic strength. Groundwater ionic strength and composition may influence the extent of particle-particle and particle-collector electrosteric interactions of surface modified-NZVI and influence transport [5, 33].

Several studies have evaluated the effect of flow velocity on surface modified-NZVI transport in column experiments. However, these studies have been conducted over a limited range of flow velocities. He et al., [34] found that transport of 12 nm diameter CMC-NZVI at flow velocities in the range of 1.1 to 4.2 $cmmin^{-1}$ showed a slight change (about 10%) in effluent concentrations with flow velocity. These groundwater velocities may be relevant to high injection rates. Natural groundwater velocities usually range between 0.006-0.6 $cmmin^{-1}$ [35] and injection rates of NZVI are in the range of 2300 cm^3min^{-1} [36]

Generally it has been observed for various colloids that with increase in collector size, particle deposition decreases [11, 15, 19, 37]. On the contrary, Phenrat el al [38] have found that with increase in collector size, attachment efficiency of surface modified-NZVI increases. Those authors have explained that with smaller collector size, the pore space is small, and thus the fluid shear will be more significant and thus lead to detachment of deposited NZVI and enhanced transportability.

Phenrat et al. [6] demonstrated the effect of particle concentration of polystyrene sulfonate (PSS)-stabilized NZVI particles on transport in porous media. The particles employed in that study were predominantly 325 nm in diameter, as measured by dynamic light scattering (DLS), and the nominal diameter of the bare NZVI as measured by TEM was 75 nm. PSS-NZVI at concentrations of 1-6 gL^{-1} showed greater deposition in packed columns compared to concentrations of 30 mgL^{-1} and this was attributed to the formation of large aggregates at gL^{-1} concentrations. Thus, aggregation of surface-modified NZVI can be an important mechanism that influences its transport characteristics.

2.2 Aggregation of NZVI in aqueous solutions

2.2.1 Inter-particle forces controlling aggregation

Several studies have reported that bare NZVI aggregate extensively and rapidly. Iron nanoparticles, can overcome electrostatic repulsion forces due to the combined effect of magnetic and van der Waals attractive forces, resulting in rapid aggregation [39-41]. The expressions for Derjaguin-Landau-Verwey-Overbeek (DLVO) interaction energies between two magnetic particles are [8, 39, 42]:

$$V_{vdw} = \frac{A}{6K_bT}\left[\frac{2a^2}{s(4a+s)} + \frac{2a^2}{(2a+s)^2} + \ln s\frac{(4a+s)}{(2a+s)^2}\right] \tag{2.4}$$

$$V_m = \frac{8\pi\mu_0 M_s a^3}{9(\frac{s}{a}+2)^3} \tag{2.5}$$

$$V_{es} = \frac{2\pi\varepsilon_r\varepsilon_0}{K_bT}a\psi^2\ln\left[1+e^{-k_{deb}s}\right] \tag{2.6}$$

where, V_{vdw} is the van der Waals interaction potential, A is Hamaker constant, K_{b} is Boltzmann constant, T in temperature, a is the radius of the colloid particles, s is the separation distance between surface of two particles. V_{m} is magnetic interaction potential, μ_0 is permeability of free space. M_{s} is saturation magnetization, V_{es} is electrostatic potential , ε_{o} is the vacuum permeability and ε_{r} is the relative permeability of water, ψ is the zeta potential at the surface and k_{deb} is Debye screening length:

$$k_{deb} = \sqrt{\frac{e^2\sum c_i z_i^2}{\varepsilon_r\varepsilon_0 K_bT}} \tag{2.7}$$

where, e is electron charge, c_{i} and z_{i} are the ion concentration and valency of i^{th} types of ion.

Surface modification of NZVI by polyelectrolytes, polymers and surfactants can limit the extent of aggregation. Phenrat et al. [43] suggests steric interaction between two surface-modified particles counteracts the particle-particle attractive forces, and significantly enhances the colloidal stability. The steric repulsion energy between two surface modified particles has been described as [8, 42-44].

$$V_{steric} = \frac{\pi^3 t_p^3 \sigma_p a}{12 N_p l^2}\left[-\ln(\frac{s}{2t_p}) - \frac{9}{5}(1-\frac{s}{2t_p}) + \frac{1}{3}(1-(\frac{s}{2t_p})^6) \right] \tag{2.8}$$

V_{steric} is the steric interaction energy, t_{p} is the polyelectrolyte layer thickness, σ_{p} and N_{p} are the surface density and number of segment and l is the length of each segment of polyelectrolyte chain. However, aggregation is usually not completely prevented by steric forces. Evidence of incomplete stabilization is also available from observations of reductions in absorbance measurements of suspensions of aqueous polymer-coated particles within minutes [7, 40, 43].

2.2.2 Aggregation kinetics

To date, the aggregation kinetics of NZVI has not been quantitatively evaluated. However, there is substantial literature on aggregation of colloidal particles. Aggregation kinetics of colloid particles are often described by Smoluchowski equation [45] as presented bellow.

$$\left(\frac{dn_k}{dt}\right) = \frac{1}{2}\alpha_{pp} \sum_{i+j=k} \beta(i,j) n_i n_j - \alpha_{pp} n_k \sum_{i=1}^{z} \beta(i,k) n_i \tag{2.9}$$

Where, n_{i}, n_{j} *and* n_{k} are the *i, j* and *k*-mer particle number concentrations, and z is the maximum number of size categories. The first term on the right hand side of Eq. 2.9 accounts for the formation of particle size k as a result of aggregation of particles of size i and j. The second term on the right hand-side accounts for the loss of particle size k as a result of collisions that lead to further aggregation.

Aggregation kinetics is mainly controlled by the particle-particle attachment efficiency, α_{pp}, and collision frequency, β, and particle number concentrations (n). Particle-particle attachment efficiency is dependent on solution chemistry and thus on particle-particle interaction energies, which are often described by DLVO interaction as described in the above section. Particle-particle collision frequency depends on the Brownian motion, fluid shear and differential sedimentation force.

Different approaches for solution of aggregation kinetics models have been suggested. For example, for particle-particle collisions, there are two approaches: (i) a rectilinear model, that assume particles are following a linear path before collision and (ii) a curvilinear model which considers that the particle motion path is not a straight line but a curve. Comparison of the two models suggests a rectilinear approach would predict more number of particle-particle collisions than the curvilinear model [46].

The shape and size of newly formed aggregates are described by two different models [45, 46]. The first model is based on coalesced sphere (CS) theory that suggests two spherical particles will form another spherical aggregate after collision. However, the forms of aggregates are more complex in reality and far from the coalesced sphere assumption. Therefore, a more advanced approach based on coalesced fractal (CF) theory assumption has been adopted to describe the aggregates. According to coalesced fractal theory the shape of the aggregates are defined by their fractal dimension, D_f, which remains unchanged during aggregation [45, 46]. A generally accepted value of D_f is in the range of 1.6-1.8 for diffusion-limited aggregation (DLA), which is the situation for aggregation under favourable conditions, and in the range of 2.0 for reaction-limited aggregation (RLA) that occur under conditions of low ionic strength aqueous solutions and/or inter-particle steric hindrance [47, 48].

Another form of aggregation kinetics, derived from Smoluchowski equation is described by Holthoff et al. [49]. Those authors demonstrated the rate of change of intensity-weighted hydrodynamic radius (r_h) is proportional to both initial primary particle number concentration (N_0) and initial aggregation rate constant (k_{11}).

$$\left(\frac{\delta r_h(t)}{\delta t}\right)_{t\to 0} \propto k_{11} N_0 \qquad (2.10)$$

Here, *t* represents time. Holthoff et al. also defined a stability ratio (W), which is the ratio of fast or diffusion controlled coagulation rate (favorable condition) to the slow or reaction controlled coagulation rate (unfavorable condition). The parameter W is an indicator of colloidal stability. Several studies [50-53] have used this method to determine α_{pp}, which is the inverse of the stability ratio. In those studies particle-particle attachment efficiency was calculated by normalizing the aggregation rate constant at low IS (k_{unfav}) to the same at high IS (k_{fav}). Beyond a certain high IS the aggregation rate constant does not does not increase, and this IS represents the critical coagulation concentration.

2.2.3 Colloid transport with aggregation

Aggregation results in changes in particle size with time. The difference in particle retention in porous media due to changes in particle size may result in differences in solid phase deposition on the collector surface or may influence straining or detachment. The influence of aggregation on polyelectrolyte-modified NZVI deposition and transport in granular media has been only evaluate qualitatively [6, 7, 38]. The aggregate size determines the magnitude of the single collector efficiency (η_0), as well as the drag forces on deposited particles, which can contribute to particle detachment and de-aggregation. The effect of colloid aggregate size on transport in porous media has also been examined by Chatterjee et al. [17]. Injection of a polydisperse suspension of inert micron-sized particles in a packed sand column resulted in larger particles being deposited at shallower bed depths compared to the smaller particles. That deposition behavior was quantitatively explained by particle-size dependent deposition rate coefficients. Although these studies have demonstrated that changes in particle size resulting from aggregation influence transport, they have not quantitatively demonstrated the effect of aggregation kinetics or time-varying particle size distributions on nanoparticle transport behavior.

The role of deposition, particle aggregation, detachment and straining in the transport of surface-modified NZVI in model granular media has been investigated in the following chapters.

Literature Cited

[1] Kuhnen, F., K. Barmettler, S. Bhattacharjee, M. Elimelech and R. Kretzschmar, *Transport of Iron Oxide Colloids in Packed Quartz Sand Media: Monolayer and Multilayer Deposition.* Journal of Colloid and Interface Science, 2000. **231**: p. 10.

[2] Tufenkji, N. and M. Elimelech, *Breakdown of colloid filtration theory: Role of the secondary energy minimum and surface charge heterogeneities.* Langmuir, 2005. **21**(3): p. 841-852.

[3] Tufenkji, N., J.A. Redman and M. Elimelech, *Interpreting deposition patterns of microbial particles in laboratory-scale column experiments.* Environmental Science and Technology, 2003. **37**(3): p. 616-623.

[4] Tufenkji, N. and M. Elimelech, *Correlation Equation for Predicting Single-Collector Efficiency in Physicochemical Filtration in Saturated Porous Media.* Environmental science and technology, 2004. **38**(Compendex): p. 529-536.

[5] Fatisson, J., S. Ghoshal and N. Tufenkji, *Deposition of carboxymethylcellulose-coated zero-valent iron nanoparticles onto silica: Roles of solution chemistry and organic molecules.* Langmuir, 2010. **26**(Compendex): p. 12832-12840.

[6] Phenrat, T., H.-J. Kim, F. Fagerlund, T. Illangasekare, R.D. Tilton and G.V. Lowry, *Particle size distribution, concentration, and magnetic attraction affect transport of polymer-modified Fe0 nanoparticles in sand columns.* Environmental science and technology, 2009. **43**(13): p. 5079-5085.

[7] Raychoudhury, T., G. Naja and S. Ghoshal, *Assessment of transport of two polyelectrolyte-stabilized zero-valent iron nanoparticles in porous media.* Journal of Contaminant Hydrology, 2010. **118**(Compendex): p. 143-151.

[8] Petosa, A.R., D.P. Jaisi, I.R. Quevedo, M. Elimelech and N. Tufenkji, *Aggregation and deposition of engineered nanomaterials in aquatic environments: Role of physicochemical interactions.* Environmental science and technology, 2010. **44**(17): p. 6532-6549.

[9] Brown, D.G., *Adaptable method for estimation of parameters describing bacteria transport through porous media from column effluent data: Optimization based on data quality and quantity.* Colloids and Surfaces A: Physicochemical and Engineering Aspects, 2007. **296**(Compendex): p. 19-28.

[10] Bradford, S.A., H.N. Kim, B.Z. Haznedaroglu, S. Torkzaban and S.L. Walker, *Coupled factors influencing concentration-dependent colloid transport and retention in saturated porous media.* Environmental science and technology, 2009. **43**(Compendex): p. 6996-7002.

[11] Bradford, S.A., J. Simunek, M. Bettahar, M.T. Van Genuchten and S.R. Yates, *Modeling colloid attachment, straining, and exclusion in saturated porous media.* Environmental science and technology, 2003. **37**(Compendex): p. 2242-2250.

[12] Li, X., C.-L. Lin, J.D. Miller and W.P. Johnson, *Role of grain-to-grain contacts on profiles of retained colloids in porous media in the presence of*

an energy barrier to deposition. Environmental science and technology, 2006. **40**(Compendex): p. 3769-3774.

[13] Liu, D., P.R. Johnson and M. Elimelech, *Colloid deposition dynamics in flow through porous media: role of electrolyte concentration.* Environmental science and technology, 1995. **29**(12): p. 2963-2963.

[14] Redman, J.A., S.L. Walker and M. Elimelech, *Bacterial Adhesion and Transport in Porous Media: Role of the Secondary Energy Minimum.* Environmental science and technology, 2004. **38**(Compendex): p. 1777-1785.

[15] Bradford, S.A., S. Torkzaban and S.L. Walker, *Coupling of physical and chemical mechanisms of colloid straining in saturated porous media.* Water Research, 2007. **41**(Compendex): p. 3012-3024.

[16] Li, X., C.-L. Lin, I.D. Miller and W.P. Johnson, *Pore-scale observation of microsphere deposition at grain-to-grain contacts over assemblage-scale porous media domains using x-ray microtomography.* Environmental science and technology, 2006. **40**(Compendex): p. 3762-3768.

[17] Chatterjee, J. and S.K. Gupta, *An agglomeration-based model for colloid filtration.* Environmental Science and Technology, 2009. **43**(10): p. 3694-3699.

[18] Solovitch, N., J. Labille, J. Rose, P. Chaurand, D. Borschneck, M.R. Wiesner and J.-Y. Bottero, *Concurrent aggregation and deposition of TiO2 nanoparticles in a sandy porous media.* Environmental science and technology, 2010. **44**(Compendex): p. 4897-4902.

[19] Bradford, S.A. and M. Bettahar, *Concentration dependent transport of colloids in saturated porous media.* Journal of Contaminant Hydrology, 2006. **82**(Compendex): p. 99-117.

[20] Tong, M. and W.P. Johnson, *Excess colloid retention in porous media as a function of colloid size, fluid velocity, and grain angularity.* Environmental science and technology, 2006. **40**(Compendex): p. 7725-7731.

[21] Johnson, W.P., X. Li and S. Assemi, *Deposition and re-entrainment dynamics of microbes and non-biological colloids during non-perturbed transport in porous media in the presence of an energy barrier to deposition.* Advances in Water Resources, 2007. **30**(Compendex): p. 1432-1454.

[22] Xu, S., B. Gao and J.E. Saiers, *Straining of colloidal particles in saturated porous media.* Water Resources Research, 2006. **42**(Compendex).

[23] Johnson, W.P., E. Pazmino and H. Ma, *Direct observations of colloid retention in granular media in the presence of energy barriers, and implications for inferred mechanisms from indirect observations.* Water Research, 2010. **44**(Compendex): p. 1158-1169.

[24] Li, X., P. Zhang, C.L. Lin and W.P. Johnson, *Role of hydrodynamic drag on microsphere deposition and re-entrainment in porous media under unfavorable conditions.* Environmental science and technology, 2005. **39**(Compendex): p. 4012-4020.

[25] Li, Y., Y. Wang, K.D. Pennell and L.M.A. Briola, *Investigation of the transport and deposition of fullerene (C60) nanoparticles in quartz sands*

under varying flow conditions. Environmental Science and Technology, 2008. **42**(Compendex): p. 7174-7180.

[26] Torkzaban, S., S.A. Bradford and S.L. Walker, *Resolving the coupled effects of hydrodynamics and DLVO forces on colloid attachment in porous media.* Langmuir, 2007. **23**(19): p. 9652-9660.

[27] Bergendahl, J. and D. Grasso, *Prediction of colloid detachment in a model porous media: Hydrodynamics.* Chemical Engineering Science, 2000. **55**(Compendex): p. 1523-1532.

[28] Torkzaban, S., S.S. Tazehkand, S.L. Walker and S.A. Bradford, *Transport and fate of bacteria in porous media: Coupled effects of chemical conditions and pore space geometry.* Water Resources Research, 2008. **44**(Compendex).

[29] Bradford, S.A., S. Torkzaban and S.L. Walker, *Coupling of physical and chemical mechanisms of colloid straining in saturated porous media.* Water Research, 2007. **41**(13): p. 3012-3024.

[30] Quevedo, I.R. and N. Tufenkji, *Influence of solution chemistry on the deposition and detachment kinetics of a CdTe quantum dot examined using a quartz crystal microbalance.* Environmental science and technology, 2009. **43**(Compendex): p. 3176-3182.

[31] He, F., D. Zhao and C. Paul, *Field assessment of carboxymethyl cellulose stabilized iron nanoparticles for in situ destruction of chlorinated solvents in source zones.* Water Research, 2010. **44**(Compendex): p. 2360-2370.

[32] Tratnyek, P.G. and R.L. Johnson, *Nanotechnologies for environmental cleanup.* Nano Today, 2006. **1**(Compendex): p. 44-48.

[33] Saleh, N., H.-J. Kim, T. Phenrat, K. Matyjaszewski, R.D. Tilton and G.V. Lowry, *Ionic strength and composition affect the mobility of surface-modified fe0 nanoparticles in water-saturated sand columns.* Environmental science and technology, 2008. **42**(9): p. 3349-3355.

[34] He, F., M. Zhang, T. Qian and D. Zhao, *Transport of carboxymethyl cellulose stabilized iron nanoparticles in porous media: Column experiments and modeling.* Journal of Colloid and Interface Science, 2009. **334**(1): p. 96-102.

[35] Elliott, D.W. and W.-X. Zhang, *Field assessment of nanoscale bimetallic particles for groundwater treatment.* Environmental science and technology, 2001. **35**(Compendex): p. 4922-4926.

[36] Zhang, W.-x., *Nanoscale iron particles for environmental remediation: An overview.* Journal of Nanoparticle Research, 2003. **5**: p. 10.

[37] Bradford, S.A., J. Simunek and S.L. Walker, *Transport and straining of E. coli O157:H7 in saturated porous media.* Water Resources Research, 2006. **42**(Compendex).

[38] Phenrat, T., H.-J. Kim, F. Fagerlund, T. Illangasekare and G.V. Lowry, *Empirical correlations to estimate agglomerate size and deposition during injection of a polyelectrolyte-modified Fe0 nanoparticle at high particle concentration in saturated sand.* Journal of Contaminant Hydrology, 2010.

[39] Phenrat, T., N. Saleh, K. Sirk, R.D. Tilton and G.V. Lowry, *Aggregation and sedimentation of aqueous nanoscale zerovalent iron dispersions.* Environmental science and technology, 2007. **41**(1): p. 284-290.

[40] Saleh, N., K. Sirk, Y. Liu, T. Phenrat, B. Dufour, K. Matyjaszewski, R.D. Tilton and G.V. Lowry, *Surface modifications enhance nanoiron transport and NAPL targeting in saturated porous media.* Environmental Engineering Science, 2007. **24**(1): p. 45-57.

[41] Schrick, B., B.W. Hydutsky, J.L. Blough and T.E. Mallouk, *Delivery vehicles for zerovalent metal nanoparticles in soil and groundwater.* Chemistry of Materials, 2004. **16**(11): p. 2187-2193.

[42] Lim, J.K., S.A. Majetich and R.D. Tilton, *Stabilization of superparamagnetic iron oxide core-gold shell nanoparticles in high ionic strength media.* Langmuir, 2009. **25**(23): p. 13384-13393.

[43] Phenrat, T., N. Saleh, K. Sirk, H.J. Kim, R.D. Tilton and G.V. Lowry, *Stabilization of aqueous nanoscale zerovalent iron dispersions by anionic polyelectrolytes: adsorbed anionic polyelectrolyte layer properties and their effect on aggregation and sedimentation.* J. Nanopart. Res., 2008. **10**(5): p. 795-814.

[44] Fritz, G., V. Schadler, N. Willenbacher and N.J. Wagner, *Electrosteric stabilization of colloidal dispersions.* Langmuir, 2002. **18**(Compendex): p. 6381-6390.

[45] Lee, D.G., J.S. Bonner, L.S. Garton, A.N.S. Ernest and R.L. Autenrieth, *Modeling coagulation kinetics incorporating fractal theories: Comparison with observed data.* Water Research, 2002. **36**(Compendex): p. 1056-1066.

[46] Lee, D.G., J.S. Bonner, L.S. Garton, A.N.S. Ernest and R.L. Autenrieth, *Modeling coagulation kinetics incorporating fractal theories: A fractal rectilinear approach.* Water Research, 2000. **34**(7): p. 1987-2000.

[47] Lin, M.Y., H.M. Lindsay, C.R. Weitz, R. Klein and P. Meakin, *Universality in colloid aggregation.* Nature, 1989. **339**: p. 3.

[48] Trinh, L.T.T., A.-L. Kjniksen, K. Zhu, K.D. Knudsen, S. Volden, W.R. Glomm and B. Nystrom, *Slow salt-induced aggregation of citrate-covered silver particles in aqueous solutions of cellulose derivatives.* Colloid and Polymer Science, 2009. **287**(12): p. 1391-1404.

[49] Holthoff, H., A. Schmitt, A. Fernandez-Barbero, M. Borkovec, M.A. Cabrerizo-Vilchez, P. Schurtenberger and R. Hidalgo-Alvarez, *Measurement of absolute coagulation rate constants for colloidal particles: Comparison of single and multiparticle light scattering techniques.* Journal of Colloid and Interface Science, 1997. **192**(Compendex): p. 463-463.

[50] Chen, K.L. and M. Elimelech, *Influence of humic acid on the aggregation kinetics of fullerene (C60) nanoparticles in monovalent and divalent electrolyte solutions.* Journal of Colloid and Interface Science, 2007. **309**(Compendex): p. 126-134.

[51] Chen, K.L. and M. Elimelech, *Interaction of fullerene (C60) nanoparticles with humic acid and alginate coated silica surfaces: Measurements, mechanisms, and environmental implications.* Environmental science and technology, 2008. **42**(Compendex): p. 7607-7614.

[52] Saleh, N.B., L.D. Pfefferle and M. Elimelech, *Aggregation kinetics of multiwalled carbon nanotubes in aquatic systems: Measurements and*

environmental implications. Environmental science and technology, 2008. **42**(21): p. 7963-7969.

[53] Saleh, N.B., L.D. Pfefferle and M. Elimelech, *Influence of biomacromolecules and humic acid on the aggregation kinetics of single-walled carbon nanotubes.* Environmental science and technology, 2010. **44**(7): p. 2412-2418.

Chapter 3

Assessment of Transport of Two Polyelectrolyte-Stabilized Zerovalent Iron Nanoparticles in Porous Media

Trishikhi Raychoudhury[1]**, Ghinwa Naja**[1,2] **and Subhasis Ghoshal**[1]

[1] *Department of Civil Engineering, McGill University, Montreal,*
Canada H3A 2K6

[2] *Everglades Foundation, Science Department, Miami, Florida 33157*

Published in

Journal of Contaminated Hydrology

3.1 Introduction

Due to their large surface area and reactivity, nanoparticles of zero-valent iron (NZVI) have recently been examined for several environmental remediation applications. NZVI are strongly reactive reducing agents capable of rapid degradation of chlorinated organic compounds, pesticides, nitramines and organic dyes and are also effective in elimination of heavy metals and inorganic anions [1-3]. Although the reactivity of NZVI towards several pollutants is well established, the large scale application of such remediation processes is hindered by a thorough lack of knowledge of transport of NZVI in porous media.

Several studies have reported that NZVI aggregate extensively and rapidly as a result of attractive magnetic and van der Waals forces, and the size and/or surface charge of these aggregates result in very high deposition on porous media grains which severely limits its transport in porous media [4, 5]. Surface modification of NZVI by polyelectrolytes, polymers and surfactants, which provide steric and electrostatic stabilization against the particle-particle attractive forces, significantly improves its transport in porous media [4, 6-8]. Groundwater ionic strength and composition may however influence the extent of particle-particle and particle-collector electrostatic interactions and influence transport [9, 10]. Sedimentation tests, which allow qualitative assessments of the degree of colloidal stabilization, indicate improvement in aggregation and stability for polymer-stabilized NZVI particles [8, 11]. The extent of colloidal stabilization of surface-modified NZVI correlates to the adsorbed polyelectrolyte mass and electrostatic charge and the thickness of the adsorbed polyelectrolyte layers [8, 12].

Phenrat et al. [13] demonstrated the effect of particle concentration of polystyrene sulfonate (PSS)-stabilized NZVI particles on transport in porous media. The particles employed in that study were predominantly 325 nm in diameter, as measured by dynamic light scattering (DLS) and PSS-NZVI at concentrations of 1-6 g•L^{-1} showed greater deposition in packed columns compared to concentrations of 30 mg•L^{-1} and this was attributed to the formation of large aggregates at g•L^{-1} concentrations.

Several studies have experimentally evaluated the effect of flow velocity on surface modified-NZVI transport. However, these studies have been conducted over a limited range of flow velocities. He et al. [14] found that transport of 12 nm diameter CMC-NZVI at flow velocities in the range of 1.1 to 4.2 cm•min^{-1} showed a slight change (about 10%) in effluent concentrations with flow velocity.

The objective of this study was to compare the transport of NZVI stabilized with two polyelectrolytes, CMC and PAA, which have been shown to be effective for stabilization of NZVI in various studies [4, 14, 15], at different flow velocities and particle concentrations. The effects of flow velocity and particle concentration on the breakthrough curves (BTC) of the CMC-NZVI and PAA-NZVI samples in packed columns were assessed. The particle concentrations were varied from 0.1 g•L^{-1} to 3 g•L^{-1}, with the highest concentration being representative of field applications [11]. The effects of particle concentrations on transport of CMC- and PAA-NZVI have not been reported to date. Darcy velocities were varied from 0.02 cm•min^{-1} to 1 cm•min^{-1} and this is representative of a range of velocities representing natural groundwater flow to flow under injection conditions. The role of particle surface potential, particle size, and aggregation kinetics as determined qualitatively through sedimentation tests and quantitatively by a Nanoparticle Tracking Analyzer (NTA) on BTC patterns have been investigated. Aggregation was accounted for, because CMC- and PAA-NZVI would aggregate while in suspension in the column feed reservoir as well as during transport in porous media.

3.2 Materials and methods

3.2.1 Chemicals.

All chemicals were reagent grade and all solutions were prepared using Milli-Q-UV Plus Ultrapure water system (>18MΩ, Millipore, MA, USA).

Sodium borohydride (≥98.5%) and sodium hydroxyl (>98%) were purchased from Sigma. Polyacrylic acid (M.W. 1.8 kg•mole^{-1}) was obtained from Aldrich while sodium carboxymethyl cellulose, (M.W. 90 kg•mole^{-1}) and the methanol (HPLC grade) were procured from Sigma-Aldrich. Ferrous sulfate heptahydrate (99%) and concentrated nitric acid (99%) were obtained from Anachemia. Concentrated hydrochloric acid was purchased from Fisher. Silica sand (Unimin corp., WI, USA), with an average diameter of 375 µm, was used as a model porous media.and The sand grains were 21.6% by weight in the size range of 212µm-300µm, 50.7% in the size range of 300µm-425µm and the remaining in the size range of 425µm-600µm), Prior to use, the sand was acid washed with concentrated hydrochloric acid to remove the background iron oxide, rinsed with water (final pH around 6.5) and dried in an oven over night at 550ºC to remove background organic matter. The oven-dried sands were stored in a sealed bottle prior to use.

3.2.2 Zero-valent iron nanoparticles synthesis and characterization.

Zero-valent iron nanoparticles (NZVI), CMC- and PAA- were prepared according to the methods described elsewhere [4, 16]. The NZVI were prepared by reducing an aqueous ferrous iron solution by sodium borohydride under a nitrogen atmosphere. To prepare CMC-and PAA-NZVI, first a polyelectrolyte suspension was prepared in degassed-DI water and refrigerated for 24 hours. Thereafter, dissolved $FeSO_4.(7H_2O)$ was added and mixed into polyelectrolyte suspension for 30 minutes to enable the formation of dissolved Fe-polyelectrolyte complexes. The Fe^{2+} ions were then reduced by adding sodium borohydride solution dropwise into the mixture. The ratio of BH_4^-/Fe^{2+} was 2.0. Once the NZVI was formed, the prepared solution was dried and stored under nitrogen.

For transmission electron microscopy (TEM) measurements samples of 0.2 g•L^{-1} suspensions were prepared in a N_2 atmosphere in degassed 1 mM $NaHCO_3$ (Sigma-Aldrich) and sonicated by a 40kHz ultrasonicator (Cole-

Palmer 8891) for 10 min. A 0.1 mL of the suspension was deposited on a carbon coated copper grid under nitrogen and dried in vacuum. Particles were imaged by a Philips CM200 TEM instrument, operated at 200 kV. The mean particle diameter (d_p) were estimated by measuring the diameters of 200 particles using the General Image Manipulating Program (GIMP software, GNU). For measuring each particle diameter, first the number of pixels were counted for the longest length of each particle and then converted to nanometers, using the scale bar.

Zeta potential was also measured for the different particle suspensions using Laser Doppler velocimetery (ZetaSizer Nano, Malvern). Stock solutions of 0.2 $g\bullet L^{-1}$ NZVI in 1mM $NaHCO_3$ were diluted to 0.1 $g\bullet L^{-1}$ to obtain consistent measurements. The pH of the suspension was determined to be 7.4±0.4) under a nitrogen atmosphere. Fourier Transform Infrared Spectroscopy (FTIR) analyses indicated that the CMC and PAA was covalently bonded to the NZVI surface, and X-ray Photoelectron Spectroscopy (XPS) analyses confirmed the presence of zerovalent iron in the particles. These analyses and data interpretation were similar to those reported by He et al. and Sun et al. [17, 18]. Particle sizes (d_p^*) over time for CMC- and PAA-NZVI in solution were also determined by nanoparticle tracking analysis (NanoSight, NTA 2.0 LM20) with a laser output of 30mW at 650 nm, to evaluate aggregation behavior. NTA measures the particle diameter based on the diffusion coefficient which in this technique is estimated by tracking the mean square displacements of single particles (from light scattering) and analyzed by NanoSight software [19]. For measurement, a concentrated stock suspension of 0.2 $g\bullet L^{-1}$ CMC- or PAA-NZVI, prepared in 1 mM $NaHCO_3$ suspension, was filled in a vial under a N_2 atmosphere. The NZVI suspensions were gently mixed and withdrawn at various time points from vials and diluted to 2 $mg\bullet L^{-1}$ for NTA measurements.

3.2.3 Sedimentation tests.

The colloidal stability of bare, CMC- and PAA-NZVI suspensions was determined by measuring the sedimentation rate of nanoparticle suspensions maintained under a N_2 headspace. The absorbance at a wavelength of 508 nm of the 0.2g•L^{-1} suspensions maintained under quiescent conditions in vials was monitored over 3 h using a spectrophotometer.

3.2.4 Column experiments.

Columns (Chromaflex, Fisher, 2.5cm i.d., and adjustable length) were packed with sand and gently vibrated at several stages to ensure uniform packing. The sand packed column was then connected to a syringe pump (KD Scientific, MA, USA). The sand packed column was first saturated with CO_2 then flushed with de-aired water for 7 pore volumes (PV) to remove the air bubbles. Tracer KNO_3 (Sigma-Aldrich) was injected from the top of the column with three different Darcy velocities of 0.02 cm•min^{-1}, 0.2 cm•min^{-1} or 1 cm•min^{-1} and the value of longitudinal dispersivity (α_x) was evaluated as 2 x10^{-3} m. The porosity of the sand packed media was determined as 0.3 (Table 3.1).

The column feeding solution containing CMC- or PAA-NZVI at several concentrations (0.1 g•L^{-1}, 0.5 g•L^{-1} or 3 g•L^{-1}) was pumped downwards through the column at a velocity of 0.2cm•min^{-1}. Additional experiments were carried out with NZVI suspensions of 0.5 g•L^{-1} where the flow velocity was 0.02cm•min^{-1}, 0.2cm•min^{-1} or 1cm•min^{-1}. CMC- and PAA-NZVI suspensions were diluted to the desired concentrations using de-aired, de-ionized water. The syringe containing the nanoparticles was continuously but moderately mixed by shaking the reservoir at 400 rpm to prevent the settlement of the particles. The inlet total Fe concentration of the suspension was monitored with time to verify a constant C_0 during the step input (Supplementary Data section, Figure 3.S1). The residence time of the particle within the syringe (reservoir) varied from 45-450 min, depending on the flow rate; and the aggregation of the NZVI occurred during that time within the influent reservoir. The average

NZVI residence time in the reservoir was at least 6 times greater than the residence time in the column. During the nanoparticle suspension injection (4 PV), the iron concentration at the outlet was monitored. Nanoparticle concentrations in the column effluent sample were determined by measuring the concentration of total iron. Total Fe was determined by dissolving the samples in concentrated HCl (1:2 v/v ratio) and 1% HNO_3 overnight and analyzed using flame atomic absorption spectrometry (AAS, Perkin Elmer 3110) at 249.7 nm wavelength. The detection limit of the AAS for Fe was 0.01 mg•L^{-1} and all effluent samples had concentrations above the detection limit.

Table 3.1: Experimental conditions and different parameters for column experiment

Column length, L	4.5 or 9 cm
NZVI concentration in column feed, C_0	0.1, 0.5 or 3 gL^{-1}
Darcy velocity v	0.02, 0.2 or 1 cm min^{-1}
Bulk density of sand in the column, ρ_b	1.95 g cm^{-3}
Porosity, ε	0.3
Median diameter of the sand particles, d_{50}	375 µm
Longitudinal dispersivity	2 $x10^{-3}$ m
pH of suspension	7.4±0.4
Ionic strength	Distilled water, 0.1, 1mM $NaHCO_3$

3.3 Results and Discussion

3.3.1 Nanoparticle characterization.

Particle sizes of bare NZVI, CMC-NZVI and PAA-NZVI obtained from TEM image analysis are listed in Table 3.2. The average particle sizes were determined by measuring the diameter of 200 particles. CMC-NZVI had an average particle diameter (d_p) of 5.7±0.9 nm and was relatively homogeneous in size, well dispersed and its appearance was similar to the smaller sub-population of PAA as shown in the TEM images (Figure 3.1a). Using a similar synthesis procedure, He et al. [12], reported that CMC-NZVI of mean diameter of 4.3 nm were obtained. PAA-NZVI were found to have a bimodal particle size distribution with mean particle diameters of 4.6 ± 0.8 nm and 30 ± 21 nm as shown in Figure 3.1a and 3.1b. The 30 nm PAA-NZVI particles comprised approximately 1% by number and 20% by mass of the suspension. The occurrence of multimodal particle size distributions during synthesis is influenced by polymer characteristics such as molecular weight, surface potential, and thickness of polymer layer [20]. NZVI particle sizes are also dependent on the synthesis procedure. Although certain steps in sample preparation for TEM, such as drying of the NZVI suspension on the TEM grid may lead to artifacts that enhance NZVI aggregation, individual particles are still distinguishable in the images and thus nominal particle sizes can be determined [19]. Measurements of particle zeta potential indicated that all three types of iron nanoparticles were negatively charged as shown in Table 3.2.

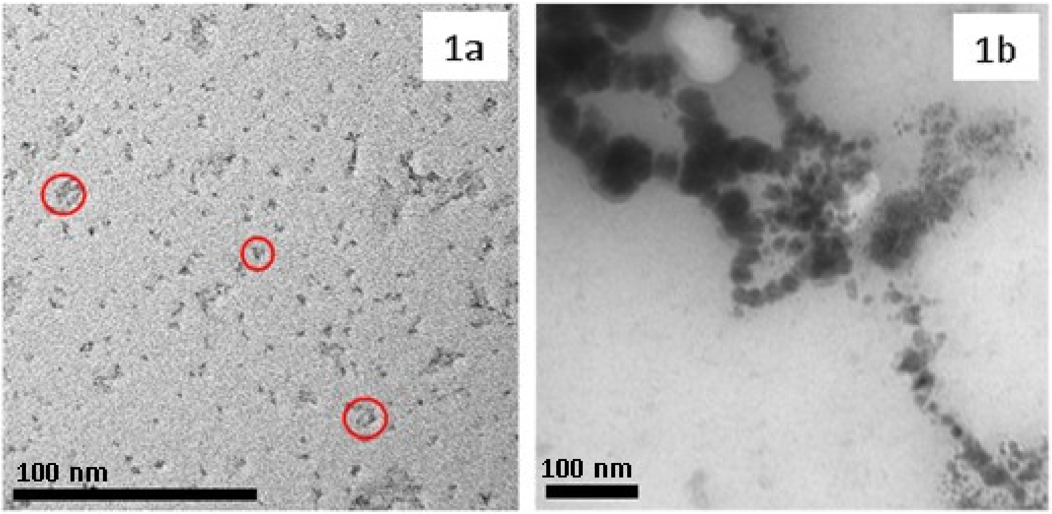

FIGURE 3.1: TEM images of PAA-NZVI: (a) smaller (3-15 nm) particle sub-population (typical particles indicated by circles). (b) larger (25-100 nm) particle sub-population.

Table 3.2. Characteristic of different types of NZVI

Particles	d_p (nm)	Zeta potential (mV)	Polyelectrolyte molecular weight (kg/mol)
Bare-NZVI	54.6±6.2	-1.45±1.11	-
CMC-NZVI	5.7±0.9	-45.8±0.99	90
PAA-NZVI	4.6±0.8, 30±21	-31.6±1.72	1.8

3.3.2 Assessment of NZVI aggregation and colloidal stability:

To compare the colloidal stability of the different nanoparticles, sedimentation tests were performed at a particle concentration of $0.2g•L^{-1}$. In vials containing a suspension of bare NZVI, the absorbance at 508 nm was reduced by almost 90% (Figure 3.2) of the initial absorbance in 3 h under quiescent conditions. Much of this change in absorbance is attributable to the rapid settling of colloidally unstable bare NZVI. In comparison, for PAA-NZVI and CMC-NZVI only about 40% and 50%, respectively, of the initial absorbance was reduced over 3 h. Similar results have been reported by Phenrat et al. and Saleh et al. [8, 11] for various polymer stabilized NZVI. The change in absorbance in these systems is attributable to aggregation of the particles, which leads to fewer but larger particles and this alters light transmittance through the suspension. However, some particles were observed to settle in the vials under quiescent conditions. Nanoparticles with diameters in the range of tens of nanometers cannot be accounted for by gravity settling of discrete particles, and it is likely that the settling of a fraction of the CMC- and PAA-NZVI is facilitated by the formation of the bridging of several polyelectrolyte covered discrete particles by the free polyelectrolytes in solution [21].

Bare NZVI aggregated and settled out of the supernatant rapidly because its larger size contributes to higher magnetic and van der Waals attractive forces between particles and it has low surface charge (-1.45 ± 1.11 mV) that does not provide significant electrostatic stabilization [9]. The CMC-NZVI were more stable in solution than PAA-NZVI. PAA-NZVI had a higher rate of absorbance change during the first 60 minutes of the sedimentation tests, and this is significant in the context of the transport experiments discussed later, as the maximum residence time of NZVI in the column feed reservoir and during column flow was within this time period for the majority of the transport experiments.

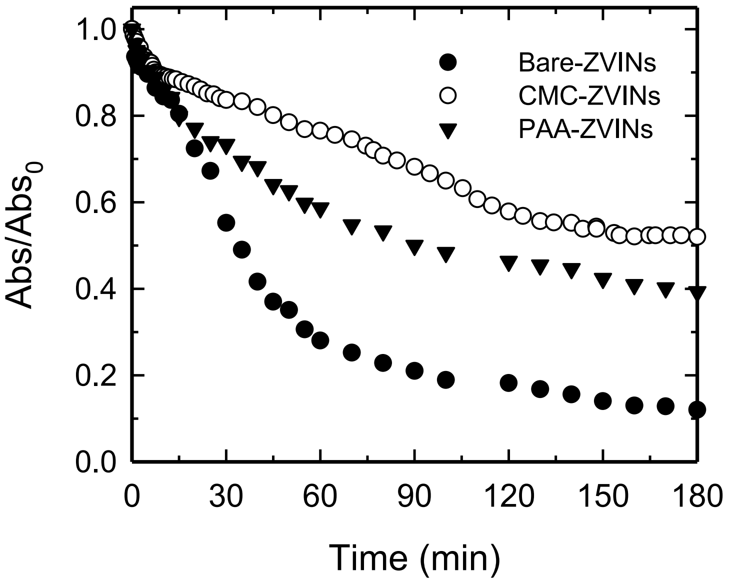

FIGURE 3.2: Changes in relative absorbance over time in sedimentation tests with different NZVI at a suspension concentration of 0.2 gL^{-1}

The extended particle-particle DLVO (XDLVO) interaction energy calculations that account for magnetic, steric, van der Waals and electrostatic interaction were performed according to the framework presented by Lim et al. [22] and Phenrat et al. [8]. For calculating the total interaction energy (V_{tot}), the magnetic, electrostatic and van der Waals interaction energies were determined from equations and parameters given in Phenrat et al. [8]; and the steric interaction energy was calculated according to Lim et al. [22]. For CMC- and PAA- NZVI a polyelectrolyte layer thickness of 7 nm was assumed, which is in the range of CMC layer thickness estimated by various studies [8, 10]. The results of these calculations are presented in Figure 3.3a, and suggest that 4.6 nm PAA-NZVI have slightly higher particle-particle attraction than similar-sized CMC-NZVI, for a 7 nm polyelectrolyte layer thickness. The XDLVO calculations shown in Figure 3.3b demonstrates that with increasing particle size the secondary energy minimum becomes more negative, which would result in more aggregation for the larger diameter (~30 nm) PAA-NZVI population. The more negative values of the secondary energy minimum with increasing particle size is attributable primarily to the increasing magnetic attraction. The XDLVO calculations thus qualitatively support the observation of lower colloidal stability of the PAA-NZVI compared to the CMC-NZVI.

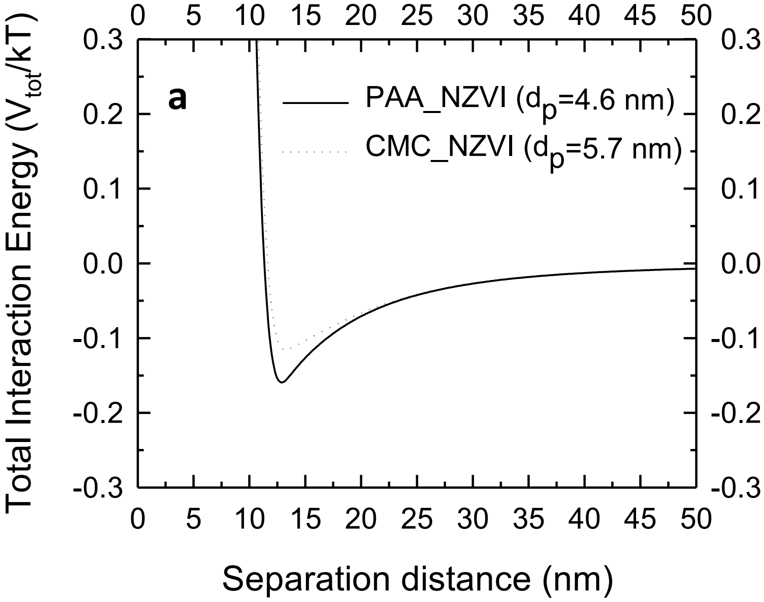

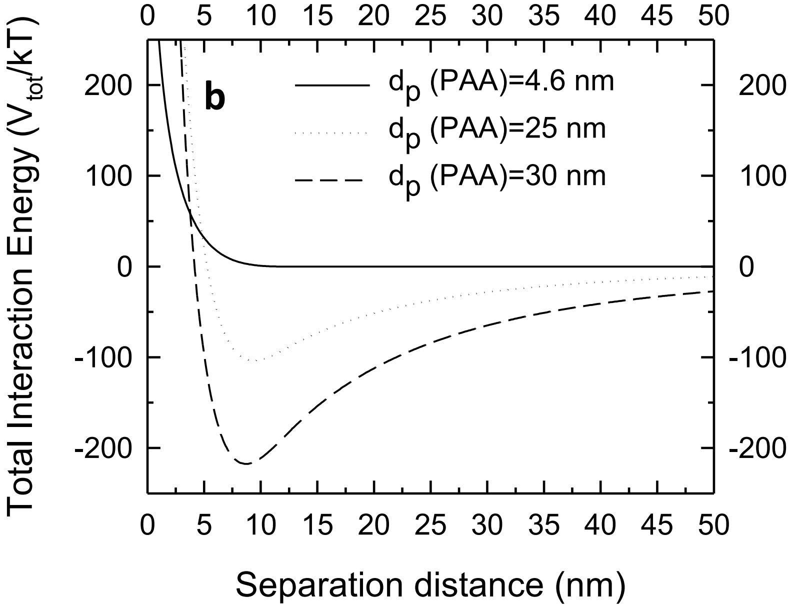

FIGURE 3.3: Particle-particle DLVO interaction with steric effect for (a) CMC-NZVI and PAA-NZVI of 5nm size and (b) for different size of PAA-NZVI

The change in particle size over time for CMC-NZVI was assessed by NTA and the results are presented in Figure 3.4. The over all size of particles, measured by NTA was higher than those determined from TEM image analyses. This is because NTA evaluates hydrodynamic diameters based on upon light scattering and bigger particles scatter significantly more light, resulting in the average particle size (d_p^*) being biased towards presence of large particles. Assuming this bias to be approximately constant over time, we observed a 7 nm increase in average particle size over a time period of 60 min (Figure 3.4). This increase in particle size indicates the extent of aggregation for CMC-NZVI. Reproducible particle sizes over time for PAA-NZVI were not obtained from NTA, because PAA-NZVI was less refractive, and was rapidly oxidized at the dilution required for the NTA analyses, and thus those results are not presented. However, based on the sedimentation test results it appears that there was more rapid and extensive aggregation.

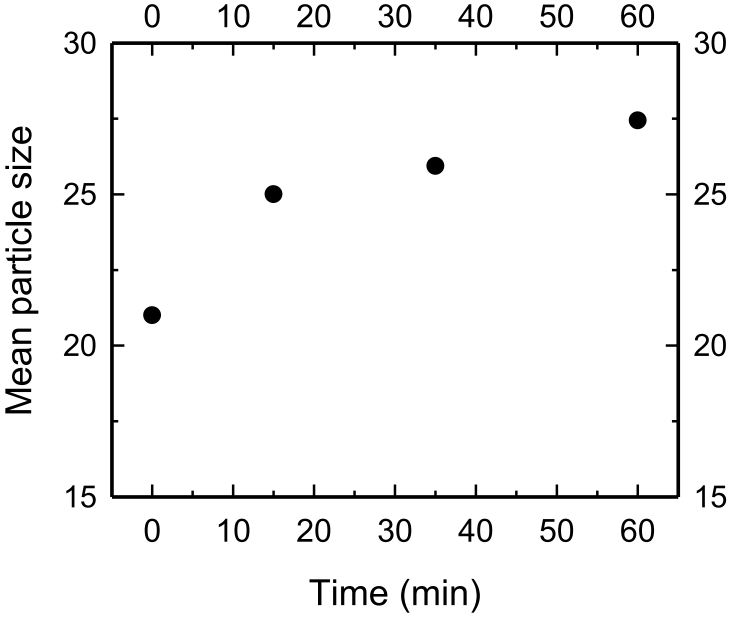

FIGURE 3.4: Changes in average particle diameter with time as determined by NTA of CMC-NZVI of particle suspension concentration of 0.2gL^{-1}.

3.3.3 Column Transport of CMC- and PAA-NZVI.

The transport of CMC-NZVI and PAA-NZVI in sand was studied in packed columns with different influent nanoparticle concentrations, C_0, average pore water velocities, v, and column length, L, as stated in Table 3.1. Column-transport experiments with bare NZVI with 0.5 g•L^{-1} concentration and 0.2 cm•min^{-1} Darcy velocity resulted in negligible transport of bare-NZVI with less than 1% effluent iron concentration.

3.3.3.1 Effect of flow velocity on nanoiron transport.

At a nanoparticle suspension mass concentration of 0.5 g•L^{-1}, nanoparticle elution from the column was dependant on the average pore velocity (Figure 3.5). At the slowest velocity of 0.02 cm•min^{-1}, representative of typical groundwater velocities, CMC-NZVI effluent concentrations reached a maximum relative concentration of nearly 0.8 (Figure 3.5a). At higher average pore water velocities of 0.2 and 1.0 cm•min^{-1} complete breakthrough was achieved, with effluent concentrations reaching influent concentrations. The above results suggest that there is greater CMC-NZVI deposition at low pore water velocities.

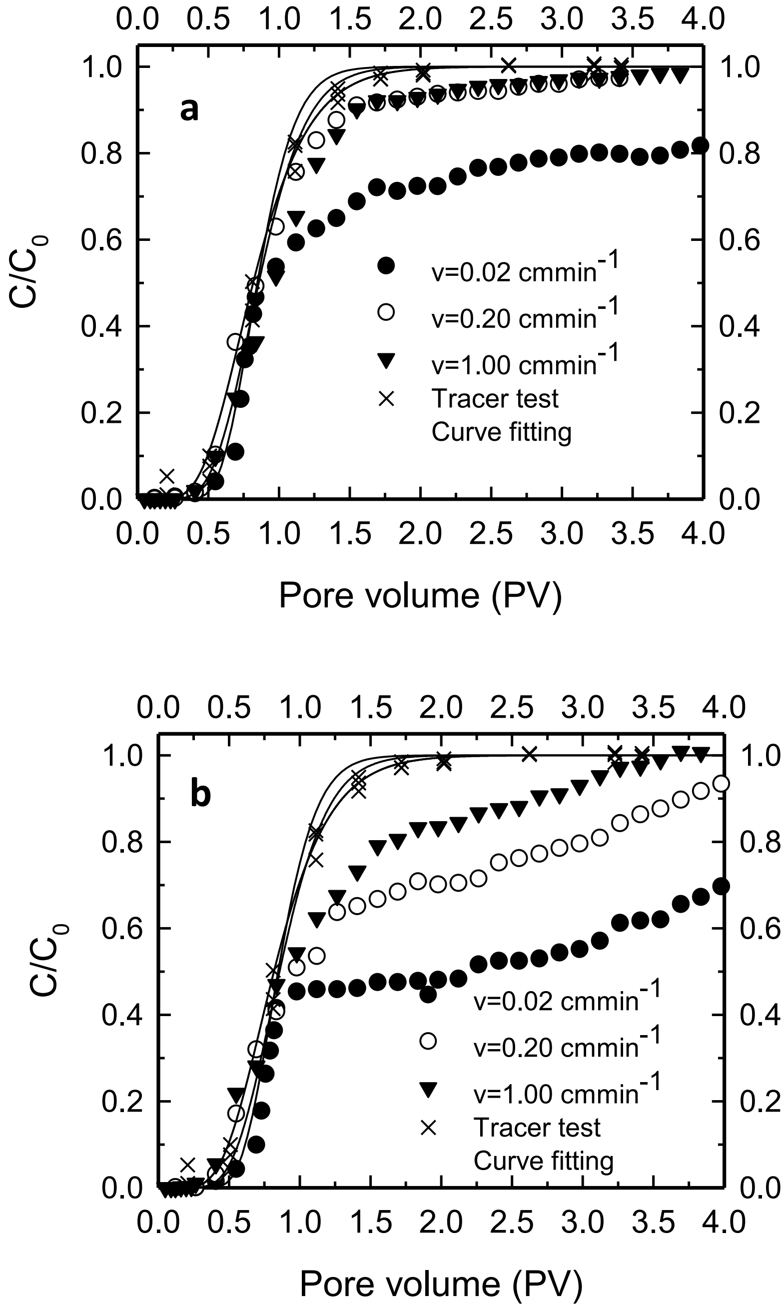

FIGURE 3.5: Experimental breakthrough curves for varying pore water velocities in packed sand columns of L =4.5 cm, C_0 = 0.5 gL^{-1}. **(a)** CMC-NZVI **(b)** PAA-NZVI

He et al. [14] also observed an increase in elution concentrations of CMC-NZVI when flow velocities were increased from 1.2 to 4.2 cm•min^{-1}. The lower retention of colloid particles at high velocities can be attributed to smaller volumes of stagnation zones and higher drag forces on attached particles which lead to greater elution [23]. Several studies have also attributed lower deposition at higher flow velocities to blocking, the reduction in particle attachment after monolayer surface coverage of collectors [24, 25] However, as discussed in the following section, blocking does not appear to be relevant for the CMC- and PAA-NZVI systems.

For PAA-NZVI the same patterns were observed with changing velocity, i.e., at the lowest velocity significantly more particle deposition occurred (Figure 3.5b). In contrast with the CMC-NZVI breakthrough curves presented in Figure 3.5a, the PAA-NZVI breakthrough curves in Figure 3.5b show a more gradual increase in effluent concentrations, especially after 1 PV. Furthermore, PAA-NZVI showed greater over all deposition than CMC-NZVI at a given PV. The XDLVO energy profiles between the sand collector surface and the PAA NZVI particles for the two major population sizes are shown in Figure 3.6a. The XDLVO energy profiles account for attractive van der Waals forces and repulsive electrostatic and steric forces between the surface modified-NZVI particles and the sand collector surface and were calculated according to procedures described in Fatisson et al. [10]. The XDLVO profile suggest bigger particles have a more negative secondary minimum and this is due to the higher van der Waals attraction with the collector surfaces. . The greater deposition of PAA-NZVI compared to CMC-NZVI is attributable primarily to the existence of the sub-population of larger particles. Although PAA-NZVI has a less negative zeta potential than CMC-NZVI, the difference in electrostatic repulsion with the collector surface for the 5 nm diameter particles, was relatively negligible, as shown in Figure 3.6a.

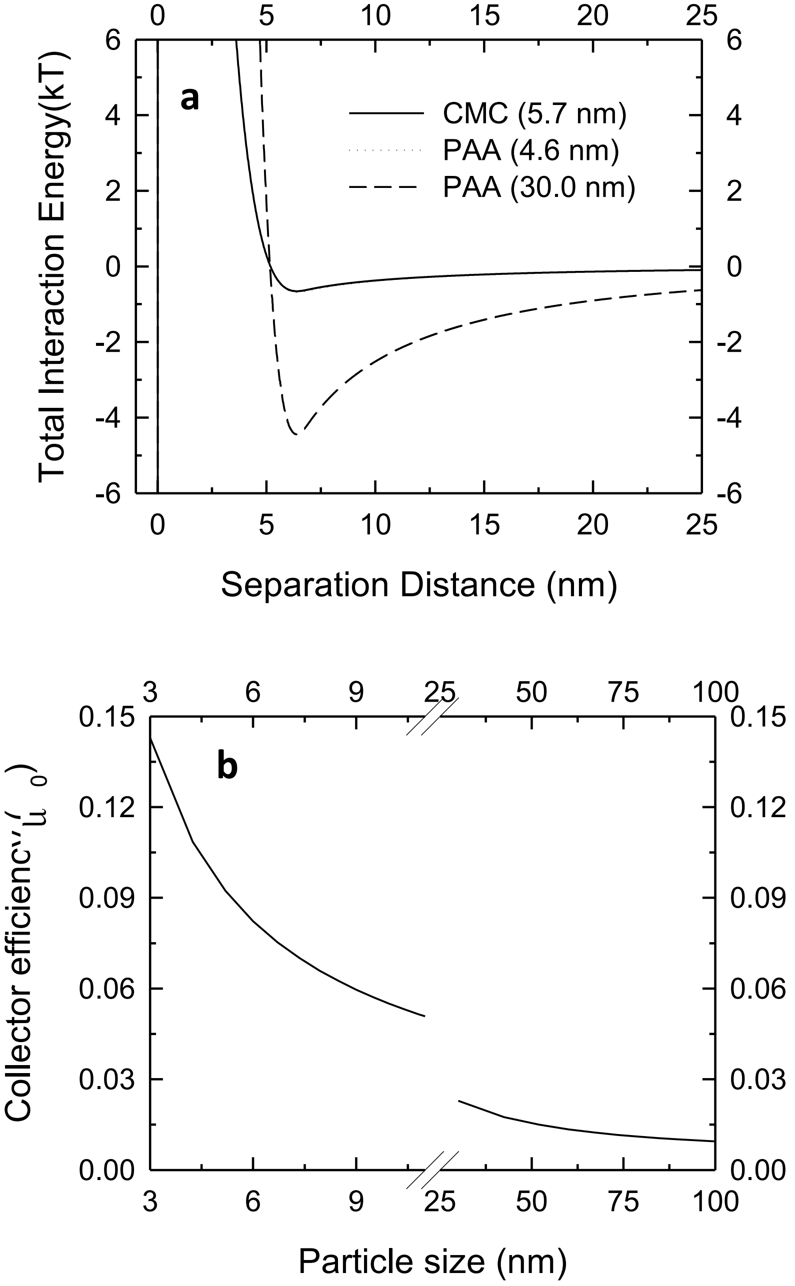

FIGURE 3.6: (a) XDLVO total interaction energies between sand collector surface and PAA-NZVI (4.6 nm, 25 nm and 50 nm diameter) and CMC-NZVI (5.7 nm diameter). The plots for PAA-NZVI (4.6 nm) and CMC-NZVI (5.7 nm) overlap (b) Change in single collector efficiency (η_0) with particle size.

The gradual increase in slope of the effluent concentrations for PAA-NZVI, compared to CMC-NZVI at all pore water velocities, can be attributed to the more rapidly decreasing single collector efficiency (η_0) over time for

PAA-NZVI. The less negative zeta potential of PAA, and the lower molecular weight of PAA will contribute to lower electrosteric repulsion between PAA-NZVI particles, and this would lead to more rapid aggregation kinetics for PAA-NZVI [8] as shown in Figure 3 3. The η_0 decreases with particle size as shown in Figure 3 6b, where the η_0 for nanoparticles ranging from 3 to 15 nm and from 25 to 100 nm are calculated by the T&E equation [26]. A decrease in η_0 causes a proportional decrease in the deposition rate constant, k_{att}, according to the clean-bed colloid filtration theory, as shown in Equation 3.1:

$$k_{att} = \left[\frac{3(1-\varepsilon)v}{2d_c\varepsilon} \alpha_{pc} \right] \eta_0 \tag{3.1}$$

Where, k_{att} is the particle deposition rate coefficient, v is the interstitial particle velocity, α_{pc} is the attachment efficiency, ε is porosity, d_{c} is the average grain (collector) size and η_0 is the single collector efficiency. The clean-bed colloid filtration theory is based on steady state effluent concentrations, which is not observed in our case. However, the clean-bed colloid filtration theory may be extended to our results by considering the BTCs obtained in our experiements as a combination of multiple effluent concentration curves, each curve relating to a certain particle size for a limited duration of the experiment. This has been demonstrated in Figure 3.7. The calculated BTC in Figure 3.7 are derived from values of η_0 in Figure 3.6b, and colloid-particle attachment efficiency (α_{pc}) ranging from 0.002 and 0.30, depending on the particle/aggregate size. He et al. [14], reported an α_{pc} of 0.0019 for 11.7 nm CMC-NZVI particles and Phenrat et al. [13] reported α_{pc} in the range of 0.30-0.32 for 63 nm PSS-NZVI particles, at NZVI concentrations comparable to our study. Larger values of α_{pc} for larger particle/aggregate sizes is supported by the XDLVO energy profiles presented in Figure 3.6a, which show more negative secondary minimum for larger particle sizes. Thus for a given attachment efficiency, a gradual decrease in the deposition rate coefficient over time with aggregation, results in an increasing trend for effluent concentrations.

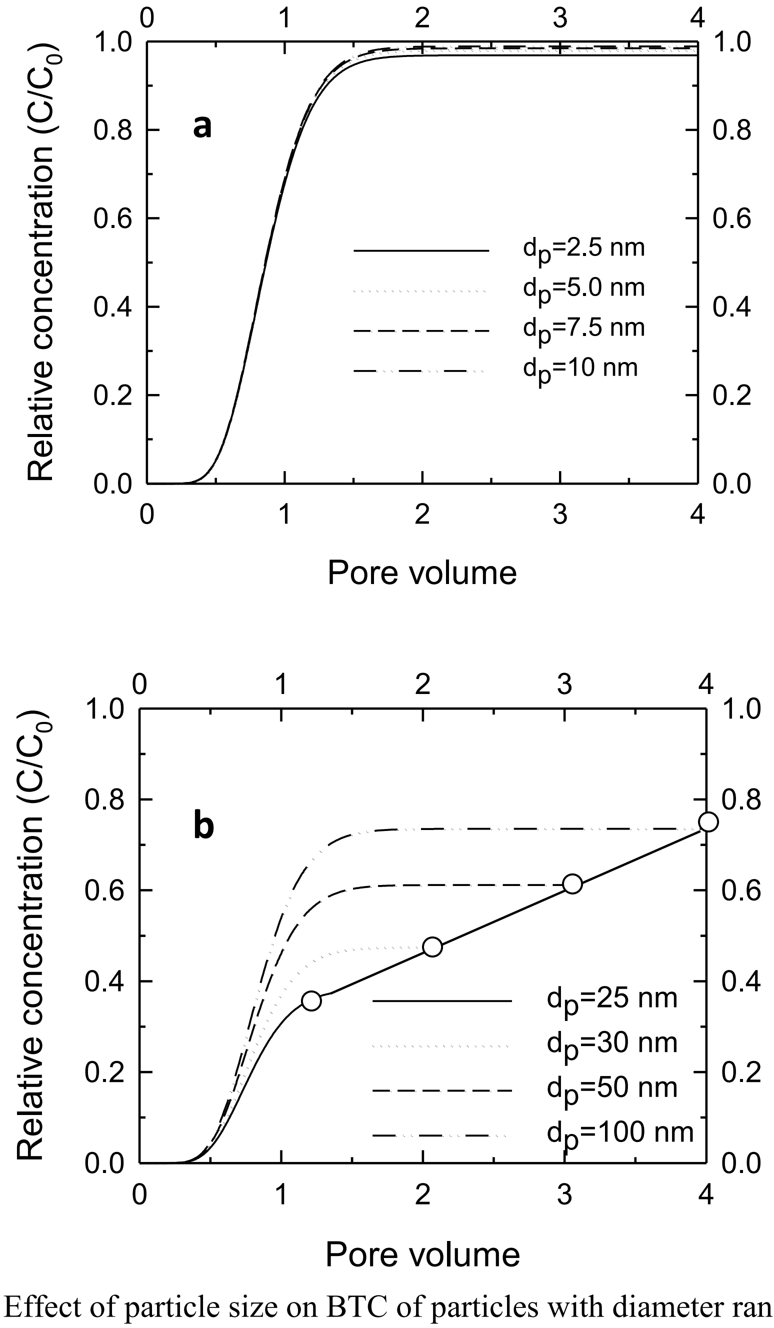

FIGURE 3.7: Effect of particle size on BTC of particles with diameter ranging between (a) 2.5-10nm and (b) 25-100nm. Each BTC corresponds to a fixed particle size, except in (b) the line connecting the circles has been drawn to illustrate the approximate BTC for particles that aggregate from 25 nm at 1 PV to 100 nm at 4 PV.

3.3.3.2 Effect of nanoparticle concentration on transport.

At a constant *v*, influent particle concentration influenced the transport of the CMC- and PAA-NZVI particles (Figure 3.8). At the lowest concentration of (0.1 g•L^{-1}), CMC-NZVI effluent concentrations after 2 PV were approximately equal to the influent concentrations. At a higher iron concentration, effluent concentrations were comparable to the influent concentrations only after 4 PV.

Clean bed colloid filtration theory suggests that changes in particle concentrations should have no effect on particle transport [27]. Processes such as blocking, ripening (the increased particle deposition resulting from attractions between deposited and suspended particles), and straining (the trapping of particles smaller than the pore sizes through which flow occurs) do however result in transport behavior that is particle concentration dependent. None of these processes appear to be strictly relevant to the CMC- and PAA-NZVI systems. With blocking, higher concentrations result in lower deposition and deposition rate constants (and thus steeper effluent curves) and higher relative effluent concentrations are observed [28, 29]. The breakthrough curves observed here show increasing deposition and deposition rates with higher concentrations and are thus inconsistent with blocking effects. Furthermore, the surface coverage is estimated to be negligible (less than 0.001%) for both CMC- and PAA-NZVI. Given that this is far less than monolayer coverage, blocking is not relevant in these experiments. Straining also leads to higher effluent concentrations with increases in particle concentration [30, 31] because the smaller pores that contribute to straining are more quickly filled up with particles at higher concentrations, leading to reductions in cross-sectional areas available for particle transport. This results in the additional (excess concentration) particles eluting faster through preferential pathways provided by larger pores. Our breakthrough patterns are again inconsistent with those observed for straining under different particle concentrations. Furthermore, straining is generally considered to be relevant with particle collector diameter ratios greater than 0.002 -0.008 [30, 32, 33].

Particle-collector ratios in our study are in the range of $8x10^{-6}$-$4x10^{-5}$ for CMC-NZVI and $8x10^{-6}$-$2.5x10^{-3}$ for PAA-NZVI. Thus simple straining processes cannot be relevant especially for CMC-NZVI whereas for PAA-NZVI the larger sub-population may experience some degree of straining. If straining was significant, the breakthrough patterns of CMC- and PAA-NZVI should have been different with the PAA-NZVI showing higher breakthrough at higher influent particle concentrations but not so for the CMC-NZVI. Ripening typically result in temporal decreases in effluent concentrations with time [34]; [35] and this was not observed in our study under any of the experimental conditions.

Phenrat et al. [13] also observed lower effluent concentrations with increasing particle concentrations using particle sizes in the range of 325 nm. Those authors have suggested that the large aggregates formed at $g•L^{-1}$ concentration ranges from those primary particles are preferentially removed from the aqueous phase during transport. In our study, the primary particles are one to two orders of magnitude smaller and thus unlikely to form very large aggregates, except may be by inter-particle bridging facilitated by free polyelectrolytes in solution [21]. Formation of large, sub-micron sized aggregates due to bridging may however result in straining. Under that scenario, the large aggregates formed at higher concentrations will lead to more particle removal by straining and thus decreased effluent concentrations with higher influent concentrations. Higher effluent concentrations with increases in influent concentrations has been observed only under conditions where the particle sizes do not change [36] and a reverse trend is possible when larger, more strainable particles are formed at higher concentrations.

At higher C_0, the collision frequency among the iron nanoparticles is increased, which would lead to increasing aggregation and larger aggregate sizes. As mentioned in the previous section, larger particles generated over time would result in a decrease in η_0 value (as Figure 3.5), which is expected to result in a gradual increase in effluent concentration as observed. This again contributes the observation of increasing effluent concentrations beyond 2 PV, rather than stable effluent concentrations. This is clearly evident with the PAA-NZVI at C_0=3 g•L^{-1} and 0.5 g•L^{-1} where effluents concentration increased steadily beyond 2 PV but less so for C_0=0.1 g•L^{-1} (Figure 3.6b).

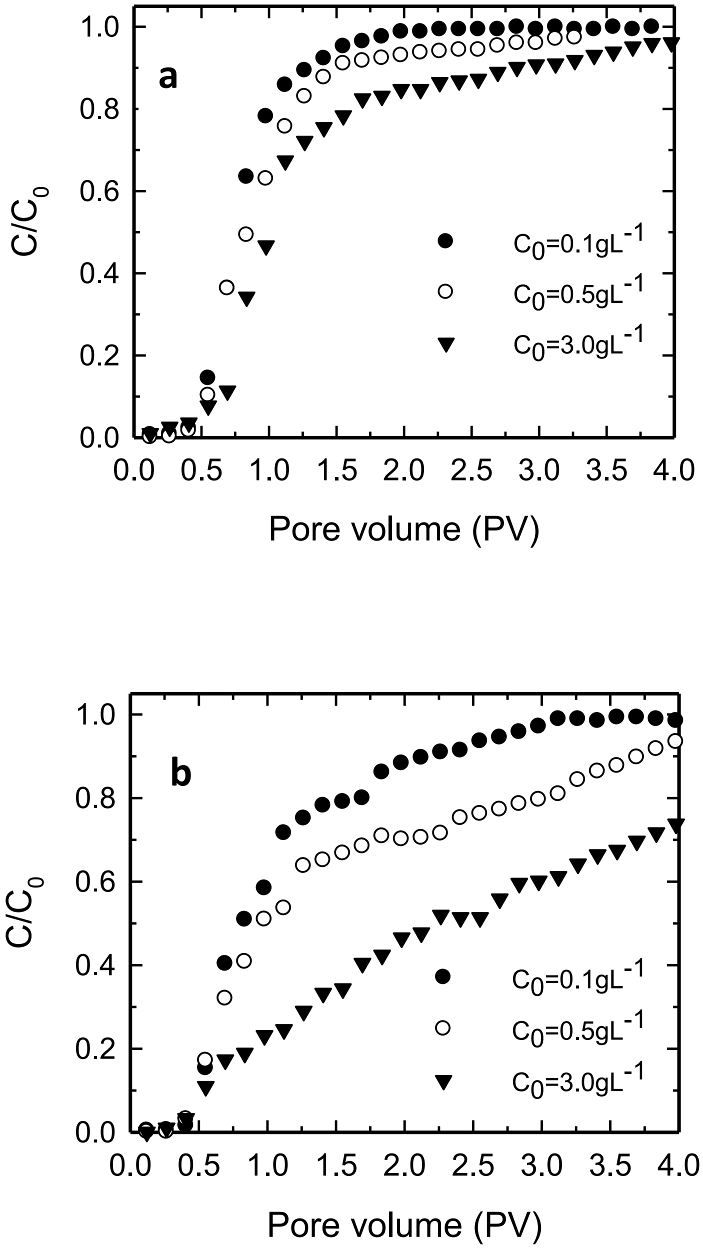

FIGURE 3.8: Experimental breakthrough curves with varying particle concentrations in packed sand columns of L =4.5 cm, v = 0.2 cm min^{-1} **(a)** CMC-NZVI (**b)** PAA-NZVI.

Theoretically, the column length should have no effect on particle breakthrough patterns. Several studies have employed longer columns compared to our study [6, 13, 37]. Thus we investigated the effect of increased column length to assess its effect on CMC-NZVI transport at a Darcy velocity of 0.2 cm min^{-1} and C_0 = 0.1 gL^{-1}. Increasing L from 4.5 to 9.5 cm had a negligible effect on the CMC-NZVI BTC (Supplementary Data, Figure 3.S2).

The change in ionic strength, from that of distilled water to 0.1mM and 1mM $NaHCO_3$, for the aqueous phase used for preparing the nanoparticle suspension for the transport experiments, had no significant influence on the BTC. The zeta potential of the CMC-NZVI is not altered significantly (-46.6 mV to 43.5 mV) in this range of ionic strength and thus the unchanged BTCs are expected.

3.4 Conclusions.

The effluent concentrations profiles for CMC- and PAA-NZVI decreased with lower flow velocities and higher influent particle concentrations. Although greater deposition of colloidal particles at low flow velocities have been reported in several studies, the greater deposition at higher influent particle concentrations has not been widely reported. Other studies have demonstrated that CMC- and PAA- are efficient polyelectrolytes for stabilization of NZVI and significantly improve NZVI transport in contrast to bare NZVI. This study presents a comparison of the transport performance of particles stabilized by these polyelectrolytes. Although both CMC- and PAA-NZVI were primarily approximately 5 nm in size, their effluent concentration profiles were significantly different. In particular, PAA-NZVI particles showed a gradual and continued increase in effluent concentrations beyond 2 PV. This pattern is attributable to the higher aggregation rate of PAA-NZVI as observed qualitatively in sedimentation tests conducted under quiescent conditions. The differences in the particle sizes and particle surface potentials of the CMC- and PAA-NZVI contribute to the different aggregation patterns. Aggregation, rather than other processes such as blocking, ripening and straining contributed to time dependent deposition rates observed from the effluent concentration profiles. Overall, the results suggest that ~ 5 nm sized polyelectrolyte-stabilized NZVI may be transported to a significant extent even at slower flow velocities, representative of natural groundwater conditions, although transport is enhanced at higher flow velocities representative of injection velocities. Although polyelectrolyte-stabilized NZVI are more colloidally stable and mobile than bare NZVI, aggregation remains an important process controlling its transport behavior.

Acknowledgements

The research was funded by the Strategic Project Grant Program of the Natural Sciences and Engineering Research Council of Canada and by Golder Associates Ltd. T.R. was supported by a McGill Engineering Doctoral Fellowship. We thank Prof. Nathalie Tufenkji, McGill University for her helpful comments on the data.

Supplementary Data

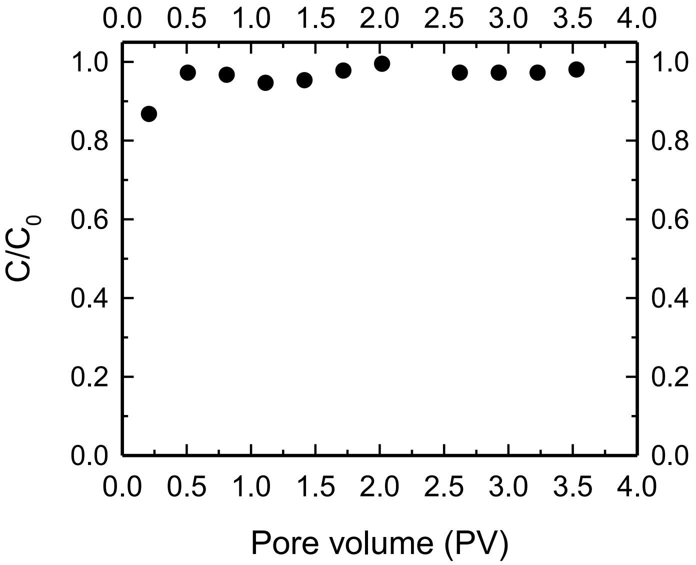

FIGURE 3.S1. Variation in influent concentration of iron nanoparticles at the inlet with time

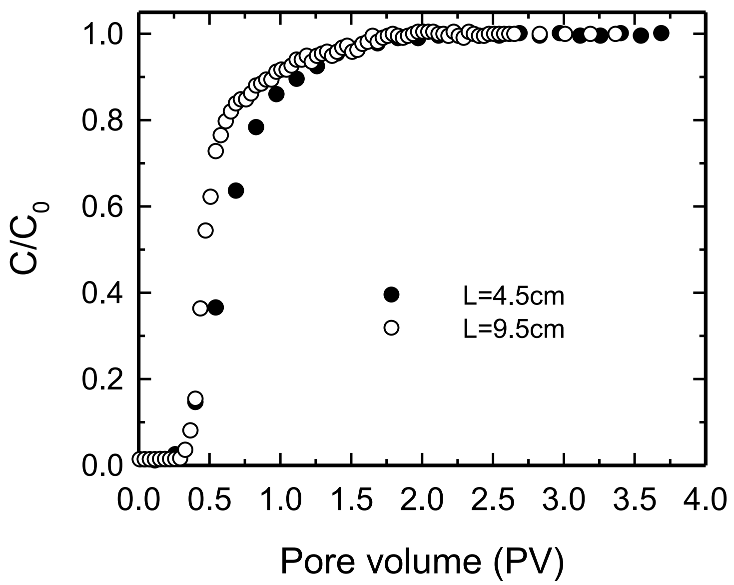

FIGURE 3.S2. Experimental breakthrough curves of CMC-NZVI with varying column lengths in packed sand columns where, $v = 0.2$ cm min^{-1} , $C_0 = 0.1$ gL^{-1}

References

[1] Kanel, S.R., J.M. Greneche and H. Choi, *Arsenic(V) removal kom groundwater using nano scale zero-valent iron as a colloidal reactive barrier material.* Environ. Sci. Technol., 2006. **40**(6): p. 2045-2050.

[2] Leupin, O.X. and S.J. Hug, *Oxidation and removal of arsenic (III) from aerated groundwater by filtration through sand and zero-valent iron.* Water Res., 2005. **39**(9): p. 1729-1740.

[3] Li, Z.H., H.R. Jones, R.S. Bowman and R. Helferich, *Enhanced reduction of chromate and PCE by palletized surfactant-modified zeolite/zerovalent iron.* Environ. Sci. Technol., 1999. **33**(23): p. 4326-4330.

[4] Schrick, B., B.W. Hydutsky, J.L. Blough and T.E. Mallouk, *Delivery vehicles for zerovalent metal nanoparticles in soil and groundwater.* Chemistry of Materials, 2004. **16**(11): p. 2187-2193.

[5] Phenrat, T., N. Saleh, K. Sirk, R.D. Tilton and G.V. Lowry, *Aggregation and sedimentation of aqueous nanoscale zerovalent iron dispersions.* Environmental science and technology, 2007. **41**(1): p. 284-290.

[6] Kanel, S., D. Nepal, B. Manning and H. Choi, *Transport of surface-modified iron nanoparticle in porous media and application to arsenic(III) remediation.* Journal of Nanoparticle Research, 2007. **9**(5): p. 725-735.

[7] Yang, G.C.C., H.-C. Tu and C.-H. Hung, *Stability of nanoiron slurries and their transport in the subsurface environment.* Separation and Purification Technology, 2007. **58**(1): p. 166-172.

[8] Phenrat, T., N. Saleh, K. Sirk, H.J. Kim, R.D. Tilton and G.V. Lowry, *Stabilization of aqueous nanoscale zerovalent iron dispersions by anionic polyelectrolytes: adsorbed anionic polyelectrolyte layer properties and their effect on aggregation and sedimentation.* J. Nanopart. Res., 2008. **10**(5): p. 795-814.

[9] Saleh, N., H.J. Kim, T. Phenrat, K. Matyjaszewski, R.D. Tilton and G.V. Lowry, *Ionic strength and composition affect the mobility of surface-modified Fe0 nanoparticles in water-saturated sand columns.* Environ. Sci. Technol., 2008. **42**(9): p. 3349-3355.

[10] Fatisson, J., S. Ghoshal and N. Tufenkji, *Deposition of carboxymethylcellulose-coated zero-valent iron nanoparticles onto silica: Roles of solution chemistry and organic molecules.* Langmuir, 2010. **26**(Compendex): p. 12832-12840.

[11] Saleh, N., K. Sirk, Y. Liu, T. Phenrat, B. Dufour, K. Matyjaszewski, R.D. Tilton and G.V. Lowry, *Surface modifications enhance nanoiron transport and NAPL targeting in saturated porous media.* Environmental Engineering Science, 2007. **24**(1): p. 45-57.

[12] He, F., D.Y. Zhao, J.C. Liu and C.B. Roberts, *Stabilization of Fe-Pd nanoparticles with sodium carboxymethyl cellulose for enhanced transport and dechlorination of trichloroethylene in soil and groundwater.* Ind. Eng. Chem. Res., 2007. **46**(1): p. 29-34.

[13] Phenrat, T., H.-J. Kim, F. Fagerlund, T. Illangasekare, R.D. Tilton and G.V. Lowry, *Particle size distribution, concentration, and magnetic attraction affect transport of polymer-modified Fe0 nanoparticles in sand columns.* Environmental science and technology, 2009. **43**(13): p. 5079-5085.

[14] He, F., M. Zhang, T. Qian and D. Zhao, *Transport of carboxymethyl cellulose stabilized iron nanoparticles in porous media: Column experiments and modeling.* Journal of Colloid and Interface Science, 2009. **334**(1): p. 96-102.

[15] Kanel, S., R.R. Goswami, T.P. Clement, M.O. Barnett and D. Zhao, *Two dimensional transport characteristics of surface stabilized zero-valent iron nanoparticles in porous media.* Environmental science and technology, 2008. **42**(3): p. 896-900.

[16] Liu, Y.Q., H. Choi, D. Dionysiou and G.V. Lowry, *Trichloroethene hydrodechlorination in water by highly disordered monometallic nanoiron.* Chem. Mat., 2005. **17**(21): p. 5315-5322.

[17] He, F. and D. Zhao, *Manipulating the size and dispersibility of zerovalent iron nanoparticles by use of carboxymethyl cellulose stabilizers.* Environmental science and technology, 2007. **41**(17): p. 6216-6221.

[18] Sun, Y.-P., X.-q. Li, J. Cao, W.-x. Zhang and H.P. Wang, *Characterization of zero-valent iron nanoparticles.* Advances in Colloid and Interface Science, 2006. **120**(1-3): p. 47-56.

[19] Domingos, R.F., M.A. Baalousha, Y. Ju-Nam, M.M. Reid, N. Tufenkji, J.R. Lead, G.G. Leppard and K.J. Wilkinson, *Characterizing manufactured nanoparticles in the environment: Multimethod determination of particle sizes.* Environmental science and technology, 2009. **43**(19): p. 7277-7284.

[20] Ditsch, A., P.E. Laibinis, D.I.C. Wang and T.A. Hatton, *Controlled clustering and enhanced stability of polymer-coated magnetic nanoparticles.* Langmuir, 2005. **21**(13): p. 6006-6018.

[21] Chen, K.L., S.E. Mylon and M. Elimelech, *Enhanced aggregation of alginate-coated iron oxide (Hematite) nanoparticles in the presence of calcium, strontium, and barium cations.* Langmuir, 2007. **23**(11): p. 5920-5928.

[22] Lim, J.K., S.A. Majetich and R.D. Tilton, *Stabilization of superparamagnetic iron oxide core-gold shell nanoparticles in high ionic strength media.* Langmuir, 2009. **25**(23): p. 13384-13393.

[23] Torkzaban, S., S.A. Bradford and S.L. Walker, *Resolving the coupled effects of hydrodynamics and DLVO forces on colloid attachment in porous media.* Langmuir, 2007. **23**(19): p. 9652-9660.

[24] Li, Y., Y. Wang, K.D. Pennell and L.M.A. Briola, *Investigation of the transport and deposition of fullerene (C60) nanoparticles in quartz sands under varying flow conditions.* Environmental Science and Technology, 2008. **42**(19): p. 7174-7180.

[25] Ko, C.-H. and M. Elimelech, *The 'shadow effect' in colloid transport and deposition dynamics in granular porous media: Measurements and mechanisms.* Environmental Science and Technology, 2000. **34**(17): p. 3681-3689.

[26] Tufenkji, N. and M. Elimelech, *Correlation Equation for Predicting Single-Collector Efficiency in Physicochemical Filtration in Saturated Porous Media.* Environmental science and technology, 2004. **38**(2): p. 529-536.

[27] T. Dabros and T.G.M. van de Ven, J., *kinatics of Coating by Colloidal Particles.* Journal of Colloid and Interface Science, 1982. **89**(2).

[28] Kuhnen, F.B., K.; Bhattacharjee, S.; Elimelech, M.; and Kretzschmar, R., *Transport of Iron Oxide Colloids in Packed Quartz Sand Media:Monolayer and Multilayer Deposition* Journal of Colloid and Interface Science 2000. **231, 32-41**

[29] Camesano, T.A. and B.E. Logan, *Influence of fluid velocity and cell concentration on the transport of motile and nonmotile bacteria in porous media.* Environmental Science and Technology, 1998. **32**(11): p. 1699-1708.

[30] Bradford, S.A. and M. Bettahar, *Concentration dependent transport of colloids in saturated porous media.* Journal of Contaminant Hydrology, 2006. **82**(1-2): p. 99-117.

[31] Bradford, S.A., H.N. Kim, B.Z. Haznedaroglu, S. Torkzaban and S.L. Walker, *Coupled factors influencing concentration-dependent colloid transport and retention in saturated porous media.* Environmental Science and Technology, 2009. **43**(18): p. 6996-7002.

[32] Bradford, S.A., S.R. Yates, M. Bettahar and J. Simunek, *Physical factors affecting the transport and fate of colloids in saturated porous media.* Water Resources Research, 2002. **38**(12): p. 631-6312.

[33] Tufenkji, N., G.F. Miller, J.N. Ryan, R.W. Harvey and M. Elimelech, *Transport of Cryptosporidium oocysts in porous media: Role of straining and physicochemical filtration.* Environmental Science and Technology, 2004. **38**(22): p. 5932-5938.

[34] Liu, D., P.R. Johnson and M. Elimelech, *Colloid deposition dynamics in flow through porous media: role of electrolyte concentration.* Environmental science and technology, 1995. **29**(12): p. 2963-2963.

[35] Tong, M., H. Ma and W.P. Johnson, *Funneling of flow into grain-to-grain contacts drives colloid-colloid aggregation in the presence of an energy barrier.* Environmental Science and Technology, 2008. **42**(8): p. 2826-2832.

[36] Bradford, S.A. and M. Bettahar, *Concentration dependent transport of colloids in saturated porous media.* Journal of Contaminant Hydrology, 2006. **82**(Compendex): p. 99-117.

[37] Saleh, N., H.-J. Kim, T. Phenrat, K. Matyjaszewski, R.D. Tilton and G.V. Lowry, *Ionic strength and composition affect the mobility of surface-modified fe0 nanoparticles in water-saturated sand columns.* Environmental science and technology, 2008. **42**(9): p. 3349-3355.

Connecting text: Chapter 3 and chapter 4

In Chapter 3, the effect of PAA- and CMC- modified NZVI on transport was evaluated. The average particle size of CMC-NZVI was in the range of 5 nm, whereas, PAA-NZV had a bimodal particle size distribution with particle sizes up to 30 nm. The experiments performed in Chapter 3 suggest that CMC-NZVI transported more efficiently than PAA-NZVI, and the results suggest that aggregation played an important role in the transport of NZVI. Therefore, in Chapter 4, the aggregation behaviour of CMC-NZVI of bigger sized particles (75 nm) was assessed and its effect on transport was evaluated.

Chapter 4

Aggregation and Deposition Kinetics of Carboxymethyl Cellulose-Modified Zero-Valent Iron Nanoparticles in Porous Media

Trishikhi Raychoudhury[1], Nathalie Tufenkji[2], Subhasis Ghoshal[1,*]

[1] *Department of Civil Engineering, McGill University, Montreal, Quebec,*
Canada H3A 2K6
[2] *Department of Chemical Engineering, McGill University, Montreal,*
Quebec, Canada H3A 2B2

Submitted to

Water Research

4.1 Introduction

An emerging remediation technique for *in situ* groundwater remediation of chlorinated solvent and heavy metal-contaminated aquifers is the injection of reactive nanoparticles of zero-valent iron (NZVI) [1, 2]. Although at appropriate doses, NZVI can eliminate or transform certain pollutants rapidly, its transport to target locations and its reactivity may be limited by its rapid aggregation [3]. Several studies have demonstrated improved colloidal stabilization of NZVI by coating them with polymers or polyelectrolytes [4-7]. Polyelectrolyte or polymer coatings can inhibit NZVI aggregation by a combination of electrostatic and steric repulsion forces when these interactions are large enough to overcome interparticle magnetic and van der Waals attractive forces. The colloidal stabilization of NZVI by polymers has been shown to reduce the extent of deposition of NZVI on granular media and thus increase its mobility, relative to that for bare NZVI [4, 5, 8].

Polymeric coatings of NZVI are unlikely to provide complete stabilization because of incomplete or insufficient surface coverage. The extent of colloidal stabilization is also dependent on the polymer characteristics, the thickness of the polymer layer on the particle surface, and on the solution chemistry [5, 6, 9]. Even at gL^{-1} doses of polymers and polyelectrolytes, which would be costly for large-scale remediation, there is evidence of incomplete stabilization within minutes [3, 5, 6, 10]. Thus, it is important to assess the changes in particle size distribution (PSD) of polymer-stabilized NZVI due to aggregation.

The influence of aggregation of polyelectrolyte-modified NZVI on the deposition and transport of these particles in granular media has been discussed in recent studies [10-13]. Those studies suggested that aggregation of the nanoparticles will influence their deposition in granular media because the particle size determines the magnitude of the single-collector contact efficiency (η_0), which is defined as the ratio of the number of collisions between the particle and the collector and the total number of particles approaching the collector. The effect of colloid aggregate size on colloid transport in porous media has been examined by Chaterjee and Gupta [14]. In their study, injection of a polydisperse suspension of inert micron-sized particles in a packed sand column resulted in larger particles being deposited at shallower bed depths compared to the smaller particles. The observed deposition behavior was quantitatively explained by particle-size dependent deposition rate coefficients. Although those studies have demonstrated that changes in particle size resulting from aggregation influence transport, the role of aggregation kinetics or time-varying particle size distributions (PSDs) on nanoparticle transport behavior has not been examined.

The objectives of this study were to assess the rates and extents of aggregation of carboxymethyl cellulose (CMC)-stabilized NZVI, as well as the effects of aggregation kinetics on CMC-NZVI transport and deposition in granular porous media at different nanoparticle concentrations. Changes in the equivalent mean diameter of a polymer-stabilized NZVI particle suspension due to aggregation were measured over a time period equivalent to the particle residence time during a transport experiment. An aggregation kinetics model was fitted to this data to obtain the particle-particle attachment efficiency (α_{pp}) and calculations were performed to determine the change in the PSD with time during the transport experiments. In an effort to better understand the role of nanoparticle aggregation kinetics on nanoparticle transport, a modified colloid transport model which couples the governing transport equation to the aggregation kinetics equation was developed. A schematic of the multiple concurrent nanoparticle aggregation, deposition and transport processes occurring in granular porous media is shown in Figure 4.1. Column transport experiments were performed for different nanoparticle concentrations, and the effluent CMC-NZVI concentrations over time were fitted to the modified colloid transport model to assess whether particle-size dependent deposition rates could account for the observed shape of the experimental breakthrough curves. The potential role of other nanoparticle deposition mechanisms such as blocking of deposition sites, detachment of nanoparticles and the changes in electrolyte composition with CMC-NZVI concentration, were also considered for explaining the observed breakthrough curves.

Nomenclature

C	Effluent particle mass concentration [ML^{-3}]	k_{dep}	Particle deposition rate coefficient [T^{-1}]
C_0	Influent particle mass concentration [ML^{-3}]	$k_{\mathrm{dep,i}}$	Deposition rate coefficient of the i$^{\mathrm{th}}$ sized particles [T^{-1}]
C_{i}	Mass concentration of ith size aggregate [ML^{-3}]	k_{det}	Particle detachment rate coefficient [T^{-1}]
D	Hydrodynamic dispersion coefficient [L^2T^{-1}]	$mass_i$	Mass of i$^{\mathrm{th}}$ particles [M]
D_{f}	Fractal dimension of aggregates	n	Particle number concentration [L^{-3}]
N_{i}	Number of single particles forming the aggregates	n_{i}	Particle number concentration of i$^{\mathrm{th}}$ aggregates [L^{-3}]
S_{dep}	Solid phase deposited mass density [MM^{-1}]	t	Time [T]
T	Temperature [T]	v	Darcy's velocity [LT^{-1}]
T_{adhesive}	Adhesive torque [ML^2T^{-2}]	x	Distance along column length [L]
T_{applied}:	Torque applied [ML^2T^{-2}]	α_{pc}	Particle-collector attachment efficiency
Z	Maximum number of size categories	α_{pp}	Particle-particle attachment efficiency
d_{Navg}	Number-averaged mean diameter measured by NTA [L]	β	Particle-particle collision frequency function [L^3T^{-1}]
d^*_{Navg}	Number-averaged mean diameter calculated from model [L]	ε	Porosity
d_{c}	Mean collector diameter [L]	η_0	Single collector contact efficiency
$d_{\mathrm{p(i)}}$	Particle diameter of i$^{\mathrm{th}}$ aggregates [L]	$\eta_{0,\mathrm{i}}$	Single collector contact efficiency of i$^{\mathrm{th}}$ sized aggregate
$d_{\mathrm{p(i=1)}}$	diameter of the smallest particle size [L]	ρ	Bulk density of sand [ML^{-3}]

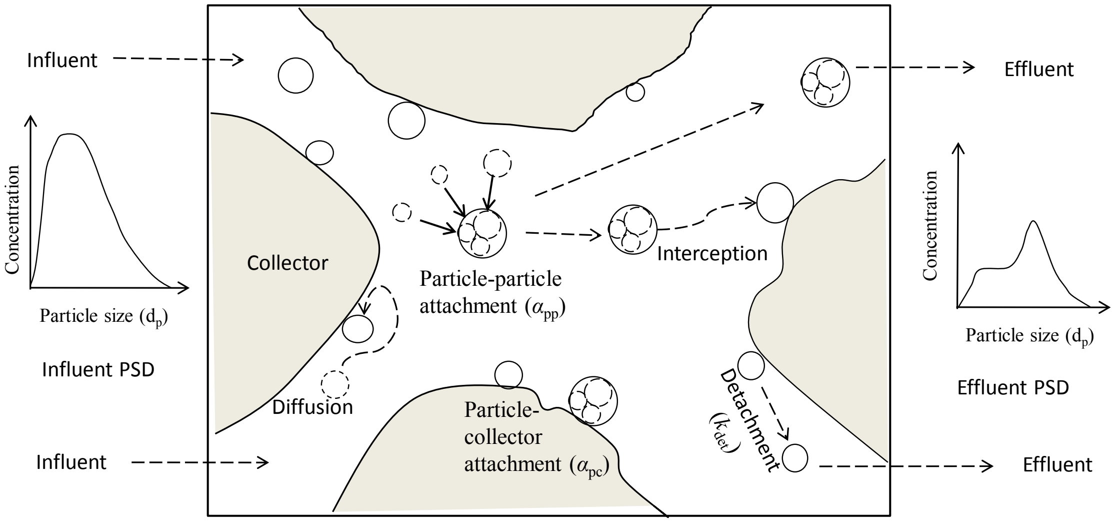

FIGURE 4.1. Schematic of concurrent aggregation and particle deposition processes in porous medium

4.2 Materials and Methods

All chemicals were reagent grade and all solutions were prepared using deionized water (Milli-Q-UV Plus, Millipore).

4.2.1 Synthesis of CMC-NZVI

CMC-NZVI was prepared according to the methods described by He et al. [15]. Briefly, an aqueous solution of 0.065M $FeSO_4{\cdot}7H_2O$ (AlfaAesar, purity greater than 99%) was added to 5 gL^{-1} of Na-CMC (90K, Aldrich) solution and mixed thoroughly for 30 minutes. The solution was then reduced by the drop-wise addition of a solution of $NaBH_4$ (Sigma-Aldrich) at rate of 55.5 mg min^{-1} under an N_2 atmosphere. The ratio of $[BH_4^-]/[Fe^{2+}]$ was set at 2.0. The mixture was then stirred for an additional 30 min before being dried overnight and finally the dry powder was stored under N_2.

4.2.2 Particle size analysis of CMC-NZVI for assessment of aggregation kinetics

The above process yielded CMC-NZVI particles with a mean diameter of 70 nm as determined by high resolution (Philips CM200) and low resolution (FEI Tecnai 12) transmission electron microscopy (TEM) operated at 200 kV and 120 kV, respectively. Samples for TEM analysis were prepared by depositing two droplets of nanoparticle suspension onto carbon-coated 400 mesh copper grids under N_2 to avoid oxidation, and the diameters were measured using the General Image Manipulating Software (GIMP Software, GNU) by averaging 100 particles on different TEM grids. From the TEM images, the CMC-layer thickness was approximated to be in the range of 5-10 nm, which is in agreement with CMC layer thicknesses reported in prior studies [10, 16]. For calculating the single-collector contact efficiency (η_0) and the particle-particle collision frequency function (β), an average CMC thickness of 7 nm was considered.

The particle sizes of CMC-NZVI over time in aqueous suspensions were determined by nanoparticle tracking analysis (NTA, NanoSight LM10). Suspensions of 0.07, 0.2 and 0.725 gL^{-1} CMC-NZVI (as total Fe) were prepared in N_2 atmosphere with filtered (0.22 μm) degassed 0.1 mM $NaHCO_3$ and sonicated by a 40kHz ultrasonic cleaner (Cole-Palmer 8891) for 10 min to ensure homogeneity of the suspensions, and the suspension was filled in a vial to zero headspace. The pH of each particle suspension was 7.4±0.4. Aliquots were withdrawn at various time points from vials subjected to slow stirring, and then diluted to 5 mgL^{-1}. The mean square displacements of single particles were determined by tracking the path of scattered light using the NanoSight software. With NTA, the diffusion coefficients are determined from a series of single-particle Brownian motion tracks over time, rather than the collective light-scattering response from all nanoparticles in dynamic light scattering which results in more biased towards the larger-sized particles in the latter technique [17].

4.2.3 Packed column experiments

A Kontes Chromoflex (Fisher Scientific) column of 1 cm i.d. and bed depth of 9 cm was used. A nylon mesh (100 µm opening size) was placed at the bottom of the packed column to prevent sand grains from being displaced into the tubing. The column was packed with graded silica sand (Unimin Corp., #4045) sieved through F30 and retained on F50 sieves. The sand was acid-washed with concentrated HCl, rinsed with DI water and oven dried for 3 hours at 550ºC. The mean size of the graded sand (d_{50}) was 375 µm. The column was dry-packed with sand at several stages with intermittent vibration to ensure uniform packing and then saturated with CO_2 to remove air bubbles. Next, 12 PVs of background electrolyte were injected in column using a syringe pump (KDS 200, KD Scientific) for conditioning of the column prior to injecting a suspension of CMC-NZVI. The porosity of the packed granular medium in the column was determined to be 0.32. The value of the hydrodynamic dispersion coefficient (D) was estimated to be 0.3 cm^2min^{-1} from breakthrough curves obtained with an inert tracer (KNO_3).

CMC-NZVI suspensions of different nanoparticle mass concentrations (0.07 gL^{-1}, 0.2 gL^{-1} and 0.725g L^{-1} as total Fe) in aqueous solution of 0.1 or 10 mM $NaHCO_3$ were prepared in a N_2 atmosphere with sonication as described above for the NTA analyses. The column influent suspension was pumped through the column at a rate of 0.445 cm min^{-1} using a syringe pump. The particle residence time in the reservoir syringe ranged from 0 to 48 minutes, and the average residence time in the column was 6 minutes. Settling of the CMC-NZVI in the syringe was prevented by gentle stirring as in the aggregation experiments. The concentration of nanoparticles entering the column was thus maintained constant over time as verified by monitoring of the column influent suspension using flame atomic absorption spectrometry (AAS) and presented in Figure 4.S1.

For AAS (Perkin Elmer 3110) analyses of Fe, the collected effluent samples were dissolved in concentrated HCl (1:2 v/v ratio), diluted with 5% HNO_3 and analyzed for total Fe at a wavelength of 249.7 nm. The detection limit of AAS for Fe measurement was 0.001 mgL^{-1} and all the samples have concentrations above the detection limit. All experiments were performed in duplicate and the presented data is the average of replicate experiments. The experimental conditions are summarized in Table 4.1.

Table 4.1. Specifications of experimental conditions

Column length, *L*	9 cm
CMC-NZVI concentration of the column feed, C_0	0.07, 0.2 or 0.725 g L^{-1}
Interstitial velocity, *v*	0.445 cm min^{-1}
Packing density of dry sand in the packed-bed, ρ_b	1.95 g cm^{-3}
Column void fraction (or porosity), ε	0.32
Mean diameter of the sand particles, d_c	375 µm
Longitudinal dispersion coefficient, *D*	0.3cm^2 min^{-1}
Density of the nanoparticles	6.7×10^3 Kg m^{-3}
Electrolyte solution for preparation of particle suspensions	0.1 mM $NaHCO_3$
pH	7.4±0.4

4.3 Results and Discussion

4.3.1 Aggregation Kinetics of CMC-NZVI

The change in the mean diameter (d_{Navg}) of the CMC-NZVI over time in a 0.07 gL^{-1}, 0.2 gL^{-1} and 0.725 gL^{-1} suspension prepared in 0.1 mM $NaHCO_3$, as determined by NTA, is presented in Figure 4.2a. The data points shown in the figure are pooled from duplicate experiments conducted for each concentration, with particle diameter measurements taken at different time points. The extent of aggregation of CMC-NZVI over the 65 minute duration resulted in an increase in d_{Navg} of 21 nm for the 0.2 gL^{-1} CMC-NZVI suspension and 65 nm for the 0.725 gL^{-1} suspension. The change in particle size with time of the 0.07 mgL^{-1} CMC-NZVI particle suspension was found to be negligible but there was aggregation at higher particle concentrations. Increasing particle concentrations result in greater number of particle-particle collisions and an increase in the extent of aggregation.

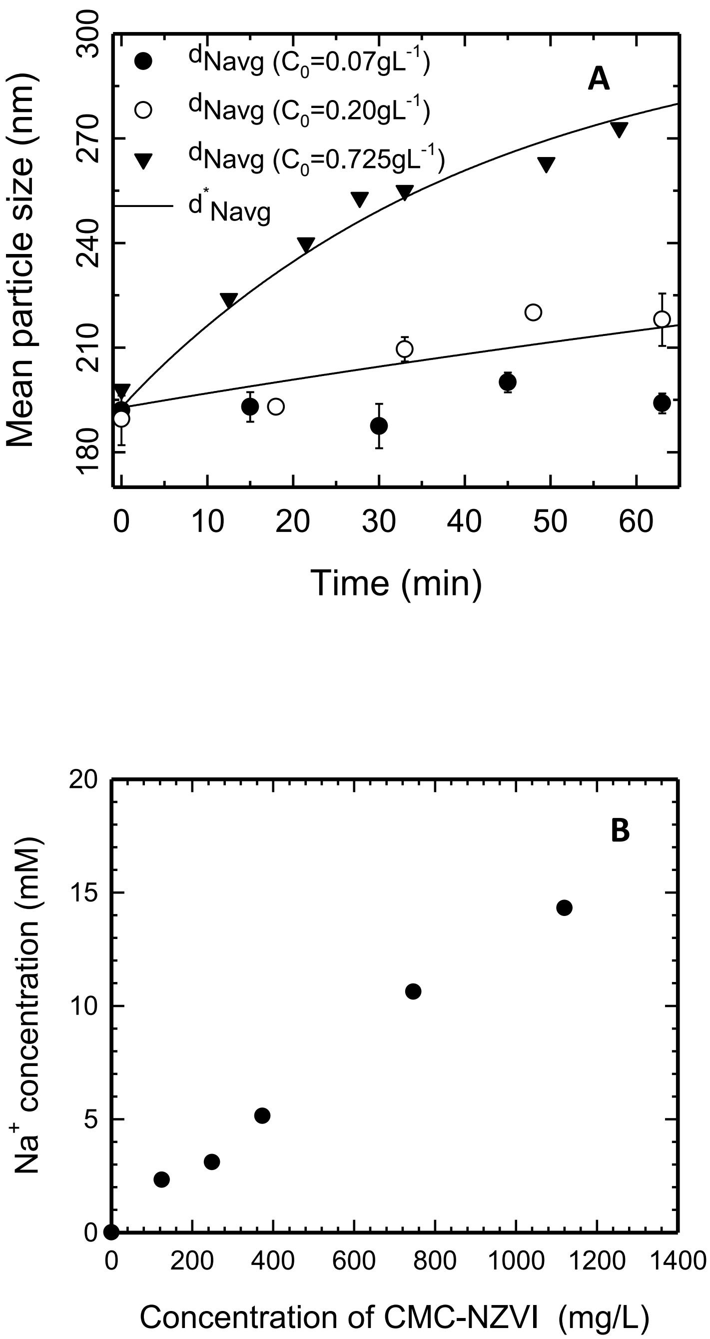

FIGURE 4.2. (A) Changes in mean particle size over time for suspensions of CMC-NZVI obtained by nanoparticle tracking analysis (NTA). The lines show the best fit of the aggregation kinetics model to the 0.2 gL^{-1} and 0.725 gL^{-1} CMC-NZVI. (B) Change in Na$^+$ concentration with increase in CMC-NZVI concentration in suspensions prepared in 0.1 mM $NaHCO_3$.

The NTA data in Figure 4.2a for the 0.2 and 0.725 gL^{-1} suspension was fitted to particle aggregation kinetics are described by the approach proposed by Lee et al. [18]

$$\left(\frac{dn_k}{dt}\right) = \frac{1}{2}\alpha_{pp}\sum_{i+j=k}\beta(i,j)n_i\,n_j - \alpha_{pp}n_k\sum_{i=1}^{z}\beta(i,k)n_i \tag{4.1}$$

where, n_i, n_j and n_k are the *i, j* and *k*-mer particle number concentrations, and z is the maximum number of size categories. The first term on the right-hand side of Equation 4.1 accounts for the formation of aggregates of size k as a result of aggregation of particles of size i and j. The second term on the right hand-side accounts for the loss of particles of size k as a result of collisions that lead to further aggregation. Aggregation kinetics are controlled by the particle-particle attachment efficiency, α_{pp}, which is the fraction of particle-particle collisions which result in attachment and is dependent on solution chemistry, and the particle-particle collision frequency function, β. The parameter β is the particle contact mechanisms that accounts for Brownian motion, fluid shear and differential sedimentation mechanism. In Equation 4.1, β was computed using the Coalesced Fractal Sphere model [18], which assumes that only binary collisions occur, and that the shape of the aggregates are defined by their fractal dimension, D_f, which remains unchanged during aggregation. A generally accepted value of D_f is in the range of 2.0 for reaction-limited aggregation that occurs under conditions of low ionic strength (IS) aqueous solutions and/or inter-particle steric hindrance [19, 20]. The aggregate sizes generated with time, are defined as follows [18]:

$$d_{p(i)}=(N_i^{1/Df})\times d_{p(i=1)} \tag{4.2}$$

where N_i is the number of single particles forming an aggregate of diameter $d_{p(i)}$ and $d_{p(i=1)}$ is the diameter of the smallest particle (45 nm) present in the suspension, and considered as the primary monomer.

The α_{pp} was determined by fitting the calculated particle number-averaged mean diameter (d^*_{Navg}) over time predicted by Equation 4.1, with the number-averaged mean diameter (d_{Navg}) measured over time by nanoparticle tracking analyses (NTA).

The fit of Equation 4.1 to NTA data is shown in Figure 4.2a. The initial (t=0) PSD was obtained from TEM image analyses of CMC-NZVI in a freshly-prepared suspension, which yielded a d_{Navg} of 70 nm, and a minimum diameter, $d_{p(i=1)}$, of 45 nm. The mean particle diameter at t=0 based on NTA was 192 nm. The difference in the mean particle sizes determined by TEM and NTA can be explained by the fact that NTA calculates particle hydrodynamic diameters based on light scattering [17]. The difference in mean particle diameters determined from TEM and NTA at the initial time point (t=0 min) was assumed to be constant over time, and the value of d^*_{Navg} was adjusted accordingly. The fitting of the 0.2 gL^{-1} and 0.725 gL^{-1} CMC-NZVI suspensions prepared in 0.1 mM $NaHCO_3$ yielded a α_{pp} of 1.7×10^{-4} and 3.0×10^{-4}, respectively. The different values of α_{pp} occurs because it was found that the two suspensions had different IS even though prepared with the same electrolyte solution of 0.1 mM $NaHCO_3$. This is because, with an increase in CMC-NZVI concentration, the dissolved Na^+ concentration released from $NaBH_4$ added during particle synthesis and from the dissociation of Na-CMC [21] also increases. CMC-NZVI particles were used without washing to prevent excessive loss of particles and to minimize oxidation of these reactive particles and thus any Na added at synthesis remained associated with the particle suspension. A linear increase in Na^+ concentration with CMC-NZVI concentration is shown in Figure 4.2b. The total Na measured in the aqueous phase, after separating the CMC-NZVI by centrifugation at 10000 rpm for 15 min, was approximated as the Na^+ concentration. Thermo gravimetric analyses showed that more than 94% of the CMC was bound to the NZVI and thus only a small amount of undissociated Na-CMC could have been present in the CMC-NZVI free solution. The effective IS accounting for the increase in Na^+ salt concentration for different CMC-NZVI suspensions are reported in Table 4.2.

The values of α_{pp} reported above were relatively small, indicating a probability of up to 3 successful collisions out of 10,000. The small values of α_{pp} are not unusual given the low effective IS of less than 10 mM [13] and the predicted high repulsive energy barrier for particle-particle interactions (Figure 4.S1a). Saleh et al. [22] reported α_{pp} of carbon nanotubes coated with humic acid to be in the range of 10^{-3} to 10^{-4} in 1 mM IS solutions. Hu et al. [23] also observed particle-particle attachment efficiencies of similar magnitude for humic acid-coated magnetite nanoparticles at IS ranging from 5-10 mM.

The particle size distributions of CMC-NZVI suspensions over time were calculated using Equations 4.1 and 4.2 with the fitted values of α_{pp}.

Changes in the PSD with time as calculated by Equation 4.1 for particle concentrations of 0.2 gL^{-1} and 0.725 gL^{-1} are presented in Figure 4.S2. The results show that at higher particle concentrations, there is a greater abundance of relatively large-sized aggregates.

4.3.2 Framework for Assessing the Effect of Aggregation on Transport of CMC-NZVI

The effects of aggregation on transport of CMC-NZVI in packed columns were assessed by accounting for the changes in PSD over the time course of the transport experiments. The classical colloid transport theory is described in the SI. The particle deposition rate coefficient (k_{dep}) is a function of the attachment efficiency (α) between suspended particles and the collector surface and the single-collector contact efficiency (η_0) which is dependent on particle size and other physical parameters [24]. Calculations using the Tufenkji and Elimelech Equation [24] show that the value of the single-collector contact efficiency decreases rapidly as the particle diameter increases up to 100 nm (Figure 4.3a) due to the decreasing contribution of Brownian diffusion. The changes in η_0 are smaller for particle diameters between 100 to 200 nm. For particles greater than 200 nm, the value of η_0 again increases due to the contributions of interception and sedimentation to particle deposition. Thus, changes in the nanoparticle suspension PSD with time as a result of aggregation will result in time-varying changes in k_{dep}. The magnitude of the overall attachment efficiency for particle deposition is given by Kuhnen et al. [25] as $\alpha = \alpha_{\mathrm{pc}}\mathrm{B}(\theta) + \alpha_{\mathrm{pp}}\theta$, where θ is the fraction of collector surface coverage and $\mathrm{B}(\theta)$ is the blocking function. The deposition of suspended particles onto previously deposited particles can be deemed negligible based on the small values of α_{pp} ($=1.7\times10^{-4}$-3×10^{-4}) and θ ($=1.5\times10^{-4}$-2.4×10^{-3}) calculated from experimental BTCs presented in the following section. Also, $\mathrm{B}(\theta)$ approaches unity for a very small value of θ. Thus, here, α can be assumed to be equal to the particle-collector attachment efficiency (α_{pc}) alone. The expressions for the deposition rate coefficient of i^{th} particle size and the resulting modified colloid transport equations are:

$$k_{dep,i} = \left[\frac{3(1-\varepsilon)v}{2d_c\varepsilon}\alpha_{pc}\right]\eta_{o,i} \tag{4.3}$$

$$C_{\mathrm{i}} = mass_{\mathrm{i}} \times n_{\mathrm{i}} \tag{4.4}$$

$$\frac{\partial C}{\partial t} = D\frac{\partial^2 C}{\partial x^2} - v\frac{\partial C}{\partial x} - \sum_{i=1}^{n} k_{dep,i}C_i \tag{4.5}$$

where $k_{\mathrm{dep,i}}$ is the deposition rate coefficient, $mass_i$ is the mass, C_i is the mass concentration in the aqueous suspension and n_i is the number concentration of the i^{th} sized particles.

Calculations using Equations 4.1 and 4.3-4.5, show that the shape of the BTC was influenced by the initial PSD. Calculated BTCs for suspensions having different initial particle size ranges of defined initial average particle sizes are shown in Figure 4.3b. These predicted BTCs were computed assuming a total number concentration of 5×10^{17} particles/mL, and with a α_{pp} of 2.5×10^{-4} and α_{pc} of 0.34, approximately average values that have been determined from fitting experimental data obtained in this study (Table 4.2). Interestingly, the results in Figure 4.3b show that aggregation may actually slightly enhance CMC-NZVI transport for aggregates with sizes ranging up to 200 nm, whereas transport may be significantly decreased for larger aggregates. When the average particle size in the suspension increases from 60 nm (at t=0) to 105 nm (at t=end) and η_0

decreases accordingly, the breakthrough nanoparticle concentration increases with time. In contrast, when the average particle size in the suspension increases from

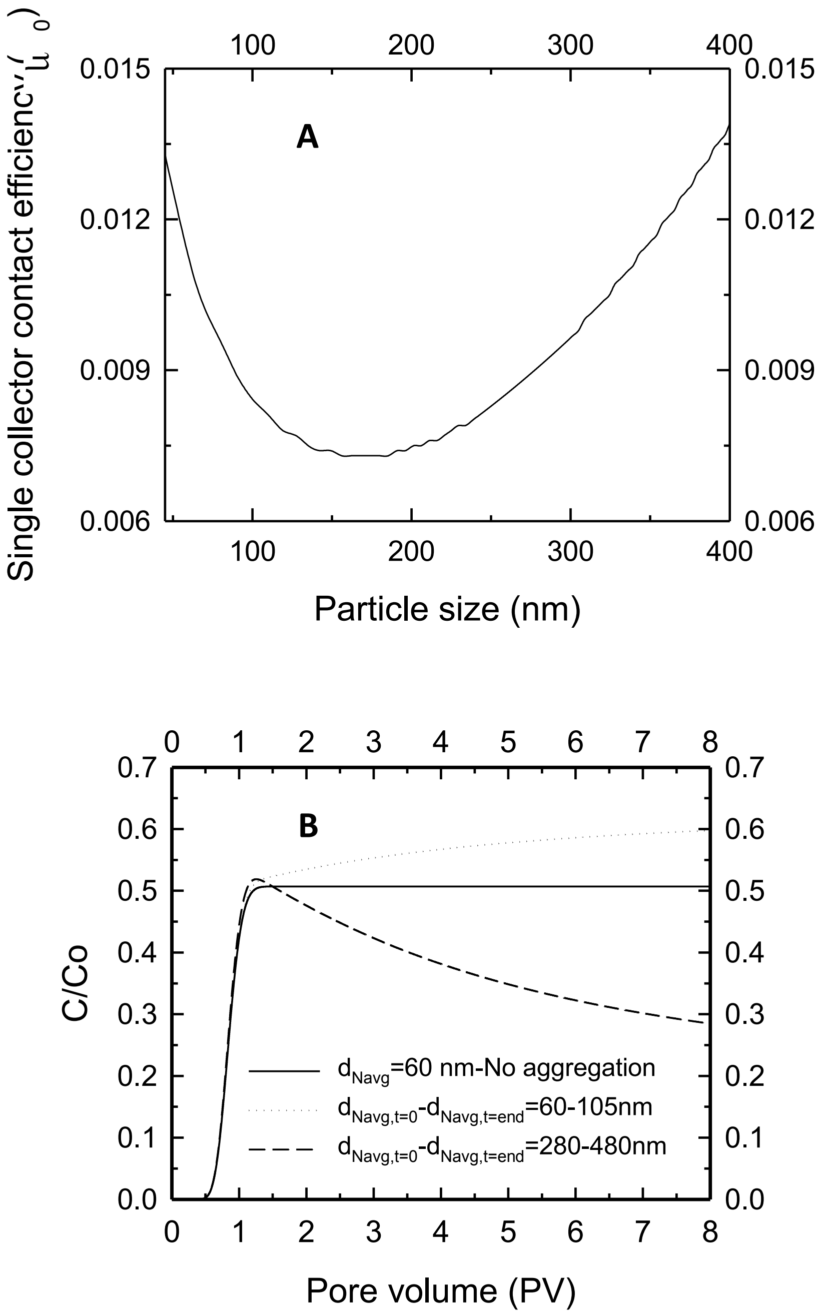

FIGURE 4.3. (A) Change in single-collector contact efficiency with particle size in the range 40-400 nm, and (B) change in CMC-NZVI breakthrough curves computed for different particle sizes with a α_{pp} = 2.5×10^4 and α_{pc}=0.34 with an assumed total particle number concentration of 5×10^{17} (number/mL). The values of α_{pp} , α_{pc} and number concentration were the average values for different experimental conditions in this study.

280 nm (at t=0) to 480 nm (at t=end) and η_0 increases over time, the breakthrough nanoparticle concentration decreases with time. The initial d_{Navg} and PSDs in the two calculated BTCs (Figure 4.3b) discussed above were chosen to highlight the possible effects of aggregation on the particle BTC and the effects may be smaller for different values of those parameters.

4.3.3 Breakthrough Curves of CMC-NZVI from Column Transport Experiments

Column transport experiments were conducted using CMC-NZVI suspensions prepared at concentrations of 0.07 gL^{-1}, 0.2 gL^{-1} and 0.725 gL^{-1}, in an electrolyte solution of 0.1 mM $NaHCO_3$. Representative BTCs shown in Figure 4.4 indicate that at the highest influent CMC-NZVI concentration of 0.725 gL^{-1}, C/C_0 at 8 PV is 0.61 which is lower compared to C/C_0 of 0.75 for the experiment conducted at 0.07 gL^{-1}.

The BTCs indicate that even after 2 PV, steady state concentrations were not achieved as the effluent concentrations slowly but continuously increase with time. The tracer (KNO_3) BTC showed steady-state effluent concentrations after 2 PV and thus the particle effluent concentrations were not influenced by artefacts arising from column packing. The CMC-NZVI BTCs are typical of blocking of collector surfaces, where deposited particles inhibit additional particle deposition once they have extensively covered collector surfaces [25-29]. However, blocking is unlikely in this system given that: (i) the surface coverage of the collector grain surfaces was comparatively small in the range of 0.015-0.24% (at 8 PVs), as calculated from the mass of particles eluted based on the BTC and the mass injected, and (ii) effluent concentrations decreased with increasing CMC-NZVI influent concentrations. Blocking generally requires more collector surface coverage by deposited particles than observed in our study. Ko et al. [30] observed blocking with as low as 5% surface coverage for sub-micron sized particles at low IS, but the surface coverage required for blocking increased with decreasing particle size. In addition, blocking results in higher effluent concentrations with increasing influent particle concentrations [25, 27].

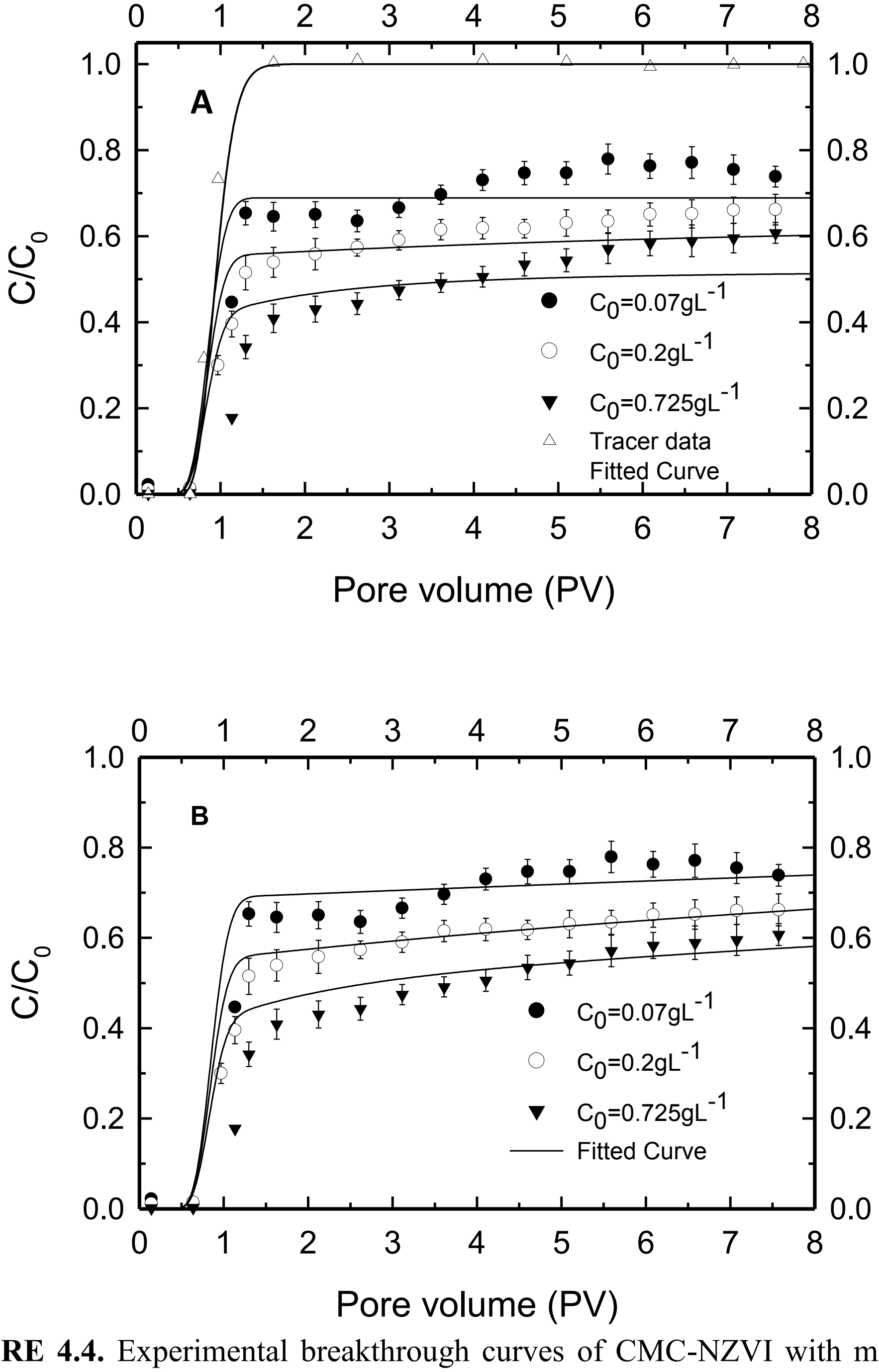

FIGURE 4.4. Experimental breakthrough curves of CMC-NZVI with model fit considering (A) particle aggregation and transport but no detachment, and (B) particle aggregation, transport and detachment. The BTCs were obtained using particle suspensions of concentrations of 0.07 gL^{-1}, 0.2 gL^{-1} and 0.725 gL^{-1}. The column bed depth was 9 cm and flow velocity 0.445 cm.min^{-1}.

Breakthrough curves for CMC-NZVI were calculated using the modified colloid transport model (Equations 4.1 and 4.3-4.5) and are shown with the experimental data in Figure 4.4a. For the 0.07 mgL^{-1} CMC-NZVI suspension, α_{pp} was set to 0. Figure 4.4a shows that the fit of the predicted BTCs matches reasonably well with the measured effluent concentrations up to 4 PVs. The particle-collector attachment efficiency (α_{pc}) was determined by fitting Equations 4.3-4.5 to the experimentally determined effluent concentrations, and the fitted values are presented in Table 4.2. The fitted BTCs show relatively little increase in effluent concentrations with increasing PVs compared to those in Figure 4.3b. This is because the PSDs for the column experiments were in the range where they exhibit smaller changes in η_0 over time compared to the particle ranges depicted in Figure 4.3b. For example, the fitted BTC for the 0.2 g/L CMC suspension (Figure 4.4a) which had a PSD (at t=0) with d_{Navg}=70 nm and minimum and maximum particle sizes of 45 and 120 nm, was associated with smaller changes in η_0 over time compared to the PSD (at t=0) for the calculated BTC shown in Figure 4.3b with d_{Navg}=60 nm, and associated minimum and maximum particle sizes of 38 nm and 96 nm. Beyond 4 PVs, the observed gradual increase in effluent concentrations for the different CMC-NZVI suspensions shown in Figure 4.4a is significantly greater than what is obtained from fitting of the modified colloid transport model. Hence, the observed increase in effluent particle concentrations (beyond 4 PVs) cannot be attributed to aggregation nor blocking as described above.

Table 4.2. Fitted values of particle-particle attachment efficiency (α_{pp}), particle-collector attachment efficiency (α_{pc}) and detachment rate constant (k_{det}) for different experimental conditions.

Experimental condition	Effective IS (mM)	α_{pp}	α_{pc}	k_{det} (min^{-1})
C_o=0.07 gL^{-1}	1.2	-	0.20	0.005
C_o=0.20 gL^{-1}	3.2	1.7×10^{-4}	0.32	0.005
C_o=0.725 gL^{-1}	9.6	3.0×10^{-4}	0.48	0.005

The increasing effluent concentrations beyond what can be accounted for by aggregation may be attributable to detachment of deposited particles. Several studies have demonstrated detachment of colloids, including nanoparticles, when deposited on silica surfaces [12, 31-33]. The results of extended Derjaguin-Landau-Verwey-Overbeek (XDLVO) [34, 35] calculations (Figure 4.S1b) for the interaction between a CMC-NZVI particle and a sand surface indicate a very high energy barrier with a sizable secondary energy minimum (on the order of 8 *kT*) where particles might be retained under this unfavorable condition for deposition [12, 36]. For particles deposited under unfavourable conditions, detachment may occur when the applied torque (T_{applied}) exceeds the adhesive torque (T_{adhesive}). The T_{adhesive} acts on a deposited particle due to particle-collector XDLVO total interaction energy and was calculated for different-sized particles in this study according to Torkzaban et al. [37]. The T_{applied} arises from the shear force and hydrodynamic drag acting on deposited particles and was calculated based on the method described by Bergendahl et al. [38]. Our calculations show that even for the smallest size particle (45 nm), $T_{\mathrm{applied}}>\mathrm{T}_{\mathrm{adhesive}}$, and with increasing particle size, $T_{\mathrm{applied}}/\mathrm{T}_{\mathrm{adhesive}}$ increases (Figure 4.S3). Therefore detachment of deposited particles due to hydrodynamic drag is likely to influence CMC-NZVI transport behavior.

To better understand the potential influence of particle detachment on the shape of the particle BTC, the aggregation-based transport model described by Equation 4.5 was extended to incorporate particle detachment from the collector surface [39] as follows:

$$\frac{\partial C}{\partial t} = D\frac{\partial^2 C}{\partial x^2} - v\frac{\partial C}{\partial x} - \sum_{i=1}^{n} k_{dep,i} C_i\ (t) + \frac{\rho k_{\mathrm{det}} S_{dep}}{\varepsilon} \tag{4.6}$$

$$\rho\frac{\partial S_{dep}}{\partial t} = \sum \varepsilon k_{dep,i} C_i\ (t) - \rho k_{\mathrm{det}} S_{dep} \tag{4.7}$$

where k_{det} is the detachment rate coefficient, S_{dep} is the concentration of particles deposited on the solid phase (mg/kg) and ρ is the bulk density of the porous medium.

According to Equations 4.6 and 4.7, as the cumulative CMC-NZVI mass deposition increases over successive PVs, the detachment of this deposited mass also increases [11, 26, 37]. The net effect is a gradual increasing trend in effluent concentrations over time. Figure 4.4b shows that the transport model that accounts for aggregation kinetics as well as particle detachment can be fitted well ($r^2>0.95$) to the experimental data obtained from column experiments. The fitted parameters in Equations 4.6 and 4.7 are k_{det} and α_{pc}, and the values are presented in Table 4.2. The single fitted value of k_{det} (0.005 min^{-1}) in this study is within the range (0.001-0.015 min^{-1}) reported in other studies conducted with latex particles of submicron to micron-sized spheres [33, 39, 40]. An additional experiment was conducted with 0.2 gL^{-1} CMC-NZVI injection for 2 PV, followed by flushing with the background electrolyte solution. A tailing of the BTC (Figure 4.S5), which is characteristic of particle detachment [40], confirmed the release of deposited CMC-NZVI from the sand grain surface. More detailed analysis on particle detachment will be addressed in future work being conducted in our laboratory.

The value of α_{pc} is expected to be constant for different concentrations of the CMC-NZVI suspensions. However, the observed increase in α_{pc} with particle concentration suggests enhanced deposition at higher influent concentrations and can be attributed to the effective increase in IS with increasing CMC-NZVI concentrations as explained in Section 3.1. The values of α_{pc} obtained in this study range from 0.20-0.48 (Table 4.2) which is comparable to those reported in other studies (0.14-0.35) conducted at a similar range of IS [9, 12].

The effect of Na^+ concentration on transport and deposition was assessed by additional column transport experiments where particle suspensions of 0.2 gL^{-1} CMC-NZVI were prepared in electrolyte solutions of 0.1 mM and 10 mM $\mathrm{NaHCO_3}$ and all other experimental parameters unchanged. The IS of 10 mM was chosen as it was similar to the effective IS of the 0.725 gL^{-1} suspension based on Na^+ concentrations (Table 4.2). Figure 4.5 shows that the relative effluent CMC-NZVI mass concentrations (C/C_0) at 8 PVs are 0.66 and 0.40 for IS of 0.1 mM and 10 mM, respectively. Indeed, the deposition of CMC-NZVI increased in the presence of higher amounts of Na^+ in the electrolyte.

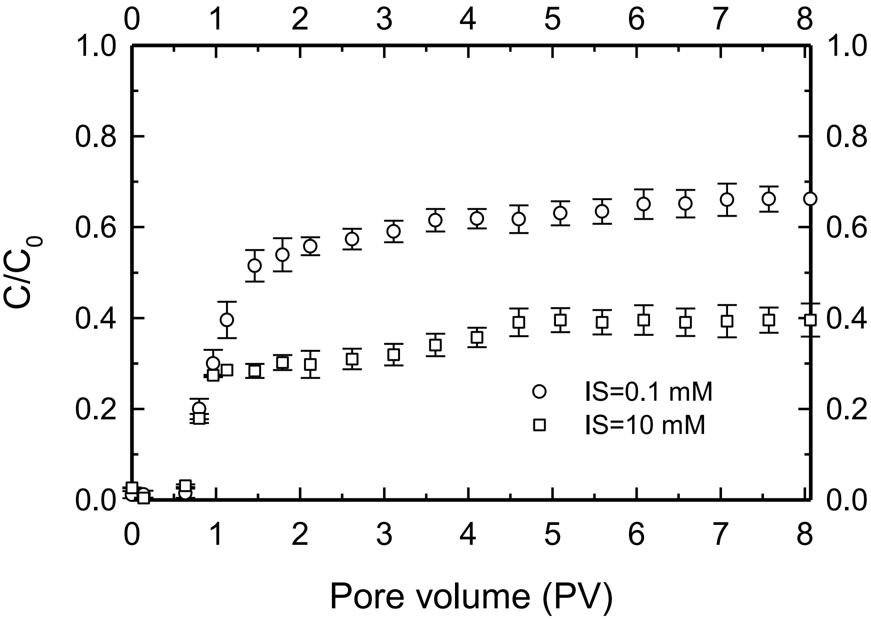

FIGURE 4.5. Breakthrough curves of CMC-NZVI for column experiments with 0.2 gL^{-1} particle suspensions prepared in 0.1 mM and 10 mM IS. The column bed depth was 9 cm and flow velocity 0.445 $cm.min^{-1}$.

4.4 Conclusion

The effects of particle concentration on aggregation and transport of CMC-NZVI was investigated. With increases in particle concentration, more rapid increase in average particle size with time was observed because of increased particle-particle attachment efficiency and number of collisions. A coupled aggregation-transport model demonstrated that the initial particle size distribution of a CMC-NZVI suspension determines the magnitude of the single-collector contact efficiency as a result of aggregation and leads to a time-dependent deposition rate coefficient. The impact of aggregation in transport is thus unsteady-state effluent concentrations. Indeed, column experiments with CMC-NZVI at different concentrations showed a gradual increase in effluent particle concentration over eight pore volumes, and the non-steady state change in effluent concentration was more rapid with increasing particle concentrations. The increases in effluent concentrations beyond approximately 4 PV were however higher than what was accounted for by fitting the coupled aggregation-transport model and it is proposed that detachment of deposited particles contributed to the increasing effluent concentrations, especially at higher PVs. Particle deposition increased with higher CMC-NZVI influent concentrations and was attributable to increases in Na^+ in solution from the higher doses of Na-CMC and $NaBH_4$ present in more concentrated particle suspensions. Such effects of CMC concentration on aqueous chemistry and transport have not been reported to date.

Acknowledgement

This research was funded by the Strategic Project Grant Program of the Natural Sciences and Engineering Research Council of Canada and by Golder Associates Ltd., as well as by Le Fonds québécois de la recherche sur la nature et les technologies Team Grant program. T.R. was supported in part by a McGill Engineering Doctoral Fellowship.

Supplementary Information

Classical colloid filtration theory

Colloid transport and deposition in granular porous media is often described by the colloid transport equation [41]

$$\frac{\partial C}{\partial t} = D\frac{\partial^2 C}{\partial x^2} - v\frac{\partial C}{\partial x} - k_{dep}C \qquad (4.S1)$$

where C is the suspended particle mass concentration, D is the hydrodynamic dispersion coefficient, v is the interstitial particle velocity and k_{dep} is the particle deposition rate coefficient, as described in the following expression:

$$k_{dep} = \left[\frac{3(1-\varepsilon)v}{2d_c\,\varepsilon}\alpha\right]\eta_0 \qquad (4.S2)$$

Here, α is the particle-collector collision efficiency, ε is porosity, d_c is the average grain size and η_0 is the single-collector contact efficiency that can be calculated using the T&E equation [42].

Physical forces acting on deposited colloids

Adhesive torque ($T_{adhesive}$) acting on a deposited particle due to particle-collector XDLVO interaction energy for different-sized particles can be calculated using the method described in Torkzaban et al. [37]. The adhesive force ($F_{adhesive} = \varphi_{min}/\delta$) was calculated from the total interaction energy at the location of the secondary minimum (φ_{min}) and the distance of the energy minimum from the particle surface (δ) as shown in Figure 4. S1b. The applied torque ($T_{applied}$) due to shear force and hydrodynamic drag ($F_{drag} = 10.2\ \pi\mu\ (\delta V/\delta r)\mathbf{a}^2$), also acts on deposited particles [38]. Here, ($\delta V/\delta r$) is the velocity gradient within the pore space due to shear on the collector surface, μ is dynamic viscosity and a is the particle radius.

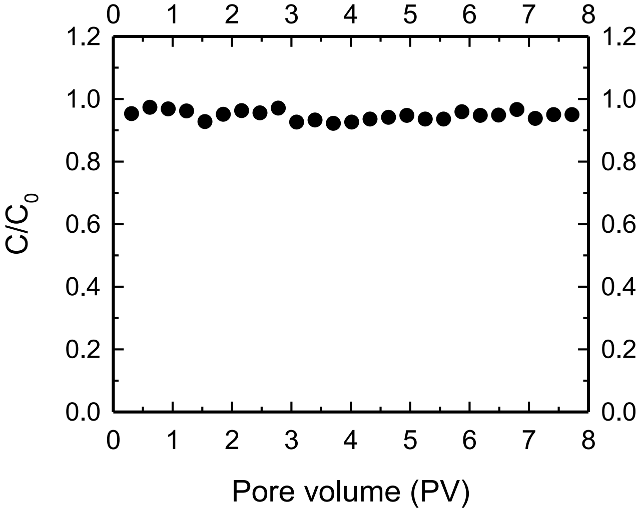

FIGURE 4.S1. CMC-NZVI concentration at inlet over time

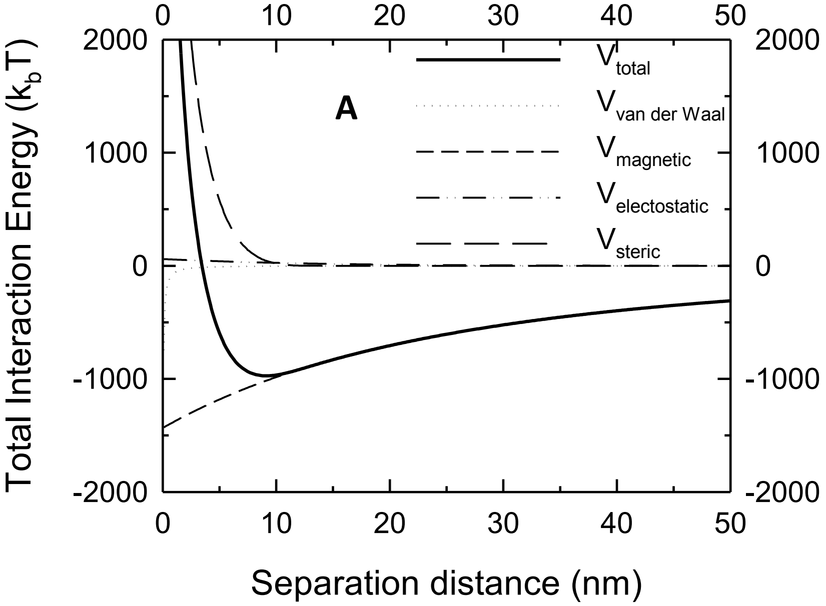

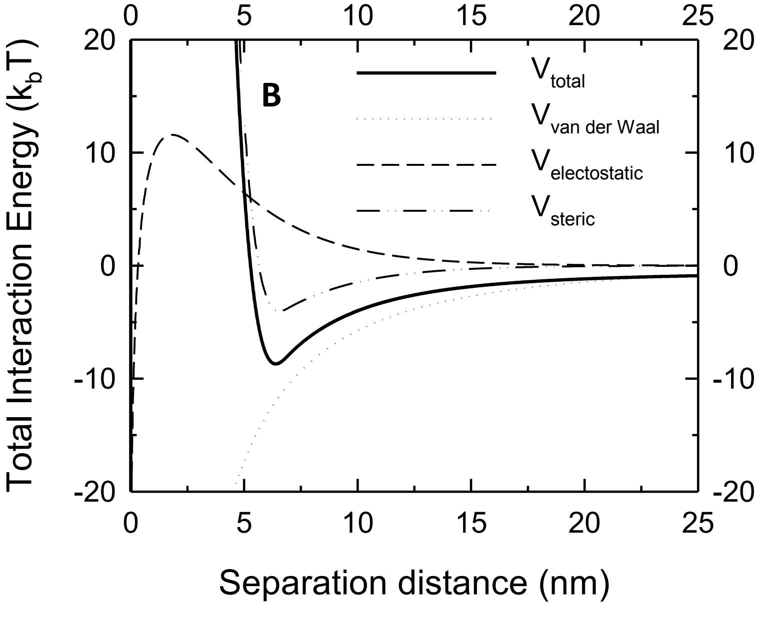

FIGURE 4.S2. Extended DLVO interaction energy calculations for CMC-NZVI (A) particle-particle and (B) sand-particle (70 nm diameter) interactions.

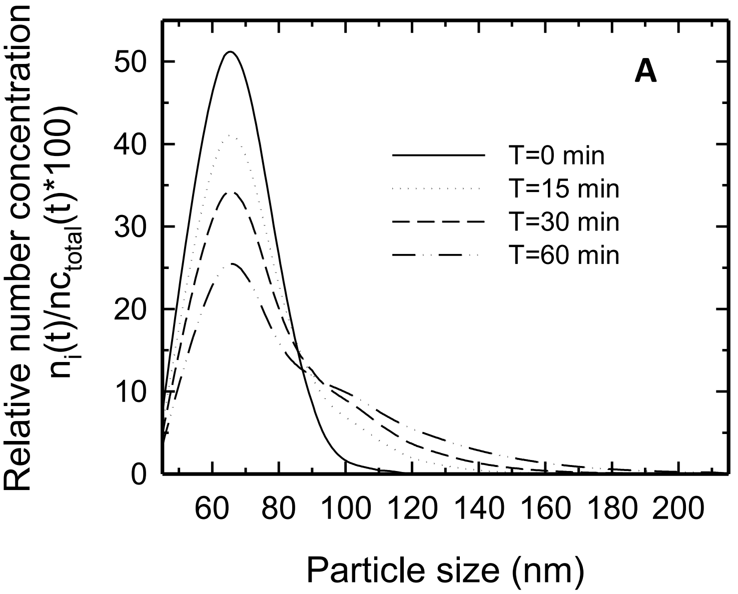

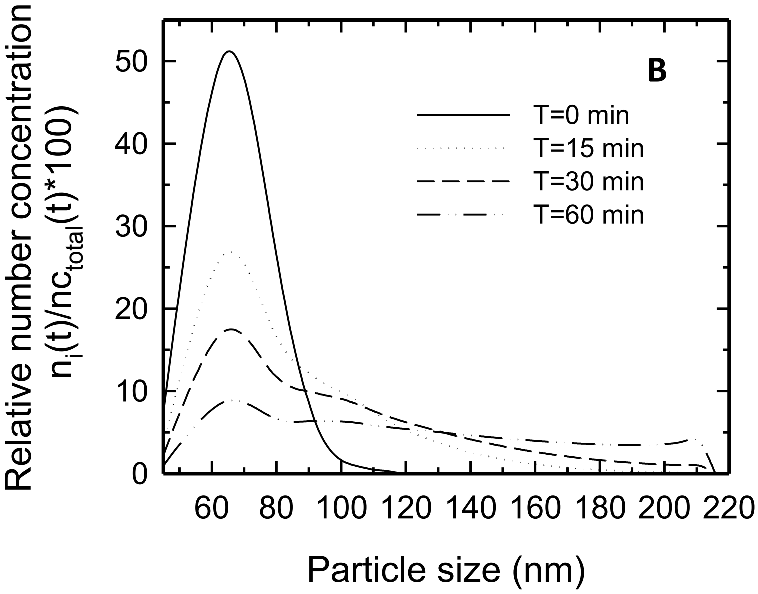

FIGURE 4.S2: Calculated particle size distributions at various times for a particle size range of 45-220 nm in particle suspensions with concentrations of (A) 0.20 gL^{-1} and (B) 0.725 gL^{-1} CMC-NZVI particles. The maximum aggregate size was set at 220 nm, as discrete aggregate sizes larger than 220 nm were not observed by TEM in particle suspensions maintained up to 65 min.

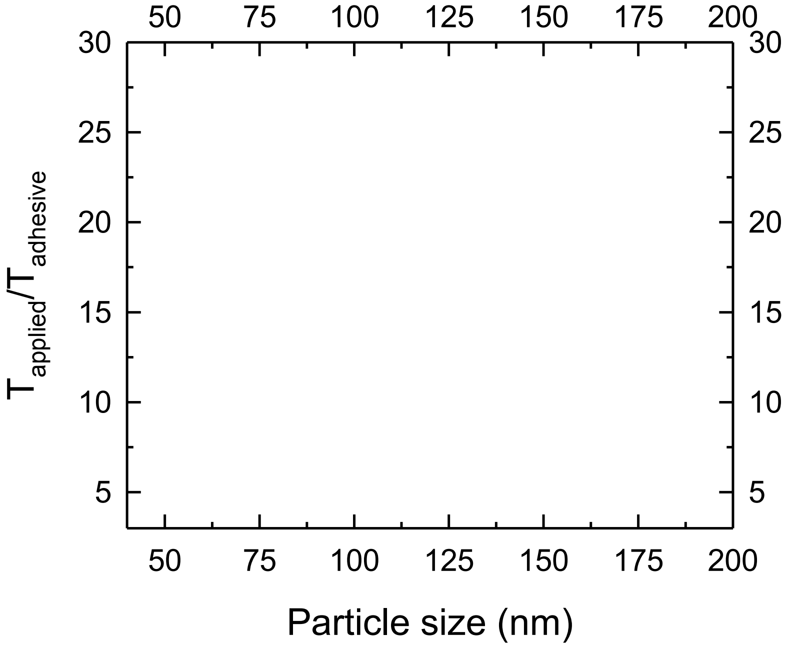

FIGURE 4.S4. Ratio of torque due to drag ($T_{applied}$) and DLVO interaction energy ($T_{adhesive}$).

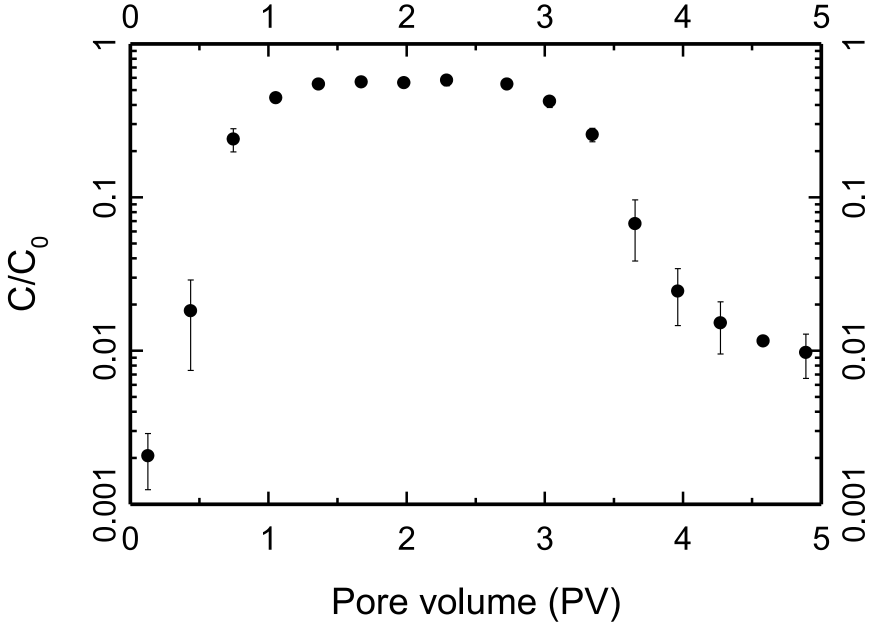

FIGURE 4.S5. Breakthrough curves of CMC-NZVI with electrolyte flushing indicate tailing effect. The column bed depth was 9 cm, particle concentration of 0.2 gL^{-1}, flow velocity 0.445 $cm.min^{-1}$ and IS was 0.1mM.

Literature Cited

[1] Tratnyek, P.G. and R.L. Johnson, *Nanotechnologies for environmental cleanup.* Nano Today, 2006. **1**(Compendex): p. 44-48.

[2] Zhang, W.-x., *Nanoscale iron particles for environmental remediation: An overview.* Journal of Nanoparticle Research, 2003. **5**: p. 10.

[3] Phenrat, T., N. Saleh, K. Sirk, R.D. Tilton and G.V. Lowry, *Aggregation and sedimentation of aqueous nanoscale zerovalent iron dispersions.* Environmental science and technology, 2007. **41**(1): p. 284-290.

[4] Kanel, S., D. Nepal, B. Manning and H. Choi, *Transport of surface-modified iron nanoparticle in porous media and application to arsenic(III) remediation.* Journal of Nanoparticle Research, 2007. **9**(5): p. 725-735.

[5] Phenrat, T., N. Saleh, K. Sirk, H.-J. Kim, R.D. Tilton and G.V. Lowry, *Stabilization of aqueous nanoscale zerovalent iron dispersions by anionic polyelectrolytes: Adsorbed anionic polyelectrolyte layer properties and their effect on aggregation and sedimentation.* Journal of Nanoparticle Research, 2008. **10**(5): p. 795-814.

[6] Saleh, N., K. Sirk, Y. Liu, T. Phenrat, B. Dufour, K. Matyjaszewski, R.D. Tilton and G.V. Lowry, *Surface modifications enhance nanoiron transport and NAPL targeting in saturated porous media.* Environmental Engineering Science, 2007. **24**(1): p. 45-57.

[7] Schrick, B., B.W. Hydutsky, J.L. Blough and T.E. Mallouk, *Delivery vehicles for zerovalent metal nanoparticles in soil and groundwater.* Chemistry of Materials, 2004. **16**(11): p. 2187-2193.

[8] He, F., M. Zhang, T. Qian and D. Zhao, *Transport of carboxymethyl cellulose stabilized iron nanoparticles in porous media: Column experiments and modeling.* Journal of Colloid and Interface Science, 2009. **334**(1): p. 96-102.

[9] Saleh, N., H.-J. Kim, T. Phenrat, K. Matyjaszewski, R.D. Tilton and G.V. Lowry, *Ionic strength and composition affect the mobility of surface-modified fe0 nanoparticles in water-saturated sand columns.* Environmental science and technology, 2008. **42**(9): p. 3349-3355.

[10] Raychoudhury, T., G. Naja and S. Ghoshal, *Assessment of transport of two polyelectrolyte-stabilized zero-valent iron nanoparticles in porous media.* Journal of Contaminant Hydrology, 2010. **118**(Compendex): p. 143-151.

[11] Phenrat, T., H.-J. Kim, F. Fagerlund, T. Illangasekare and G.V. Lowry, *Empirical correlations to estimate agglomerate size and deposition during injection of a polyelectrolyte-modified Fe0 nanoparticle at high particle concentration in saturated sand.* Journal of Contaminant Hydrology, 2010.

[12] Phenrat, T., H.-J. Kim, F. Fagerlund, T. Illangasekare, R.D. Tilton and G.V. Lowry, *Particle size distribution, concentration, and magnetic attraction affect transport of polymer-modified Fe0 nanoparticles in sand columns.* Environmental science and technology, 2009. **43**(13): p. 5079-5085.

[13] Petosa, A.R., D.P. Jaisi, I.R. Quevedo, M. Elimelech and N. Tufenkji, *Aggregation and deposition of engineered nanomaterials in aquatic*

environments: Role of physicochemical interactions. Environmental science and technology, 2010. **44**(17): p. 6532-6549.

[14] Chatterjee, J. and S.K. Gupta, *An agglomeration-based model for colloid filtration.* Environmental Science and Technology, 2009. **43**(10): p. 3694-3699.

[15] He, F. and D. Zhao, *Manipulating the size and dispersibility of zerovalent iron nanoparticles by use of carboxymethyl cellulose stabilizers.* Environmental science and technology, 2007. **41**(17): p. 6216-6221.

[16] Fatisson, J., S. Ghoshal and N. Tufenkji, *Deposition Behavior of Carboxymethylcellulose Coated Zero-valent Iron Nanoparticles onto Silica: Role of Solution Chemistry and Organic Macromolecules.* Langmuir, 2010. **26**(15).

[17] Domingos, R.F., M.A. Baalousha, Y. Ju-Nam, M.M. Reid, N. Tufenkji, J.R. Lead, G.G. Leppard and K.J. Wilkinson, *Characterizing manufactured nanoparticles in the environment: Multimethod determination of particle sizes.* Environmental science and technology, 2009. **43**(19): p. 7277-7284.

[18] Lee, D.G., J.S. Bonner, L.S. Garton, A.N.S. Ernest and R.L. Autenrieth, *Modeling coagulation kinetics incorporating fractal theories: A fractal rectilinear approach.* Water Research, 2000. **34**(7): p. 1987-2000.

[19] Lin, M.Y., H.M. Lindsay, C.R. Weitz, R. Klein and P. Meakin, *Universality in colloid aggregation.* Nature, 1989. **339**: p. 3.

[20] Trinh, L.T.T., A.-L. Kjniksen, K. Zhu, K.D. Knudsen, S. Volden, W.R. Glomm and B. Nystrom, *Slow salt-induced aggregation of citrate-covered silver particles in aqueous solutions of cellulose derivatives.* Colloid and Polymer Science, 2009. **287**(12): p. 1391-1404.

[21] Milonjic, S.K., *Aggregation/dispersion of amorphous silica particles by simultaneous adsorption of two polymers in an aqueous phase.* Colloids and Surfaces, 1992. **63**(Compendex): p. 113-113.

[22] Saleh, N.B., L.D. Pfefferle and M. Elimelech, *Influence of biomacromolecules and humic acid on the aggregation kinetics of single-walled carbon nanotubes.* Environmental science and technology, 2010. **44**(7): p. 2412-2418.

[23] Hu, J.-D., Y. Zevi, X.-M. Kou, J. Xiao, X.-J. Wang and Y. Jin, *Effect of dissolved organic matter on the stability of magnetite nanoparticles under different pH and ionic strength conditions.* Science of the Total Environment, 2010. **408**(16): p. 3477-3489.

[24] Tufenkji, N. and M. Elimelech, *Correlation Equation for Predicting Single-Collector Efficiency in Physicochemical Filtration in Saturated Porous Media.* Environmental science and technology, 2004. **38**(2): p. 529-536.

[25] Kuhnen, F., K. Barmettler, S. Bhattacharjee, M. Elimelech and R. Kretzschmar, *Transport of Iron Oxide Colloids in Packed Quartz Sand Media: Monolayer and Multilayer Deposition.* Journal of Colloid and Interface Science, 2000. **231**: p. 10.

[26] Bradford, S.A. and M. Bettahar, *Concentration dependent transport of colloids in saturated porous media.* Journal of Contaminant Hydrology, 2006. **82**(Compendex): p. 99-117.

[27] Brown, D.G., *Adaptable method for estimation of parameters describing bacteria transport through porous media from column effluent data: Optimization based on data quality and quantity.* Colloids and Surfaces A: Physicochemical and Engineering Aspects, 2007. **296**(Compendex): p. 19-28.

[28] Johnson, P.R. and M. Elimelech, *Dynamics of colloid deposition in porous media. Blocking based on random sequential adsorption.* Langmuir, 1995. **11**(Compendex): p. 801-812.

[29] Song, L. and M. Elimelech, *Dynamics of colloid deposition in porous media. Modeling the role of retained particles.* Colloids and Surfaces A: Physicochemical and Engineering Aspects, 1993. **73**(Compendex): p. 49-63.

[30] Ko, C.-H., S. Bhattacharjee and M. Elimelech, *Coupled Influence of Colloidal and Hydrodynamic Interactions on the RSA Dynamic Blocking Function for Particle Deposition onto Packed Spherical Collectors.* Journal of Colloid and Interface Science, 2000. **229**: p. 554-567.

[31] Bradford, S.A., S. Torkzaban and S.L. Walker, *Coupling of physical and chemical mechanisms of colloid straining in saturated porous media.* Water Research, 2007. **41**(13): p. 3012-3024.

[32] Quevedo, I.R. and N. Tufenkji, *Influence of solution chemistry on the deposition and detachment kinetics of a CdTe quantum dot examined using a quartz crystal microbalance.* Environmental science and technology, 2009. **43**(Compendex): p. 3176-3182.

[33] Tong, M. and W.P. Johnson, *Excess colloid retention in porous media as a function of colloid size, fluid velocity, and grain angularity.* Environmental science and technology, 2006. **40**(Compendex): p. 7725-7731.

[34] Gregory, J., *Interaction of Unequal Double Layers at Constant Charge.* Journal of Colloid and Interface Science, 1975. **51**(1): p. 45-51.

[35] de Gennes, P.G., *POLYMERS AT AN INTERFACE: A SIMPLIFIED VIEW.* Advances in Colloid and Interface Science, 1987. **27**(Compendex): p. 189-209.

[36] Chen, K.L. and M. Elimelech, *Interaction of fullerene (C60) nanoparticles with humic acid and alginate coated silica surfaces: Measurements, mechanisms, and environmental implications.* Environmental science and technology, 2008. **42**(Compendex): p. 7607-7614.

[37] Torkzaban, S., S.A. Bradford and S.L. Walker, *Resolving the coupled effects of hydrodynamics and DLVO forces on colloid attachment in porous media.* Langmuir, 2007. **23**(19): p. 9652-9660.

[38] Bergendahl, J. and D. Grasso, *Prediction of colloid detachment in a model porous media: Hydrodynamics.* Chemical Engineering Science, 2000. **55**(Compendex): p. 1523-1532.

[39] Bradford, S.A., J. Simunek, M. Bettahar, M.T. Van Genuchten and S.R. Yates, *Modeling colloid attachment, straining, and exclusion in saturated porous media.* Environmental science and technology, 2003. **37**(Compendex): p. 2242-2250.

[40] Li, X., P. Zhang, C.L. Lin and W.P. Johnson, *Role of hydrodynamic drag on microsphere deposition and re-entrainment in porous media under unfavorable conditions.* Environmental science and technology, 2005. **39**(Compendex): p. 4012-4020.

[41] Tufenkji, N., J.A. Redman and M. Elimelech, *Interpreting deposition patterns of microbial particles in laboratory-scale column experiments.* Environmental Science and Technology, 2003. **37**(Compendex): p. 616-623.

[42] Tufenkji, N. and M. Elimelech, *Correlation Equation for Predicting Single-Collector Efficiency in Physicochemical Filtration in Saturated Porous Media.* Environmental science and technology, 2004. **38**(Compendex): p. 529-536.

Connecting text: Chapter 4 and chapter 5

In Chapter 4, the aggregation behaviour of CMC-NZVI and its effect on particle transport were assessed and detachment of particles at higher pore volumes was observed. This is because the particles are deposited in the secondary energy minima and hydrodynamic drag force applied on deposited particles resulted in detachment when the solid phase deposited mass is significant. Considering the fact that particles are deposited in secondary minima, significance of physical colloid retention mechanisms such as straining on CMC-NZVI transport in porous media was evaluated in Chapter 5.

Chapter 5

Straining of CMC-NZVI during Transport through Porous Media

Trishikhi Raychoudhury[1], Nathalie Tufenkji[2], Subhasis Ghoshal[1,*]

[1] *Department of Civil Engineering, McGill University, Montreal, Quebec,*
Canada H3A 2K6
[2] *Department of Chemical Engineering, McGill University, Montreal, Quebec,*
Canada H3A 2B2

To be submitted to
Environmental Science and Technology

5.1 Introduction

The direct injection of reactive nanoscale zero valent iron (NZVI) particles into aquifers is an emerging technology for *in situ* remediation of groundwater contaminated by chlorinated organic compounds [1-3]. A number of studies have demonstrated that colloidal stabilization of NZVI particles by coating with polymers or polyelectrolytes is necessary for facilitating particle transport in subsurface porous media [4, 5]. Several biodegradable and non-toxic polyelectrolytes have been identified, which when sorbed or bonded to the NZVI particle surface, provide significant electrosteric stabilization against the strong inter-particle magnetic attractive forces [4-9].

The deposition of NZVI particles in subsurface granular porous media is influenced by several factors such as the size and aggregation state of the nanoparticles, the surface chemistry of the nanoparticles, the chemistry of the pore fluid, the fluid velocity, and porous media properties (e.g., grain size, shape and surface chemistry) [8, 10-12]. Due to charge screening, the surface potential at the polyelectrolyte-coated NZVI and collector surfaces becomes less negative with increasing IS of the background electrolyte solution, and this may lead to greater particle-particle aggregation and particle deposition [8, 13, 14]. The extent to which the IS can impact NZVI particle deposition however depends on the electrostatic and steric repulsion of the polyelecrolyte coating on the NZVI, the cation type, as well as the presence of polymeric macromolecules in the aqueous solution [8]. The retention of surface-modified NZVI has been reported to decrease with increasing approach velocities and this is attributed to the significant drag forces at higher velocities that promote detachment of deposited particles [5, 6, 12, 14].

However, even under unfavourable deposition conditions, such as low ionic strength where there is high electrostatic repulsion between similarly charged colloid and collector surfaces, significant colloid retention has been observed, and is attributed to mechanisms such as straining and wedging of colloids between collector grains, attachment of particles at the secondary minimum or at charge heterogeneities on collector surfaces [8, 15-18]. To assess the patterns and extent of colloid retention specifically due to straining, Bradford et al. [19, 20] injected sub-micron or micron-sized latex colloids (0.45 μm to 3.2 μm) into columns packed with sands of different diameters (150 μm to 740 μm). Their studies showed that particle straining or entrapment of particles in pore throats that are too small to allow their passage, resulted in hyper-exponential particle retention profiles along the column depth. Straining was found to be significant for ratios of particle diameter (d_p) to collector diameter (d_c) in the range of 0.002 to 0.06, and straining increased with decreasing sand grain size. Johnson et al. [21] demonstrated that wedging or particle retention at grain-to-grain contacts is favourable for d_p/d_c ratios greater than 0.005 and wedging increased with decreasing water flow velocity. They also suggested that the effect of flow stagnation zones on colloid retention becomes important with a d_p/d_c ratio less than 0.005. Tong et al. [22] demonstrated that retention of polystyrene latex particles of 0.1 -2 μm in porous media not only depends on colloid-collector size ratio, but also on grain angularity, grain-to-grain contact length and the drag force on the deposited particles. Bradford et al [23] have suggested that the small pore region surrounded by grain-to-grain contact points are unfavourable locations for hydrodynamic drag, and thus may be potential locations for particle retention or straining sites.

Recently, a few studies have suggested that nanoparticles of haematite, maghemite and maghemite/nickel of diameters in the range of 15-50 nm, and single-walled carbon nanotubes of hydrodynamic diameters of 122 nm can be retained in packed columns of sand or soil due to straining [24, 25]. Tosco and Sethi [26] have also suggested that straining increases the retention of xanthun gum stabilized NZVI particles of 70 nm diameter in porous media. However, these studies have not characterized and confirmed the straining patterns systematically by assessing transport and retention of the particles in range of sand sizes.

The objective of this study is to assess whether straining can be a dominant retention mechanism during transport of CMC-NZVI in subsurface granular media. Column transport experiments were conducted where the CMC-NZVI effluent breakthrough patterns were assessed as a function of time. The size of CMC-NZVI particles in the suspensions injected in the column was stable with time. Following each transport experiment, the packed columns were sectioned and the CMC-NZVI retention profile along the column length was analyzed. Because straining is dependent on pore size and thus on sand grain size, four different sand sizes were selected for this study. The application of NZVI for remediation requires its injection into aquifers at concentrations up to several gL^{-1}. Thus, the column experiments were conducted with CMC-NZVI concentrations ranging up to 1.7 gL^{-1}. Two colloid transport models considering 1) particle deposition by attachment and 2) straining along with particle deposition by attachment were fitted to the experimental data to evaluate the significance of straining.

5.2 Theoretical Background

Nanoparticle transport in granular porous media is often described by the colloid transport equation that accounts for advection, dispersion and deposition of colloids due to attachment to collector surfaces [17, 27, 28]. Particle retention due to straining could be represented by modifications to the colloid transport equations as shown in Equations 5.1-5.3 [19]. Conceptually, particle retention due to straining and/or wedging occurs primarily at the column inlet. This is because at the inlet, colloids enter a larger number of grain-to-grain contact points or small pores that are too narrow for the colloids to pass through. Colloids entering the column after these pores are clogged are channelled through larger pores and eventually the colloids are transported selectively through connected wider pore networks. Transport through wide pore networks and bypassing of narrow pores towards the end of the column causes limited straining at greater depths.

To incorporate depth-dependent straining, a colloid straining function, $\psi_{str,}$ was introduced with the straining rate coefficient as shown in Equation 5.1. The straining function ψ_{str} is inversely related with the column length x as described below.

$$\frac{\partial C}{\partial t} = D\frac{\partial^2 C}{\partial x^2} - v_x\frac{\partial C}{\partial x} - k_{att}C - k_{str}\psi_{str}C \tag{5.1}$$

$$\rho\frac{\delta S_{att}}{\delta t} = \varepsilon k_{att}C \tag{5.2}$$

$$\rho\frac{\delta S_{str}}{\delta t} = \varepsilon k_{str}\psi_{str}C \tag{5.3}$$

where, C (ML^{-3}) is the suspended particle mass concentration and varies with the distance x (L) and time t (T). D (L^2T^{-1}) is the hydrodynamic dispersion coefficient, v_x (LT^{-1}) is the pore water velocity, ρ (ML^{-3}) is the bulk density of sandand k_{att} (T^{-1}) is the particle attachment rate coefficient accounting for the deposition of particles due to the net interaction energies due to electrostatic, steric and van der Waals forces. . k_{str} (T^{-1}) is the straining rate coefficient, and ψ_{str} is the dimensionless colloid straining function expressed by $\psi_{str} = (\frac{d_c}{d_c + x})^{\beta'}$. The parameter β' describes the shape of the spatial distribution of strained particles and S_{att} is the attached mass and S_{str} is the strained mass of particles. In the absence of straining, k_{str} (T^{-1}) is zero, and the equation reduces to the traditional colloid transport equation [17, 27, 28].

The overall particle attachment rate coefficient (k_{att}) presented in Equation 5.4 is related to the attachment efficiency (α_{pc}) between a particle and a collector and the single-collector contact efficiency (η_0).

$$k_{att} = \left[\frac{3(1-\varepsilon)v}{2d_c\varepsilon}\alpha_{pc}\right]\eta_0 \tag{5.4}$$

where, α_{pc}, is the attachment efficiency, v (LT^{-1}) is the_Darcy's velocity, d_c (L) is the average grain size and η_0 is the single-collector contact efficiency which can be calculated using the Tufenkji and Elimelech equation [29].

In this study, the experimental data was compared with two colloid transport models. Model 1 accounts for colloid transport due to 1-D advection, dispersion, and deposition only due to particle attachment. The solid phase deposition of CMC-NZVI due to particle attachment was evaluated by considering Equation 5.2

which neglects straining of particles. In Model 2, the solid phase deposition due to attachment and straining (S=S_{att}+S_{str}) was calculated using Equations 5.2 and 5.3. The straining rate coefficient was fitted to the experimentally determined CMC-NZVI breakthrough curves and retention profiles. The Marquardt algorithm for nonlinear least square optimization was used to determine the best fit straining parameters [30, 31]. The sum of least squares for the effluent concentration and the solid phase deposition data from the column experiments and the model calculations were minimized simultaneously.

5.3 Materials and Method

All chemicals were reagent grade and all solutions were prepared using Milli-Q-UV Plus Ultrapure water (Millipore, MA, USA).

5.3.1 Synthesis and Characterization of CMC-NZVI:

The CMC-NZVI preparation method was adapted from He and Zhao [32]. Briefly, an aqueous solution of 0.055M ferrous sulphate heptahydrate ($FeSO_4 \cdot 7H_2O$, AlfaAesar, purity greater than 99%) was added to 5 gL^{-1} of CMC (90K, Sigma-Aldrich) solution and mixed thoroughly for 30 minutes and then the solution was reduced by the drop-wise addition of sodium borohydride solution ($NaBH_4$, Sigma-Aldrich) under N_2 atmosphere. The mixture was then dried overnight and stored under N_2.

CMC-NZVI suspensions having three different concentrations (0.085 gL^{-1}, 0.35 gL^{-1} and 1.7gL^{-1}) prepared in 0.1 mM $NaHCO_3$, by sonicating with a 40 kHz ultrasonic cleaner (Cole-Palmer 8891) for 10 min to ensure homogeneity of the suspensions and then the suspensions were stirred for 90 min. The application of NZVI for remediation requires its injection into aquifers at concentrations up to several gL^{-1}. Thus, a range of particle concentrations up to 1.7 gL^{-1} were employed. Particles sizes were assessed at different time points to ensure that 90 min was sufficient to attain stable particle sizes. The mean hydrodynamic diameter was determined by nanoparticle tracking analyzer (NTA, NanoSight LM10). Concentrated stock suspension of CMC-NZVI of three different concentrations (0.085, 0.35 and 1.7gFe L^{-1}) in 0.1 mM $NaHCO_3$ was filled in a vial under N_2 atmosphere to zero headspace and was diluted to 6 mgL^{-1} immediately prior to NTA measurement. The NTA calculates the mean square displacements of single particles by tracking the path of scattered light. The mean particle hydrodynamic diameters were derived from the diffusion coefficients which are determined from a series of single-particle Brownian motion tracked over time [33].

The particle hydrodynamic diameters after 90 min of mixing, d_p, for the three CMC-NZVI suspensions of different concentrations, as measured by NTA are presented in Table 5.2. These hydrodynamic diameters were used to calculate BTCs and retention profiles for all experimental conditions. The particle hydrodynamic diameters were in the range of 167 to 185 nm. The mean diameter of the NZVI particles from TEM analyses of CMC-NZVI suspensions after 90 min of mixing was in the range of 85±15 nm. Thus the zero valent iron particles in this study are referred to as nanoparticles. The details of the TEM analyses are given elsewhere [5].

5.3.2 Packed column experiments:

A glass column (Konets Chromoflex) of 1 cm i.d. and packed bed length of 9 cm was used. A nylon mesh (100 μm) was placed at the bottom of the packed column to prevent sand grains from being displaced into the end adapters. Two batches of UNIMIN sand (UNIMIN Corp, WI, USA), Unimin 4020 and Unimin 2030 were acid washed with 12 N concentrated HCl, rinsed with DI water and oven-dried for 3 hours at 550ºC. The washed sands were sieved using nylon mesh and the average size of sands was determined by averaging the sieve sizes, as the sands had very limited particle size distributions. The sample labelled as F2025 passed through a 850 μm sieve (F20) and was retained on a 700 μm (F25) sieve, and thus its average particle diameter was 775 μm. The F3040 sand passed through 600 μm (F30) mesh sieve and was retained on 420 μm (F40) sieve, and had an average diameter of 510 μm. The finer sand, F5070 passed through 300 μm (F50) sieve and was retained on 210 μm (F70) sieve, with an average diameter of 250 μm and, finally, the finest sand, F70140, passed through 210 μm (F70) sieve and was retained on a 100 μm (F140) sieve, with an average diameter of 150 μm. Details of sand sizes and other properties are given in Table 5.1.

Table 5.1 Experimental conditions and different parameters for column transport experiments

Column length, *L*	9 cm
Nanoiron concentration of the column feed, C_0	0.085, 0.35 or 1.7 gL^{-1}
Interstitial velocity, *v*	0.445 cmmin^{-1}
Packing density of dry sand in the packed-bed, ρ_b	1.95 g cm^{-3}
Thickness of CMC layer	7 nm
Density of the nanoparticles	6.7 x10^{3} kgm^{-3}
pH of the CMC-NZVI suspension	7.4±0.4
Ionic strength of electrolyte solution as prepared	0.1 mM of NaHCO3
Dispersion coefficient, *D*	0.13 cm^{2}min^{-1} (775-150 μm)
Porosity, ε	0.35 (775 μm), 0.32 (510-150 μm)

The column was dry-packed with sand and vibrated intermittently to ensure uniform packing and then saturated with CO_2 to ensure removal of air bubbles. The column was then connected to a syringe pump (KD Scientific) and eight pore volumes (PVs) of background electrolyte of 0.1 mM $NaHCO_3$ were injected (0.89 cm min^{-1}) from the bottom of the column to equilibrate the granular medium. Next, 7 PVs of the electrolyte were injected at 0.445 cm min^{-1} from the top of the column prior to injecting a suspension of CMC-NZVI or the tracer (KNO_3). The KNO_3 solution was injected at the same flow rate through all four types of sand packed columns to determine the hydrodynamic dispersion coefficient (*D*). The porosity (ε) and the value of dispersion coefficient, *D* of the columns containing the different sands are presented in Table 5.1.

The influent CMC-NZVI suspensions were prepared at different Fe particle concentrations of 0.085, 0.35 and 1.7 gL^{-1} in 0.1 mM $NaHCO_3$ as described earlier andpumped downwards at a velocity of 0.445 cm min^{-1} using a syringe pump. The particle suspension pH was 7.4±0.4. Settling of the CMC-NZVI in the syringe was prevented by internal stirring. CMC-NZVI was injected for 2.1 PVs for the three finer sized sands (510-150μm) and 1.8 PVs for the coarser sand of 775 μm diameter (F2025). Thereafter, several PVs of electrolyte were flushed from the top of the column at the same flow rate as CMC-NZVI injection. At the end of the transport experiment, the porous media was dissected to obtain the mass of iron distributed along the column length. During the sectioning process the column was not tapped or otherwise disturbed to avoid displacement of CMC-NZVI from the sand grain surfaces. The sectioned sand samples were digested in the HCl-HNO_3 mixture for 48 hours such that the deposited iron particles on the sand were dissolved in the solution. The collected samples were analyzed for total iron as mentioned below. The sand samples were washed with DI water and oven-dried for 24 hours to obtain the dry weight of each segment of the sand bed. The iron concentration in samples was determined by dissolving the samples in concentrated HCl-HNO_3 mixture, and analyzing for total iron using flame atomic absorption spectrometry (Perkin Elmer 3110) at a wavelength of 249.7 nm. All experiments were done in duplicate and the average of replicate experiments is reported.

5.4 Results and Discussion

5.4.1 Transport of CMC-NZVI at Different Concentrations through Coarse and Fine Sands

CMC-NZVI transport experiments were conducted using columns packed with clean sand having four different mean grain diameters (150 μm, 250 μm, 510 μm and 775 μm) at three different CMC-NZVI influent concentrations of 0.085 gL^{-1}, 0.35 gL^{-1} and 1.70 gL^{-1}, in a solution of 0.1 mM IS. Figure 5.1 shows the breakthrough curves (BTCs) and retention profiles of the solid-phase associated CMC-NZVI for the experiments conducted with 0.085 gL^{-1} (Fe) nanoparticle suspensions using four different-sized sands. Similar results were obtained with the 0.35 and 1.70 gL^{-1} CMC-NZVI suspensions and are shown in Figure 5.S1 and S2.

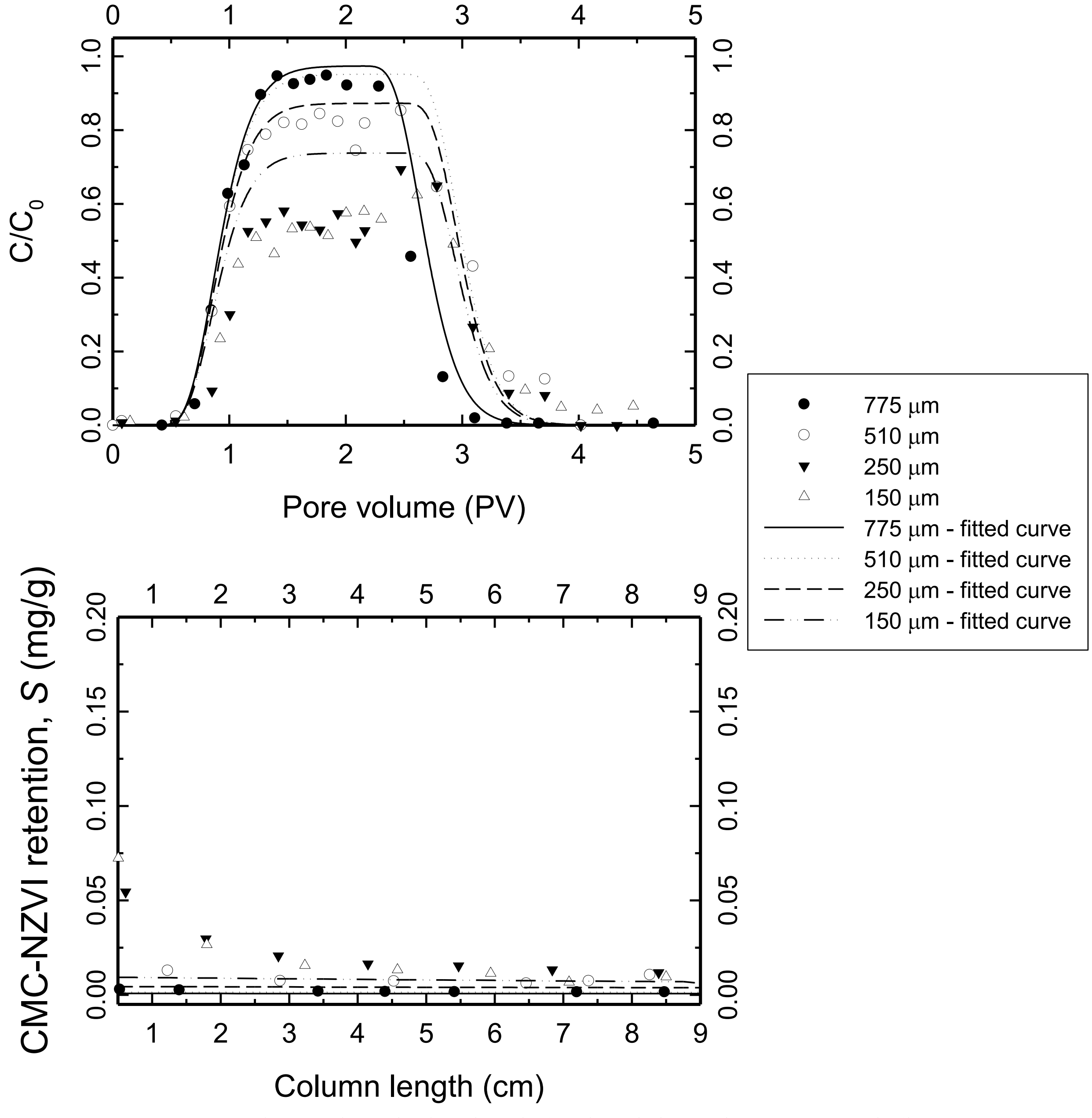

FIGURE 5.1. Experimental and simulated (a) breakthrough curves and (b) retention profiles along the column length of CMC-NZVI through different sized sands packed columns of L =9.0 cm, C_0 = 0.085 g•L^{-1}, considering Model 1

Figure 5.1 demonstrates that for the coarsest sand (775 μm) there was near-complete breakthrough of the 0.085 gL^{-1} CMC-NZVI suspension with a relative effluent concentration (C/C_0) of 0.95 at 2 PVs. Furthermore, with decreasing average diameter of the sand, the breakthrough value of C/C_0 decreased, indicating greater CMC–NZVI retention. The C/C_0 decreased from 0.84 for the 510 μm diameter sand to 0.57 for the 250 μm diameter sand and to 0.55 for the 150 μm sand (Table 5.2). Figure 5.1b (and Figures 5.S1b, 5.S2b) suggests that retention of CMC-NZVI particles at the column inlet increases as the sand size decreases for all three CMC-NZVI influent concentrations. A tailing effect in the BTC with continued flushing beyond 3 PV, was observed for all cases. This result can be attributed to particle detachment [34, 35].

The mass of CMC-NZVI (measured as total Fe) retained in the column as determined from the sectioning data and the mass of CMC-NZVI eluted based on the BTC were used to evaluate the mass balances of Fe. The overall mass balances of total CMC-NZVI injects (denoted as M_{balance}) were achieved approximately 87-99 % for the various experiments, and are presented in Table 5.2. The increase in colloid deposition with decreasing collector grain size and the hyper-exponential particle retention patterns along the column length, have been previously attributed to straining in several studies [18-20].

Transport conducted with different CMC-NZVI concentrations showed that normalized effluent concentrations did not vary significantly with changes in influent concentrations in the range 0.085-1.70 gL^{-1} (Figures 5.1, 5.S1 and 5.S2). Phenrat et al. [11] characterized the transport of polyelectrolyte-coated hematite and zero valent iron nanoparticle. In that study, there was no significant effect of particle concentration on the transport if PSS-modified *hematite* nanoparticles in the concentration range of 30 mg/L to 6 g/L or for PSS-*NZVI* in the concentration range of 1-6 g/L. However, the C/C_0 of PSS-NZVI was lower at influent concentrations at the g/L level compared to mg/L levels. It was proposed that only with PSS-NZVI at the g/L concentration, there were formation of large aggregates that resulted in greater retention. In our study, the mean particle diameters for the range of CMC-NZVI concentrations in the influent (0.085-1.7 gL^{-1}) varied to a limited extent (167-185 nm) compared to the range reported by Phenrat et al (45-367 nm) for PSS-NZVI.

Table 5.2: Transport results and strained mass at different experimental conditions

Sand grade	d_c (μm)	d_p (NTA)	C_0 (g/L)	C/C_0	η_0	M_{balance} (%)	k_{att} (min^{-1})	k_{str} (min^{-1})	$M_{\text{str, L=0-2}}$ (%)	$M_{\text{str, L=2-9}}$ (%)	r_{C/C_0}^2	r_S^2
F2025	775	167	0.085	0.95	0.0029	88.5	0.0039	0.00	0.00	0.00	0.99	1.00
	775	183	0.35	0.97	0.0029	92.5	0.0039	0.09	2.45	3.17	0.93	0.99
	775	185	1.70	0.89	0.0029	94.8	0.0039	0.09	2.45	3.17	0.97	0.99
F3040	510	167	0.085	0.84	0.0034	98.0	0.007	0.37	6.70	7.98	0.98	0.89
	510	183	0.35	0.82	0.0034	95.5	0.007	0.43	7.88	9.26	0.93	0.95
	510	185	1.70	0.77	0.0034	97.6	0.007	0.43	7.88	9.26	0.95	0.90
F5070	250	167	0.085	0.57	0.0048	98.9	0.0202	1.21	13.10	13.62	0.92	0.90
	250	183	0.35	0.67	0.0046	95.5	0.0194	1.12	12.41	13.04	0.90	0.99
	250	185	1.70	0.6	0.0046	92.0	0.0194	1.12	12.41	13.04	0.96	0.99
F70140	150	167	0.085	0.55	0.0062	92.8	0.0436	1.61	12.58	12.17	0.96	0.99
	150	183	0.35	0.62	0.0060	92.7	0.0421	1.74	13.50	12.98	0.90	0.99
	150	185	1.70	0.60	0.0060	86.7	0.0482	1.74	13.50	12.98	0.93	0.99

Several studies have reported an effect of concentration on colloid retention. For example, Bradford et al. [23] and Bradford and Bettahar [18] conducted column transport experiments with micron sized latex particles, and showed that the C/C_0 increases with influent concentration. Those authors explained that these observations were caused by the fraction of the total injected colloid mass that is retained due to straining decreasing with the total injected colloid mass. The existence of a maximum straining capacity [27] , or hindered straining at high colloid concentrations has been discussed in the literature [23, 37, 38]. Kuhnen et al. [27], have demonstrated that with increase in influent iron oxide particles concentrations, a higher C/C_0 was achieved due to blocking of collector surface. However, our results showed that the normalized effluent particle concentration only varies slightly (less than 10%) with changes in input concentration suggesting that blocking of collector grain surfaces or hindered straining did not play a significant role in this study.

Generally, the reasons for increased CMC-NZVI retention with decreasing sand size could be: a) change in single-collector contact efficiency with average sand grain size (e.g., η_0 increases ~two fold (from 0.0029 to 0.006) as the sand size decreases from 775 μm to 150 μm); b) straining and/or wedging at small pores or grain-to-grain contact points; and c) larger specific surface area available for attachment on finer sands compared to coarser sands. However, the sand surface coverage by retained particles were calculated according to methods described elsewhere [36], which suggests that the fraction of collector surface covered by CMC-NZVI is quite low (in the range of 10^{-5}-10^{-4}) for the different sands. In addition, particle transport with different concentration as described above revealed blocking of collector surface is not relevant here. Therefore, in this study the increased retention in columns for finer sands cannot be accounted for by their higher available surface area for CMC-NZVI attachment. Thus the following sections discuss the relevance of the single collector contact efficiency and straining of CMC-NZVI during transport through sand packed column.

5.4.2 Model 1: Particle Attachment to Sand Surfaces

The CMC-NZVI BTCs and mass retention profiles along the column length were compared to results calculated using Model 1, which represents CMC-NZVI retention by attachment on collector surfaces only, without consideration of straining. The model calculations are presented in Figures 5.1 (and 5.S1, 5.S2). In this model, particle attachment rate coefficients vary with sand size due to the change in the single-collector contact efficiency (η_0). Single-collector contact efficiencies (η_0) for the four different sands at three different CMC-NZVI concentrations (which produced three different d_p) were calculated using the Tufenkji and Elimelech equation [37] and are presented in Table 5.2. A value of α_{pc}=0.085 was obtained by fitting Model 1 to the BTC and retention profile corresponding to the lowest CMC-NZVI concentration (0.085 gL^{-1}) in the coarsest sand (775 μm) which had negligible straining of CMC-NZVI as discussed in the following section (Table 5.2). The same value of α_{pc} was employed for calculating the BTCs and retention profiles for all other scenarios.

Figure 5.1, showed that calculated BTC and retention profile of 0.085gL^{-1} CMC-NZVI (d_p=167 nm) transported through 775 μm sand, which have a lowest d_p/d_c ratio of 0.0022, fitted well with the experimental data with r^2 (r_s^2 and r_{c/c_0}^2) > 0.99 (Table 5.2). The predicted BTC using α_{pc}=0.085, for the coarsest sand (d_c=775 μm) with higher CMC-NZVI concentrations of 0.35 and 1.7 gL^{-1} (d_p=183nm and 185nm), were close to the experimental data (Figure 5.S1a, 5.S2a), however the measured particle retention towards the column inlet were slightly higher compared to the model prediction (Figure 5.S1b, 5.S2b). For sands of other sizes (d_c=510 μm, d_c=250 μm and d_c=150 μm), the calculated BTCs exceed the measured normalized effluent particle concentration for all of the experimental conditions (Figures 5.1a, 5.S1a and 5.S2a). In the case of the sands ranging from 510 to 150μm mean size the measured particle retention near the column inlet for all CMC-NZVI suspension conditions were much higher compared to the model predictions (Figures 5.1b, 5.S1b and 5.S2b). Thus, Model 1, which accounts for particle attachment on different-sized collectors, does not adequately account for the retention profiles observed for the three different CMC-NZVI suspensions.

5.4.3 Model 2: Particle Attachment and Straining

The clear trend of increasing retention of CMC-NZVI in finer sands and high CMC-NZVI mass retention at the column inlet is likely attributable to straining (Figures 5.1, 5.S1-5.S2). Figures 5.2-5.4 show that predictions with Model 2, which account for both straining and deposition of CMC-NZVI are in good agreement (r_s^2 and $r_{c/c_0}^2 > 0.9$) with the experimental BTCs and retention profiles for twelve individual experimental scenarios. Model 2 has two fitting parameters, the straining rate coefficient (k_{str}), which is dependent on the relative size of particles and sands, and β'. A single value of β' is used to describe the spatial distribution of strained particles over a wide range of colloid and collector sizes [19]. The best fits shown in Figures 5.2-5.4 were achieved with fixed values of α_{pc} (=0.085) and a fitted value of β' (=0.67). The value of k_{att} was calculated from η_0 and α_{pc}. All parameter values are presented in Table 5.2.

The straining rate coefficients determined in this study vary from 0.09 min^{-1} to 1.74 min^{-1}, and are within the range of reported values. Bradford et al. [19] have reported k_{str} in the range of 7×10^{-3}-1.2 min^{-1} for carboxyl functionalized latex particles of 0.45-3.2 μm diameter through Ottawa sand of 150-740 μm in size. Xu et al. [38] have obtained straining rate coefficients in the range of 4×10^{-3}-0.6 min^{-1}, with latex particles 0.5-5 μm in diameter through 98-780 μm diameter sand grains. Tosco and Sethi [26] have found straining rate coefficients in the range of 0.5 min^{-1} to 25.6 min^{-1} with micro- (1.1 μm) and nano- (70 nm) scale polymer-coated zero valent iron particles transported through 690 μm diameter silica sand. Several studies have found that nanoparticles can be removed from pore waters by straining [24-26]. Hong et al. [39] have suggested that haematite, maghemite and maghemite/nickel particles of diameters in the range of 15-50 nm (as measured by TEM), can be retained during transport due to straining. In their study, it was observed that particles that were more magnetic, and thus aggregated more significantly, had a higher retention in the column during transport experiments, and the retention was particularly significant at the column inlet. Tosco and Sethi [26] also suggest that straining contributed to the retention of xanthum gum-stabilized NZVI particles of diameter 70 nm (as determined by TEM imaging). However, none of the above studies performed systematic analysis of straining with a range of sand size, which is very sensitive parameter for assessing straining, as was done in this study. BTCs and NZVI retention profiles had a better fit to colloid transport equations that accounted for straining along with attachment.

The change in the straining rate coefficient as a function of the ratio of the mean CMC-NZVI particle hydrodynamic diameter (based on NTA image analysis) and the mean sand diameter is presented in Figure 5.5. The straining rate coefficient shows a linear relationship with the d_p/d_c ratio (r^2=0.97). In this study, the CMC-NZVI particle hydrodynamic diameters fall within a narrow range for all transport experiments and the results in Figure 5.5 suggests that the straining rate coefficient increases linearly with the diameter of the sand grains. The d_p/d_c ratio varied from 2.2×10^{-4} to 1.23×10^{-3}, which is within the range observed previously [19, 24, 26, 40]. Changes in the straining rate coefficient with the d_p/d_c ratio have also been reported elsewhere. Xu et al. [38] found that the straining rate coefficient varies linearly within a d_p/d_c range of 0.008-0.052, whereas Bradford et al. [19] demonstrated a power relationship of $(d_p/d_c)^{1.42}$ with the straining rate coefficient.

From the Figures (Figure 5.2-5.4), it was observed that the particle retention was very high towards the column inlet due to straining. To better understand the spatial distribution of strained mass the percentage of strained mass (to the total injected CMC-NZVI) at the inlet (within 2 cm of column length) and beyond 2cm of column length was calculated from the model. The percentage at the column inlet was denoted by $M_{str,L=0-2}$ and beyond this point it was denoted by $M_{str,L=2-9}$ and presented in Table 5.2.

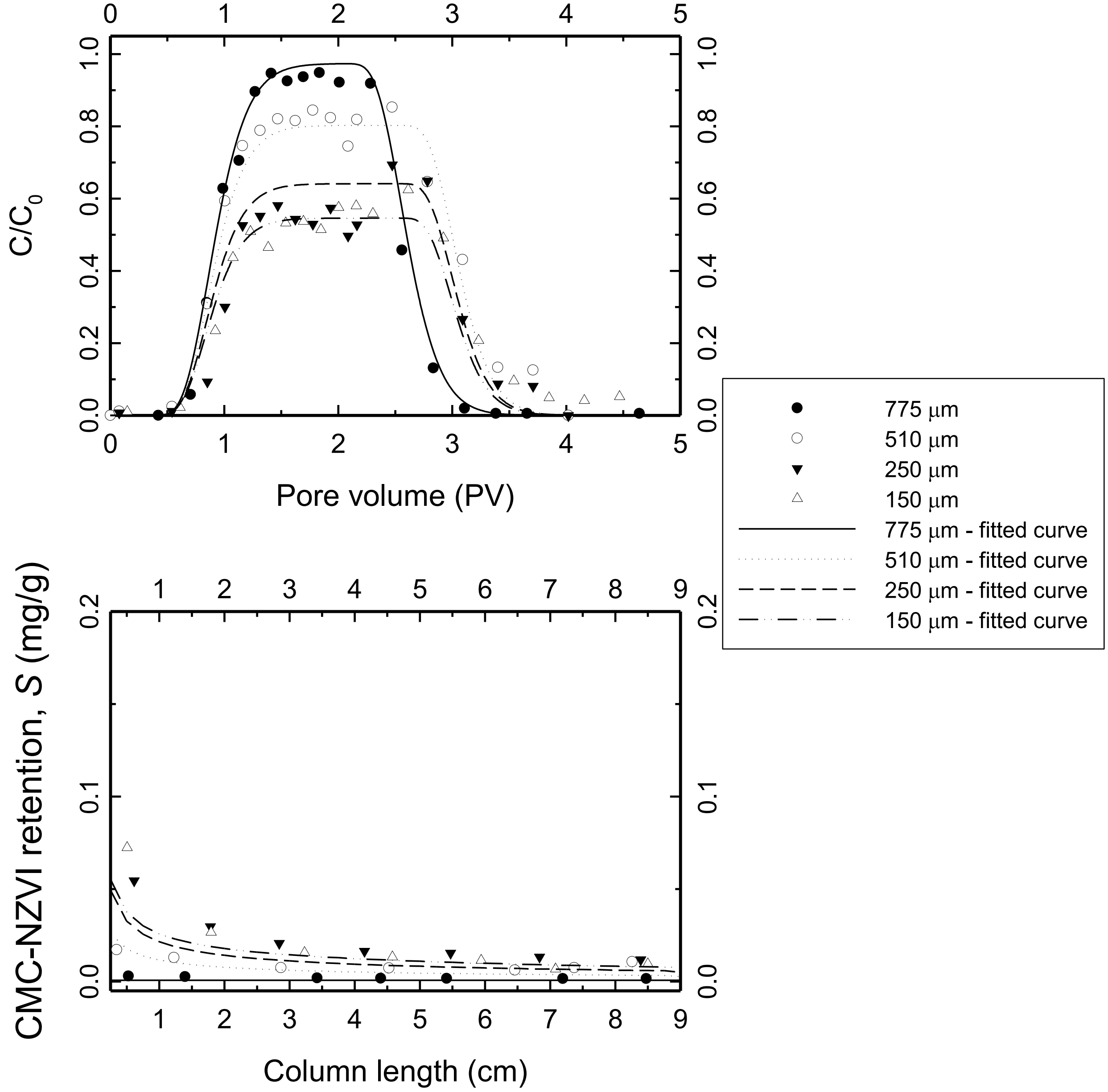

FIGURE 5.2. Experimental and simulated (a) breakthrough curves and (b) retention profiles along the column length of CMC-NZVI through different sized sands packed columns of L =9.0 cm, C_0 = 0.085 g•L^{-1},considering Model 2.

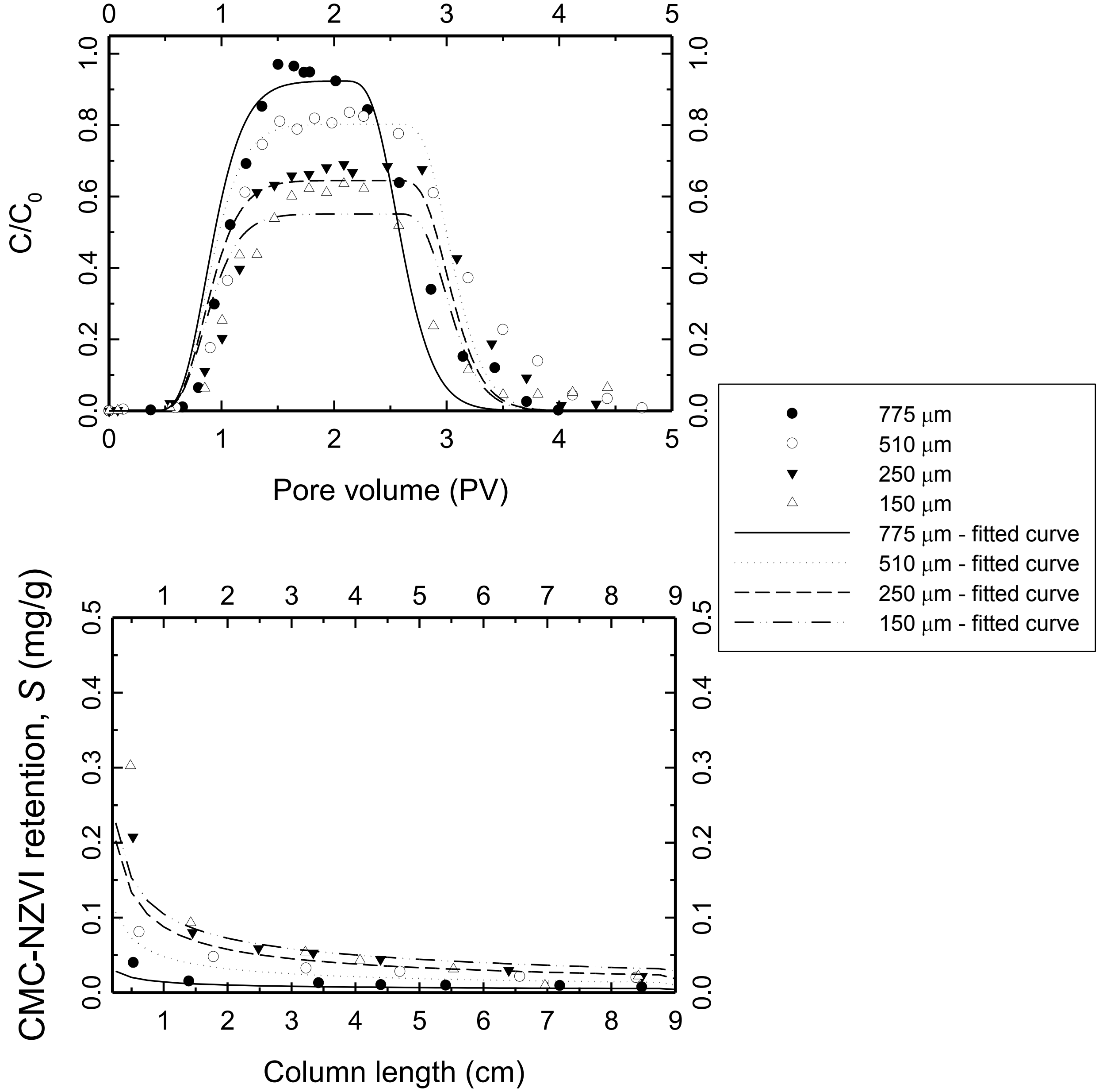

FIGURE 5.3. Experimental and simulated (a) breakthrough curves and (b) retention profiles along the column length of CMC-NZVI through different sized sands packed columns of *L* =9.0 cm, C_0 = 0.35 g•L^{-1},considering Model 2

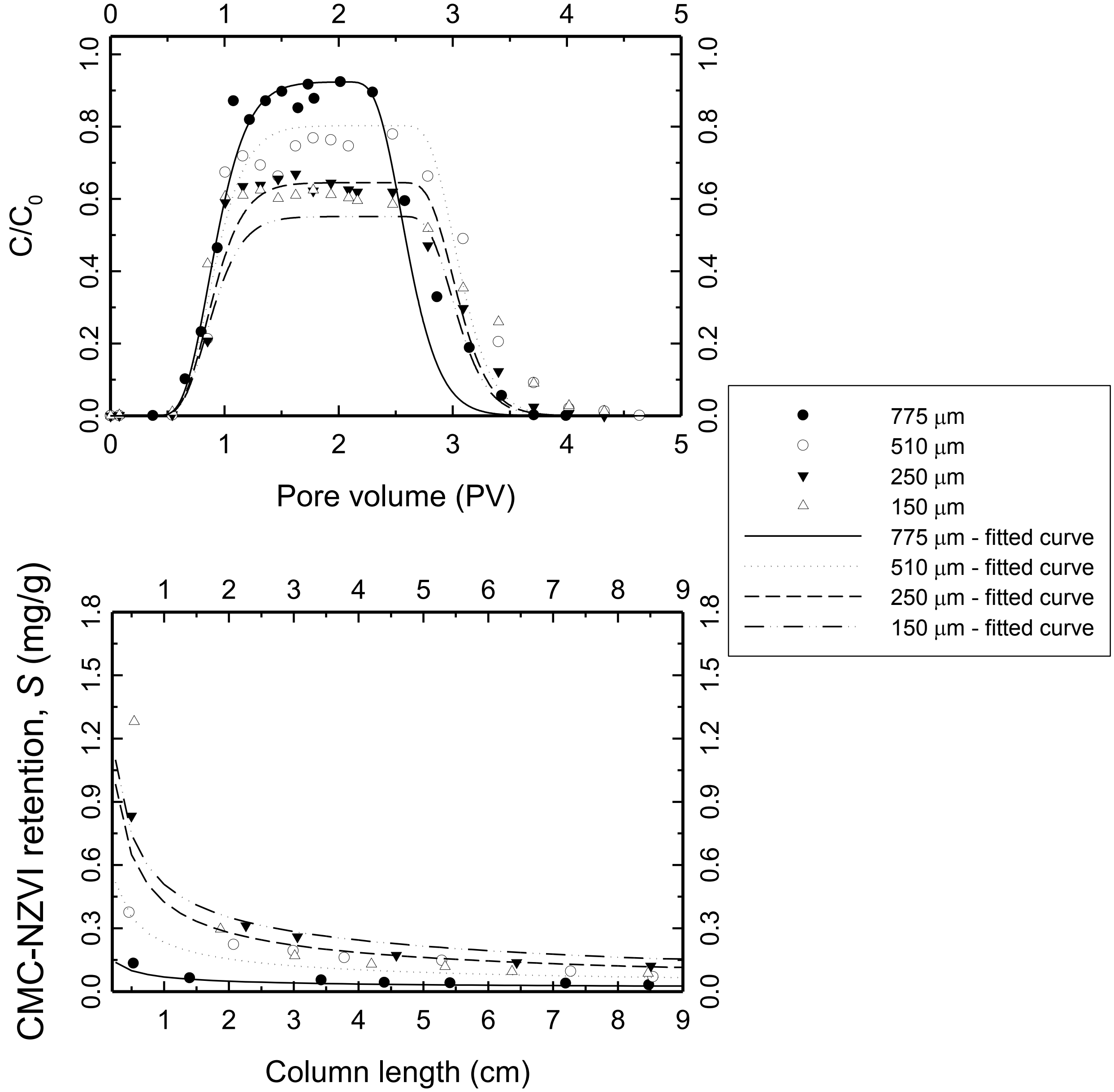

FIGURE 5.4. Experimental and simulated (a) breakthrough curves and (b) retention profiles along the column length of CMC-NZVI through different sized sands packed columns of *L* =9.0 cm, C_0 = 1.70 g•L^{-1},considering Model 2.

From Table 5.2, it could be confirmed that for the coarsest (775μm) sand and with lowest CMC-NZVI concentration (0.085 gL^{-1}) there is no straining. With decreasing sand size the percentage of strained mass increases steadily. For example, the percentage of strained mass at inlet for 0.35gL^{-1} CMC-NZVI increases from 2.45 % to 7.88 % to 12.41 % to 13.50 % for sand sizes of 775 to

510 to 225 to 150 μm, respectively. Similar trendw were observed for the other CMC-NZVI concentrations throughout the column length (Table 5.2).

Interestingly, the percentage of strained mass reduces after 2cm of column length for all sand sizes and concentrations. Within the first 2cm of the inlet around 13.5 % of the CMC-NZVI mass injected was retained due to straining with the finest sand and 0.35 gL^{-1} CMC-NZVI). In the remaining 7cm of the column, only an additional 12.98 % was retained by straining. Similarly, approximately half of the CMC-NZVI was retained within 2 cm of column length for the other sand sizes and CMC-NZVI concentrations. This suggests that straining can be an important retention mechanism during polymer stabilized-NZVI transport.

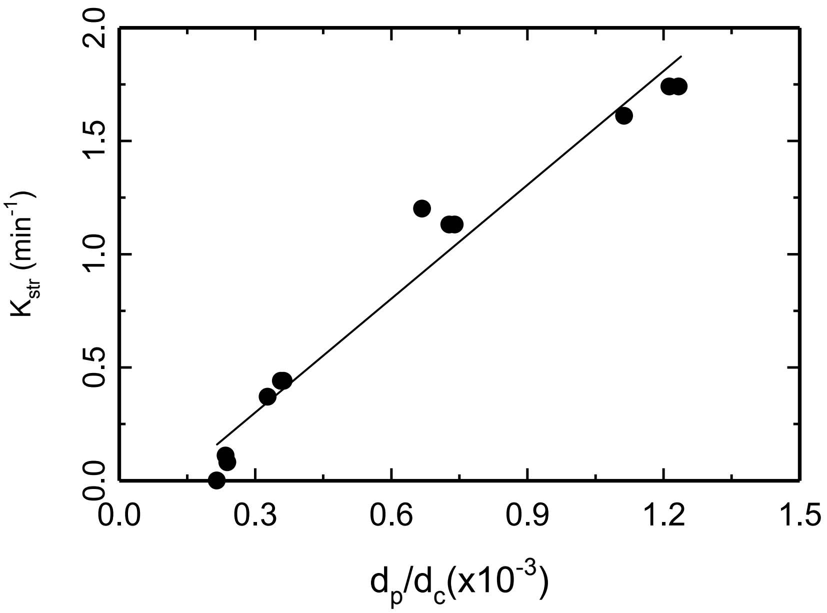

FIGURE 5.5. Fitted straining rate coefficient, evaluated using Model 2, varies linearly with d_p/d_c ratio. Here, d_p is based on NTA image analysis.

Supporting Information

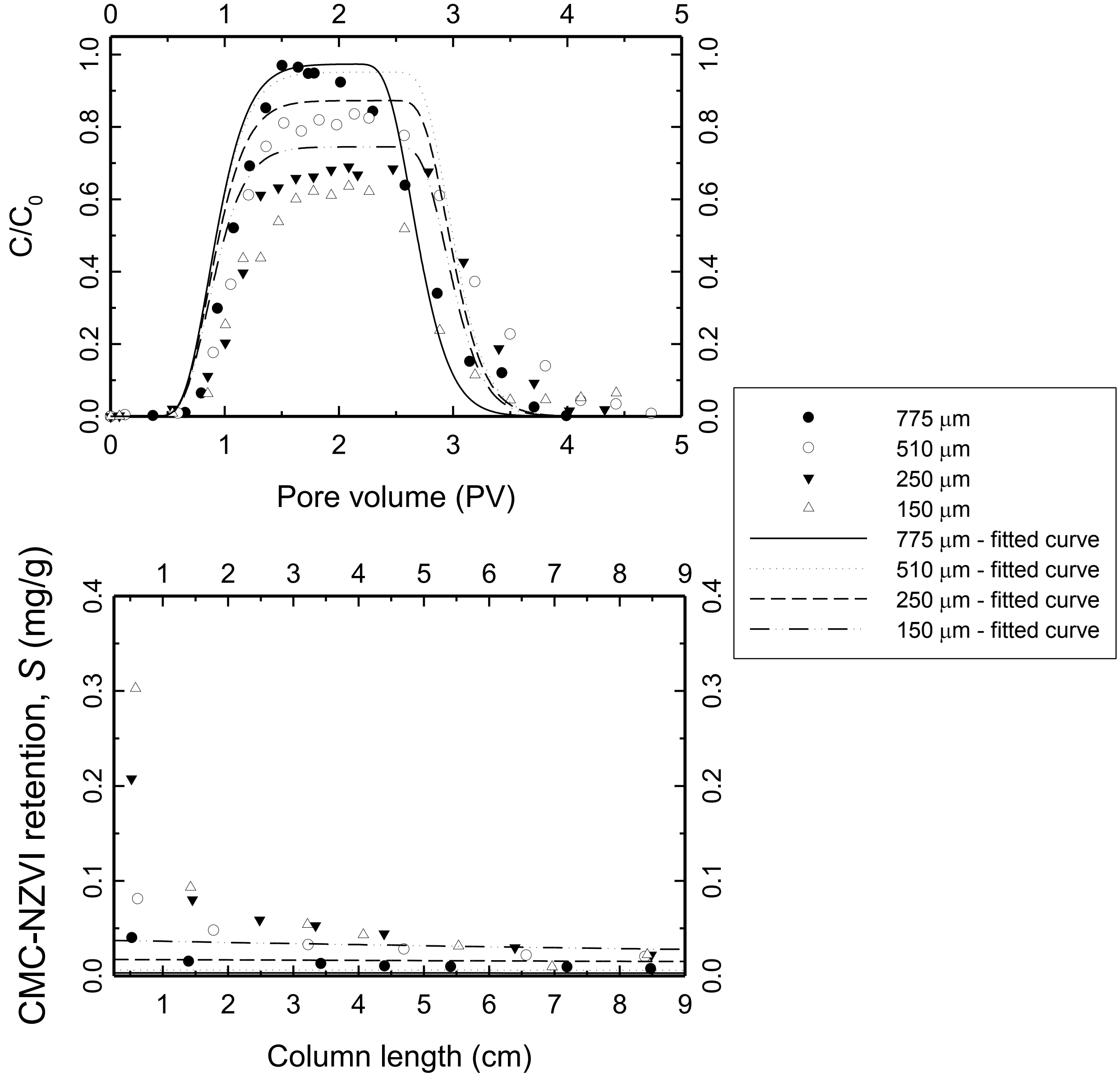

FIGURE 5.S1: (a) Experimental breakthrough curves and (b) retention profiles along with simulated plot considering Model Approach 1, for different graded sands packed columns of *L* =9.0 cm, C_0 = 0.35 g•L^{-1}.

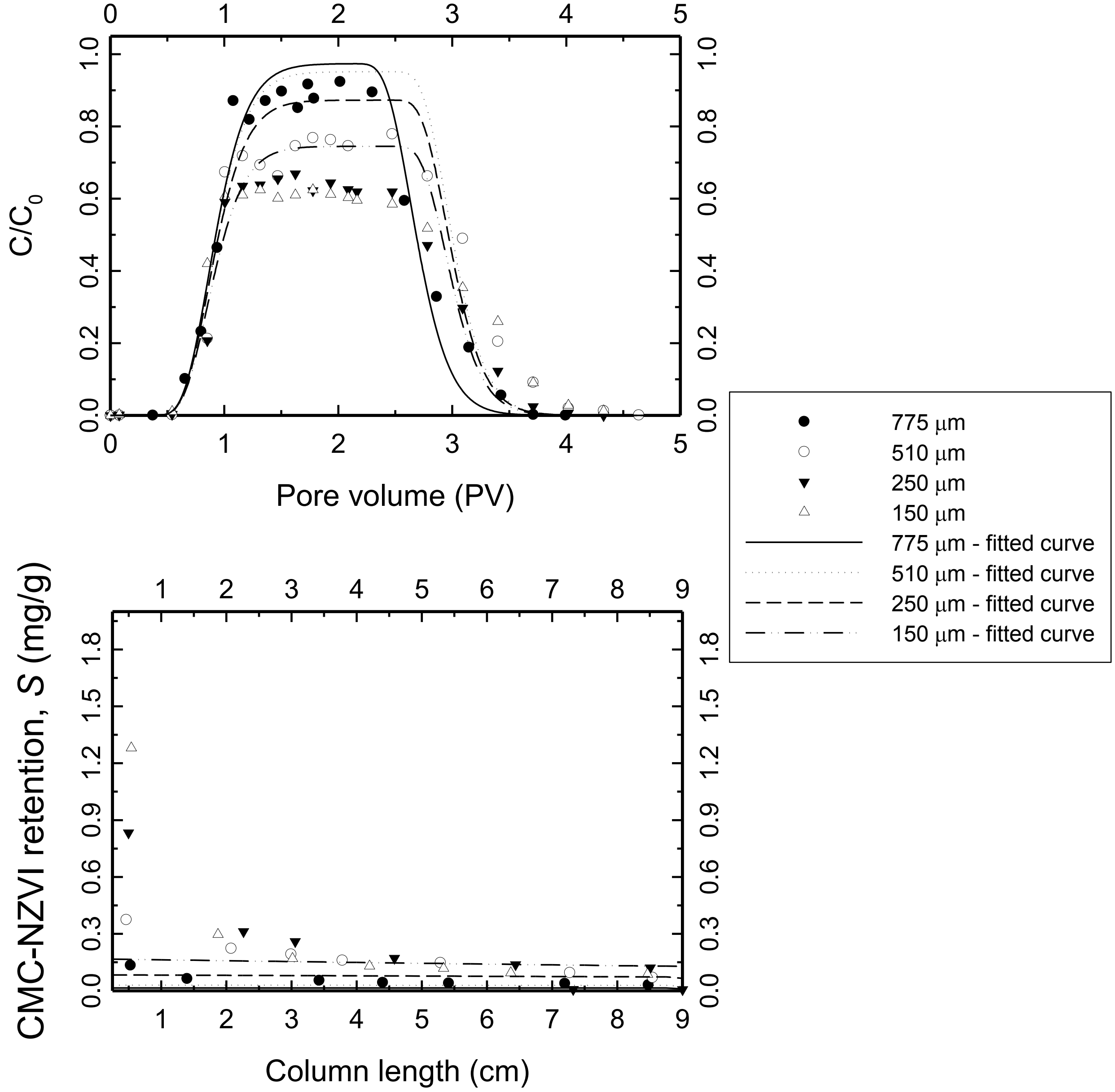

FIGURE 5.S2: (a) Experimental breakthrough curves and (b) retention profiles along with simulated plot considering Model Approach 1, for different graded sands packed columns of L =9.0 cm, C_0 =1.70 g•L^{-1}.

References

[1] Kim, H.-J., T. Phenrat, R.D. Tilton and G.V. Lowry, *Fe0 nanoparticles remain mobile in porous media after aging due to slow desorption of polymeric surface modifiers.* Environmental science and technology, 2009. **43**(10): p. 3824-3830.

[2] Phenrat, T., N. Saleh, K. Sirk, R.D. Tilton and G.V. Lowry, *Aggregation and sedimentation of aqueous nanoscale zerovalent iron dispersions.* Environmental science and technology, 2007. **41**(1): p. 284-290.

[3] Zhang, W.-x., *Nanoscale iron particles for environmental remediation: An overview.* Journal of Nanoparticle Research, 2003. **5**: p. 10.

[4] Phenrat, T., N. Saleh, K. Sirk, H.-J. Kim, R.D. Tilton and G.V. Lowry, *Stabilization of aqueous nanoscale zerovalent iron dispersions by anionic polyelectrolytes: Adsorbed anionic polyelectrolyte layer properties and their effect on aggregation and sedimentation.* Journal of Nanoparticle Research, 2008. **10**(5): p. 795-814.

[5] Raychoudhury, T., G. Naja and S. Ghoshal, *Assessment of transport of two polyelectrolyte-stabilized zero-valent iron nanoparticles in porous media.* Journal of Contaminant Hydrology, 2010.

[6] He, F., M. Zhang, T. Qian and D. Zhao, *Transport of carboxymethyl cellulose stabilized iron nanoparticles in porous media: Column experiments and modeling.* Journal of Colloid and Interface Science, 2009. **334**(1): p. 96-102.

[7] Kanel, S., D. Nepal, B. Manning and H. Choi, *Transport of surface-modified iron nanoparticle in porous media and application to arsenic(III) remediation.* Journal of Nanoparticle Research, 2007. **9**(5): p. 725-735.

[8] Saleh, N., H.-J. Kim, T. Phenrat, K. Matyjaszewski, R.D. Tilton and G.V. Lowry, *Ionic strength and composition affect the mobility of surface-modified fe0 nanoparticles in water-saturated sand columns.* Environmental science and technology, 2008. **42**(9): p. 3349-3355.

[9] Schrick, B., B.W. Hydutsky, J.L. Blough and T.E. Mallouk, *Delivery vehicles for zerovalent metal nanoparticles in soil and groundwater.* Chemistry of Materials, 2004. **16**(11): p. 2187-2193.

[10] Petosa, A.R., D.P. Jaisi, I.R. Quevedo, M. Elimelech and N. Tufenkji, *Aggregation and deposition of engineered nanomaterials in aquatic environments: Role of physicochemical interactions.* Environmental science and technology, 2010. **44**(17): p. 6532-6549.

[11] Phenrat, T., H.-J. Kim, F. Fagerlund, T. Illangasekare, R.D. Tilton and G.V. Lowry, *Particle size distribution, concentration, and magnetic attraction affect transport of polymer-modified Fe0 nanoparticles in sand columns.* Environmental science and technology, 2009. **43**(13): p. 5079-5085.

[12] Raychoudhury, T., G. Naja and S. Ghoshal, *Assessment of transport of two polyelectrolyte-stabilized zero-valent iron nanoparticles in porous media.* Journal of Contaminant Hydrology, 2010. **118**(Compendex): p. 143-151.

[13] Fatisson, J., S. Ghoshal and N. Tufenkji, *Deposition Behavior of Carboxymethylcellulose Coated Zero-valent Iron Nanoparticles onto*

Silica: Role of Solution Chemistry and Organic Macromolecules. Langmuir, 2010. **26**(15).

[14] Phenrat, T., H.-J. Kim, F. Fagerlund, T. Illangasekare and G.V. Lowry, *Empirical correlations to estimate agglomerate size and deposition during injection of a polyelectrolyte-modified Fe0 nanoparticle at high particle concentration in saturated sand.* Journal of Contaminant Hydrology, 2010.

[15] Redman, J.A., S.L. Walker and M. Elimelech, *Bacterial Adhesion and Transport in Porous Media: Role of the Secondary Energy Minimum.* Environmental science and technology, 2004. **38**(Compendex): p. 1777-1785.

[16] Tufenkji, N., G.F. Miller, J.N. Ryan, R.W. Harvey and M. Elimelech, *Transport of Cryptosporidium oocysts in porous media: Role of straining and physicochemical filtration.* Environmental science and technology, 2004. **38**(Compendex): p. 5932-5938.

[17] Tufenkji, N. and M. Elimelech, *Breakdown of colloid filtration theory: Role of the secondary energy minimum and surface charge heterogeneities.* Langmuir, 2005. **21**(3): p. 841-852.

[18] Bradford, S.A. and M. Bettahar, *Concentration dependent transport of colloids in saturated porous media.* Journal of Contaminant Hydrology, 2006. **82**(Compendex): p. 99-117.

[19] Bradford, S.A., J. Simunek, M. Bettahar, M.T. Van Genuchten and S.R. Yates, *Modeling colloid attachment, straining, and exclusion in saturated porous media.* Environmental science and technology, 2003. **37**(Compendex): p. 2242-2250.

[20] Bradford, S.A., S. Torkzaban and S.L. Walker, *Coupling of physical and chemical mechanisms of colloid straining in saturated porous media.* Water Research, 2007. **41**(13): p. 3012-3024.

[21] Johnson, W.P., X. Li and S. Assemi, *Deposition and re-entrainment dynamics of microbes and non-biological colloids during non-perturbed transport in porous media in the presence of an energy barrier to deposition.* Advances in Water Resources, 2007. **30**(Compendex): p. 1432-1454.

[22] Tong, M. and W.P. Johnson, *Excess colloid retention in porous media as a function of colloid size, fluid velocity, and grain angularity.* Environmental science and technology, 2006. **40**(Compendex): p. 7725-7731.

[23] Bradford, S.A., H.N. Kim, B.Z. Haznedaroglu, S. Torkzaban and S.L. Walker, *Coupled factors influencing concentration-dependent colloid transport and retention in saturated porous media.* Environmental science and technology, 2009. **43**(Compendex): p. 6996-7002.

[24] Hong, Y., R.J. Honda, N.V. Myung and S.L. Walker, *Transport of iron-based nanoparticles: Role of magnetic properties.* Environmental Science and Technology, 2009. **43**(23): p. 8834-8839.

[25] Jaisi, D.P. and M. Elimelech, *Single-walled carbon nanotubes exhibit limited transport in soil columns.* Environmental science and technology, 2009. **43**(Compendex): p. 9161-9166.

[26] Tosco, T. and R. Sethi, *Transport of non-newtonian suspensions of highly concentrated micro- and nanoscale iron particles in porous media: A modeling approach.* Environmental science and technology, 2010. **44**(Compendex): p. 9062-9068.

[27] Kuhnen, F., K. Barmettler, S. Bhattacharjee, M. Elimelech and R. Kretzschmar, *Transport of Iron Oxide Colloids in Packed Quartz Sand Media: Monolayer and Multilayer Deposition.* Journal of Colloid and Interface Science, 2000. **231**: p. 10.

[28] Tufenkji, N., J.A. Redman and M. Elimelech, *Interpreting deposition patterns of microbial particles in laboratory-scale column experiments.* Environmental science and technology, 2003. **37**(3): p. 616-623.

[29] Tufenkji, N. and M. Elimelech, *Correlation Equation for Predicting Single-Collector Efficiency in Physicochemical Filtration in Saturated Porous Media.* Environmental science and technology, 2004. **38**(Compendex): p. 529-536.

[30] Marquardt, D.W., *An algorithm for least-squares estimation of nonlinear parameters.* Journal of the Society for Industrial and Applied Mathematics, 1963. **11**(2): p. 431-441.

[31] Deb, K., *Optimization for Engineering Design: Algorithm and Examples*. Seventh ed. ISBN 812030943X2004, New Delhi: Prentice Hall of India Privale Limited.

[32] He, F. and D. Zhao, *Manipulating the size and dispersibility of zerovalent iron nanoparticles by use of carboxymethyl cellulose stabilizers.* Environmental science and technology, 2007. **41**(17): p. 6216-6221.

[33] Filipe, V., A. Hawe and W. Jiskoot, *Critical Evaluation of Nanoparticle Tracking Analyzer (NTA) by Nanosight for Measurement of Nanoparticles and Protein Aggregation.* Pharmaceutical Research, 2010. **27**(5): p. 796-810.

[34] Li, X., P. Zhang, C.L. Lin and W.P. Johnson, *Role of hydrodynamic drag on microsphere deposition and re-entrainment in porous media under unfavorable conditions.* Environmental science and technology, 2005. **39**(Compendex): p. 4012-4020.

[35] Tong, M., X. Li, C.N. Brow and W.P. Johnson, *Detachment-influenced transport of an adhesion-deficient bacterial strain within water-reactive porous media.* Environmental science and technology, 2005. **39**(Compendex): p. 2500-2508.

[36] Torkzaban, S., Y. Kim, M. Mulvihill, J. Wan and T.K. Tokunaga, *Transport and deposition of functionalized CdTe nanoparticles in saturated porous media.* 2010.

[37] Tufenkji, N. and M. Elimelech, *Correlation Equation for Predicting Single-Collector Efficiency in Physicochemical Filtration in Saturated Porous Media.* Environmental science and technology, 2004. **38**(2): p. 529-536.

[38] Xu, S., B. Gao and J.E. Saiers, *Straining of colloidal particles in saturated porous media.* Water Resources Research, 2006. **42**(Compendex).

[39] Hong, Y., R.J. Honda, N.V. Myung and S.L. Walker, *Transport of iron-based nanoparticles: Role of magnetic properties.* Environmental science and technology, 2009. **43**(Compendex): p. 8834-8839.

[40] Jaisi, D.P., N.B. Saleh, R.E. Blake and M. Elimelech, *Transport of single-walled carbon nanotubes in porous media: Filtration mechanisms and reversibility.* Environmental science and technology, 2008. **42**(Compendex): p. 8317-8323.

Chapter 6
Intellectual contributions

The remediation of aquifers contaminated by chlorinated organics by injection of nanoparticles of zero valent iron (NZVI) is considered to be a promising clean-up approach as NZVI can degrade such pollutants rapidly. However, the efficient remediation of DNAPL source zones in aquifers will depend on the feasibility of transport of NZVI from injection wells to DNAPL pools and zones of residual saturation. The transport of bare NZVI in porous media is limited because of their strong tendency to aggregate and thus plug pores.

Certain polymers can colloidally stabilize NZVI and limit aggregation, and thereby significantly enhance its transport in porous media. Different polyelectrolyte can stabilize NZVI up to different extents depending upon the molecular property of specific surface modifier. In my doctoral research, the colloidal stability of NZVI by different surface modifier were assessed by sedimentation test and presented in Appendix.

Among different polymer PAA and CMC were found to most suitable (Appendix) from colloidal stabilization point of view and selected for further study. Transport and deposition of PAA- and CMC-NZVI modified particles varied depending upon particle size distribution, aggregation kinetics and groundwater velocity.

Aggregation of surface-modified NZVI can influence particle transport through porous media Aggregation kinetics depends upon particle number concentrations. Considering the fact, the effect of particle concentration on aggregation and thus on transport was examined experimentally and compared with an aggregation based transport model.

Surface-modified NZVI particles are expected to deposit on secondary minima due presence of high energy minima and transport of these particles are likely to be governed by different physical mechanism such as wedging and/or straining. Thus the significance of straining of CMC-NZVI transport through porous media was evaluated by comparing experimental data with model prediction. Findings and contribution of each specific objective are discussed in details bellow.

6.1 This study presents the assessment of the transport performance at different flow velocities and particle concentrations of NZVI particles stabilized with PAA and CMC and in the size range of 5 to 30 nm.

Overall, polyelectrolyte-stabilized NZVI transported to a significant extent even at slower flow velocities, representative of natural groundwater conditions, and the transport efficiency has enhanced at higher flow velocities representative of injection velocities. To date no other studies have examined NZVI transport under a range of velocities reflecting natural groundwater flow and flow during injection conditions.

CMC-NZVI transported more extensively than PAA. The effluent concentrations profiles for CMC- and PAA-NZVI decreased with lower flow rate and higher influent particle concentrations. To date this has not been demonstrated for CMC- or PAA- stabilized NZVI. In particular, PAA-NZVI particles showed a gradual and continued increase in effluent concentrations beyond 2 PV. It was established that this pattern is attributable to the higher aggregation rate of PAA-NZVI as observed qualitatively in sedimentation tests conducted under quiescent conditions. The differences in the particle sizes and particle surface potentials of the CMC- and PAA-NZVI contribute to the different aggregation patterns. Although polyelectrolyte-stabilized NZVI are more colloidly stable and mobile than bare NZVI, aggregation remains an important process controlling its transport behaviour.

s

6.2 This study assesses the effect of concentration on CMC-NZVI aggregation and its implication on transport. The study presents the first mathematical approach which links an aggregation kinetics model with a colloid transport model.

The extent of aggregation was quantified by evaluating the increase in particle size with time from the experimental data and aggregation model calculation. With increase in concentration, more rapid increase in average particle size with time was observed. Though the overall aggregation was not very significant, but due to very high particle number concentrations, increase in particle-particle collision frequency resulted in measurable aggregation.

CMC-NZVI effluent concentration profiles showed a gradual increasing slope with time; the increasing trend is more rapid for higher concentration. Gradual increases in effluent concentrations were explained by combined effects of aggregation and detachment. The particle-collector collision frequency changed with particle size, which resulted in a time dependent deposition rate coefficient. The aggregation model, fitted with NTA data gave the particle size distribution with time, which was inserted in the transport model. Comparison of transport model with experimental data suggests that for the range of CMC-NZVI particle size encountered in the experiments, the aggregation kinetics does not affect the deposition pattern at higher pore volumes (>4PVs). Detachment due to drag seems to have more predominant effect on transport at higher pore volumes.

Particle deposition at higher CMC-NZVI influent concentration was higher. Increasing deposition with influent concentration, particularly for this batch of sand, was attributable to changes in the ionic strength of the suspension increase due to sodium dissolved from the Na-CMC. Such effects of CMC concentration on aqueous chemistry and transport have not been reported to date.

6.3 This study is the first to quantitatively demonstrate that straining is a significant mechanism contributing to CMC-NZVI retention in granular porous media during transport.

CMC-NZVI transport in porous media can be governed by straining and/or wedging, which is blocking of small dead-end pores near the inlet of column and/or excess particle retention at the grain-to-grain contact point. Straining resulted in more particles retained through finer sand (as finer sand would have more number of small pores and/or more number of grain-to-grain contact points) and at column inlet. Therefore, transport experiments were designed to assess the effect of straining by selecting sands of different diameter with different influent concentration. In addition, the CMC-NZVI particle retention along the column length was evaluated by sectioning the packed column after electrolyte flushing.

Effluent particle concentration decreases with decrease in sand size. In addition very high particle retention at column inlet suggests straining. There was not much significance difference in BTC with different concentration. This may be because the experiment was carried out after stabilizing the particles for 90 min to avoid aggregation.

Comparison of experimental data with transport model considering 1) particle deposition and 2) particle deposition along with straining, suggests the effect of straining of CMC-NZVI retention is significant. The straining rate co-efficient varied linearly with the d_p/d_c ratio. A comparison of experimental data with model prediction suggests some degree of detachment for finest sand.

In the different studies discussed above, the effect of particle concentration on CMC-NZVI retention in packed columns was investigated. In Chapter 4, where the aggregation and deposition kinetics was studied, a decrease in C/C_0 with increase in influent concentration was reported. In Chapter 5, where the significance of straining was evaluated, though CMC-NZVI of similar particle size range was used, no such trend in the breakthrough behavior with concentration was observed. The main differences in these two sets of experiments were i) in the first case, CMC-NZVI was injected when the aggregation was an ongoing process, whereas for the second case, particles were injected once the aggregation process has reached steady state and ii) two different batches of sands were used for these two different sets of experiments.

The aggregation process may have some additional contribution on transport beyond what was proposed in Chapter 4. For example, at initial time, a greater number of small particles are expected at low concentration compared to high concentration. Therefore, more straining at high concentrations (due to more larger sized particles) might affect the retention (or C/C_0 at 2PV) of particles by straining, which was not considered in the modified aggregation-transport model. Whereas in Chapter 5, the experiments are carried out once the particles are stabilized (no more aggregation); therefore, not much difference in particle size at different concentrations was observed. So the effect of straining was similar at different concentrations resulting in insignificant change in BTC with influent concentrations. In future, further analysis needs to be carried out that incorporate aggregation and straining together to explain the data (in Chapter 4 and Chapter 5) in more comprehensive manner.

Second, in experiments of Chapter 4, there is an increase in deposition with which occurs, at least in part, as a result of increase in IS of the background aqueous solution with increase in CMC-NZVI concentration. The effect of IS on CMC-NZVI deposition appears to be different with the two different batches of sands. Surface characterization of these different batches of sands at different IS could be done in future to understand this phenomenon completely.

APPENDIX

Synthesis and characterization of NZVI

Nano-scale zero valent iron (NZVI) is synthesized in the laboratory by reduction of ferric ($FeCl_3$ $6H_2O$) or ferrous ($FeSO_4 7H_2O$) ions by borohydride ($NaBH_4$), to zero valent iron Fe(0) as shown below [1-3].

$FeCl_3$ Reduction: $4Fe^{+3} + 3BH_4^- + 9H_2O \Rightarrow 4Fe^{0} + 3H_2BO_3^- + 12H^+ + 6H_2$ (A.1)

$FeSO_4$ Reduction: $Fe^{+2} + 2BH_4^- + 9H_2O \Rightarrow Fe^{0} + 2H_2BO_3^- + 8H^+ + 7H_2$ (A.2)

The characteristics of NZVI have been extensively reported. Average diameter of NZVI without surface modification was commonly found in the range of 50-100 nm before aggregate formation, resulting in surface areas of 18-35 m^2/g [3-5]. Their zeta potential has been reported to be in the range of +10 mV at pH 7.8 to –25 mV at pH 8.4 [6]. X-ray Diffraction (XRD) and X-Ray photoelectron Spectroscopy (XPS) analyses show zero valent iron (Fe^0) nanoparticles are comprised of a shell of iron oxides and hydroxides and a core of Fe^0 [4-7].

However, the main concern about *in situ* NZVI application is its tendency to aggregate rapidly. Several studies demonstrated the stabilization of NZVI improved by polyelectrolyte coating. There are two different approaches for polymer-coating, such as (i) polymers can be post grafted to the bare NZVI [8, 9] and (ii) alternatively NZVI may be synthesized in the presence of polymer [1].

In this study we have adopted the pre-grafted approaches described in He and Zhao [1]. Detail of the synthesis and characterization procedures for CMC-NZVI are described in Chapter 3 and chapter 4. To compare performance of different polymer the Fe/polymer weight ratio has been kept as 2:5 (adopted in Chapter 4). The surface modified-NZVI was characterized for surface charges, pH and particle sizes as presented in Table A1. The colloidal stability of these particles is evaluated by sedimentation test as described in Chapter 3 and the results are presented in Figure A.1.

Table A.1. Characteristics of bare and different polymer-NZVI

Characterization	NZVI	CMC-NZVI	PSS-NZVI	PAM-NZVI	PAA-NZVI
Molecular weight	-	90K	70K	5000K	1.8K
ζ Potential (mV)	-1.45±1.1	-41.4±1.7	-34.5±1.8	0.18±1.6	-27.6±1.0
pH	7.8	7.5	7.9	8.3	8.0
Average particle size (nm)	59.1±20.9	84.5±18.9	182±78.1	101±29.1	189.3±20.9

**Here, CMC is Carboxymethylcellulose (weak anionic polysaccharide, PSS is Polystyrenesulfonate (strong anionic polyelectrolyte), PAM is Polyacrylamide (nonionic polymer) and PAA is Polyacrylic acid (weak anionic polyelectrolyte).

Table A1 suggests the zeta potential of NZVI and PAM-NZVI are nearly zero (-1.45 ± 1.11 and 0.18 ± 1.68, respectively), wheras, for PAA, PSS and CMC-NZVI more negative zeta potential (-27.57, -34.5 and -41.4 respectively) with a similar range of pH (7.5-8.3). Average particles size of bare NZVI is 59.1±20.9 which is within the reported range mentioned above.

From sedimentation tests, it could be stated that CMC and PAA acts as the most efficient dispersant compared to other polymers. The colloidal stability of PSS-NZVI is relatively poor compared to that of CMC, though they have similar ζ –potential values and molecular weight [10]. This may be explained by the fact that PSS have much bigger diameter compared to CMC-NZVI which would result in greater magenetic attraction and thus more aggregation. PAA-NZVI was approximately 20% more stable compared to PSS-NZVI despite similar particle sizes, higher molecular weight for PSS, and a more negative zeta potential of PSS-NZVI. It is likely that the poor stability of the PSS-NZVI is due to the hydrophobic domains in the molecules [11]

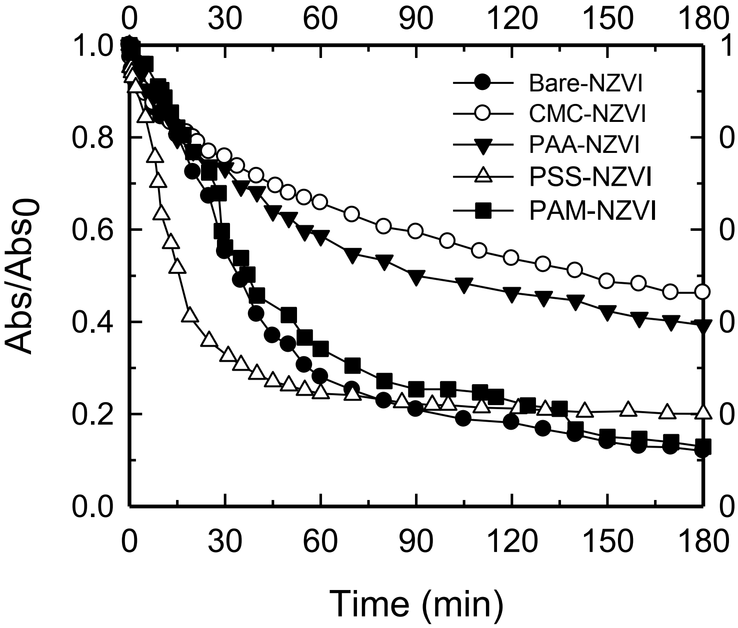

Figure A.1: Sedimentation test results of bare and different surface modified NZVI.

Table A.2 and Table A.3 represents equation and parameter values used for particle-particle and particle-collector DLVO interaction energy calculations as presented in Chapter 3 and Chapter 4.

Table A.2: DLVO interaction energies between particle-particle and particle-collector

Particle-particle DLVO interaction energies (*V/K_bT*) **Sphere-sphere DLVO interaction**
van der Waals attraction energy (Gregory 1981, [12]) $V_{vdw} = \frac{A}{6K_bT}\left[\frac{2a^2}{s(4a+s)} + \frac{2a^2}{(2a+s)^2} + \ln s\frac{(4a+s)}{(2a+s)^2}\right]$

Magnetic attraction energy (Phenrat et al. 2007, [13])

$$V_m = \frac{8\pi\mu_0 M_s a^3}{9(\frac{s}{a}+2)^3}$$

$$M_s = -0.0913Fe_0^2 + 18.093Fe_0 + 329.99$$

Electrostatic repulsion energy (Gregory 1975, [14])

$$V_{es} = \frac{2\pi\varepsilon_r\varepsilon_0}{K_b T} a\psi_1^2 \ln\left[1+e^{-k_{deb}s}\right]$$

$$k_{deb} = \sqrt{\frac{e^2\sum c_i z_i^2}{\varepsilon_r\varepsilon_0 K_b T}}$$

Steric repulsion interaction (Lim et al. 2009, [15])

$$V_{steric} = \frac{\pi^3 t_p^3 \sigma_p a}{12N_p l^2}\left[-\ln(\frac{s}{2t_p}) - \frac{9}{5}(1-\frac{s}{2t_p}) + \frac{1}{3}(1-(\frac{s}{2t_p})^6)\right]$$

Particle-collector DLVO interaction energies (*V*)

Sphere-flat plate DLVO interaction

van der Waals attraction energy (Gregory 1981, [12])

$$V_{vdw-pc} = \frac{-Aa}{6s}\left[1-\frac{bs}{\lambda}\ln(1+\frac{\lambda}{bs})\right]$$

Electrostatic repulsion energy (Hogg et al. 1966, [16])

$$V_{es-pc} = \frac{2\pi a n_\infty k_b T}{\kappa_{deb}^2}\left(\psi_1^2+\psi_2^2\right)\left[\frac{2\psi_1\psi_2}{\psi_1^2+\psi_2^2}\ln\left(\frac{1+e^{-\kappa_{deb}s}}{1-e^{-\kappa_{deb}s}}\right) - \ln(1-e^{-2\kappa_{deb}s})\right]$$

Steric repulsion interaction (Lim et al. 2009, [15])

$$V_{steric-pc} = 2\pi a\frac{k_b T}{h^3}\left\{\frac{4t_d}{5}\left[\left(\frac{t_d}{s}\right)^{\frac{5}{4}}-1\right] + \frac{4t_d}{7}\left[\left(\frac{s}{t_d}\right)^{\frac{7}{4}}-1\right]\right\}$$

Table A.3. Parameter values used for DLVO calculation

Symbol	Parameters	Adopted values	References
A	Hamaker constant	$1*10^{-19}$ (J)	Fatisson et al. 2010
Fe_0	Percentage of zerovalent iron in NZVI	25 %	Phenrat et al. 2008
K_b	Boltzmann constant	$1.38*10^{-23}$ (J/K)	-
N_a	Avogadro’s constant	$6.023*10^{23}$	-
N_p	Number of segment of polyelectrolyte chain	100	Lim et al. 2009
T	Temperature	295 (K)	Measured
a	Radius of the colloid particles	4-200 (nm)	Gregory, 1975
b	Constant	5.32	Gregory, 1975
c_i	Ion concentration of i^th^ ion	0.1-10 (10^{-3}M)	Prepared
E	Charge of electron	$1.6*10^{-19}$	-
h	Distance between polymer chain at surface	2 (nm)	Fatisson et al. 2010
l	Length of segment of polyelectrolyte chain	0.3 (nm)	Lim et al. 2009
n_∞	Bulk ion density	$N_\mathrm{a}*\sum c_\mathrm{i}$ (ion.m^{-3})	Fatisson et al. 2010
s	Separation distance	Variable (nm)	
t_p	Polyelectrlyte layer thickness	7 (nm)	Fatisson et al. 2010
z_i	Valancy of i^{th} ion	1 (Na^+ and HCO_3^-)	-
ε_0	Vacuum permeability	80	-
ε_r	Relative permeability of water	$8.85*10^{-12}$ (Fm^{-1})	-
σ_p	Surface density of polyelectrolyte chain	1 (molecules.nm^{-2})	Lim et al. 2009
λ	Retardation Factor	10^{-7}	Fatisson et al. 2010
μ_0	Magnetic permeability of free space	$1.256*10^{-6}$ (NA^{-2})	-

Ψ_1	Zeta potential at particle surface	-40 to -47 mV	Measured
Ψ_2	Zeta potential at collector surface	-20 mV	Assumed

Literature cited

[1] He, F. and D. Zhao, *Manipulating the size and dispersibility of zerovalent iron nanoparticles by use of carboxymethyl cellulose stabilizers.* Environmental science and technology, 2007. **41**(17): p. 6216-6221.

[2] Kanel, S., B. Manning, L. Charlet and H. Choi, *Removal of arsenic(III) from groundwater by nanoscale zero-valent iron.* Environmental science and technology, 2005. **39**(Compendex): p. 1291-1298.

[3] Zhang, H., Z.-H. Jin, L. Han and C.-H. Qin, *Synthesis of nanoscale zero-valent iron supported on exfoliated graphite for removal of nitrate.* Transactions of Nonferrous Metals Society of China (English Edition), 2006. **16**(Compendex): p. s345-s349.

[4] Nurmi, J.T., P.G. Tratnyek, V. Sarathy, D.R. Baer, J.E. Amonette, K. Pecher, C. Wang, J.C. Linehan, D.W. Matson, R.L. Penn, and M.D. Driessen, *Characterization and properties of metallic iron nanoparticles: Spectroscopy, electrochemistry, and kinetics.* Environmental science and technology, 2005. **39**(Compendex): p. 1221-1230.

[5] Song, H. and E.R. Carraway, *Catalytic hydrodechlorination of chlorinated ethenes by nanoscale zero-valent iron.* Applied Catalysis B: Environmental, 2008. **78**(Compendex): p. 53-60.

[6] Li, L., M. Fan, R.C. Brown, J. Van Leeuwen, J. Wang, W. Wang, Y. Song and P. Zhang, *Synthesis, properties, and environmental applications of nanoscale iron-based materials: A review.* Critical Reviews in Environmental Science and Technology, 2006. **36**(Compendex): p. 405-431.

[7] Sun, Y.-P., X.-q. Li, J. Cao, W.-x. Zhang and H.P. Wang, *Characterization of zero-valent iron nanoparticles.* Advances in Colloid and Interface Science, 2006. **120**(1-3): p. 47-56.

[8] Kanel, S., D. Nepal, B. Manning and H. Choi, *Transport of surface-modified iron nanoparticle in porous media and application to arsenic(III) remediation.* Journal of Nanoparticle Research, 2007. **9**(5): p. 725-735.

[9] Phenrat, T., N. Saleh, K. Sirk, H.J. Kim, R.D. Tilton and G.V. Lowry, *Stabilization of aqueous nanoscale zerovalent iron dispersions by anionic polyelectrolytes: adsorbed anionic polyelectrolyte layer properties and their effect on aggregation and sedimentation.* J. Nanopart. Res., 2008. **10**(5): p. 795-814.

[10] Cirtiu, M.C., T. Raychoudhury, S. Ghoshal and A. Moores, *Systematic Comparison of the Size, Surface Characteristics and Colloidal Stability of*

Zero Valent Iron Nanoparticles Preand Post-Grafted with Common Polymers. Colloids and Surfaces A: Physicochem. Eng. Aspects, 2011. doi:10.1016/j.colsurfa.2011.09.011.

[11] Ditsch, A., P.E. Laibinis, D.I.C. Wang and T.A. Hatton, *Controlled clustering and enhanced stability of polymer-coated magnetic nanoparticles.* Langmuir, 2005. **21**: p. 6006-6018.

[12] Gregory, J., *Approximate expression for retarded van der Waals interaction.* Journal of Colloid and Interface Science, 1981. **83**: p. 138-145.

[13] Phenrat, T., N. Saleh, K. Sirk, R.D. Tilton and G.V. Lowry, *Aggregation and sedimentation of aqueous nanoscale zerovalent iron dispersions.* Environmental science and technology, 2007. **41**(1): p. 284-290.

[14] Gregory, J., *Interaction of Unequal Double Layers at Constant Charge.* Journal of Colloid and Interface Science, 1975. **51**(1): p. 45-51.

[15] Lim, J.K., S.A. Majetich and R.D. Tilton, *Stabilization of superparamagnetic iron oxide core-gold shell nanoparticles in high ionic strength media.* Langmuir, 2009. **25**(23): p. 13384-13393.

[16] Hogg, R.I., T.W. Healey and D.W. Fuerstenau, *Mutual coagulation of colloid dispersions.* Trans Faraday Soc., 1966. **62**: p. 1638-1651.